공학석사 학위논문

Reinjection Experiment at the Patuha Geothermal Field, West Java, Indonesia: A Field Experience and Numerical Analysis

인도네시아 파투하 지열 저류층에서의 재주입 실험 :

현장 적용과 수치 해석

2018 년 8 월

서울대학교 대학원

에너지시스템공학부

Ali Mehrabifard

Reinjection Experiment at the Patuha Geothermal Field, West Java, Indonesia: A Field Experience and Numerical Analysis

인도네시아 파투하 지열 저류층에서의 재주입 실험 :

현장 적용과 수치 해석

지도 교수 민 기 복

이 논문을 공학석사 학위논문으로 제출함
2018 년 8 월

서울대학교 대학원
에너지시스템공학부
Ali Mehrabifard

Ali Mehrabifard의 공학석사 학위논문을 인준함
2018 년 8 월

위 원 장 전 석 원 (인)

부위원장 민 기 복 (인)

위 원 송 재 준 (인)

Abstract
Reinjection Experiment at the Patuha Geothermal Field, West Java, Indonesia: A Field Experience and Numerical Analysis

Ali Mehrabifard
Department of Energy Systems Engineering
Rock Mechanics & Rock Engineering Laboratory
The Graduate School
Seoul National University

The status of the geothermal power capacity is about 13.3 Gigawatts as of January 2016, spread across the world, 25% of which is being produced by vapor-dominated reservoir. It would be more significant to bring in mind the fact that only 5.7% of all the operating geothermal reservoirs are vapor-dominated. Vapor-dominated reservoirs are prized because virtually all high-enthalpy produced-fluid is piped to the power turbines. Hence, the associated expense of injection wells and phase separation systems could be minimized. Vapor-dominated field requires a proper strategic management to be well-developed. The Patuha geothermal field is considered as a vapor-dominated system, located in West java, Indonesia. The site has a significant potential of 210 MWe, while the current installed-capacity is 55 MWe. This study is firstly focused to find the reason behind the poor production of idle wells and high production decline rate, and secondly to propose a suitable solution to the diagnosed-problem in order to enhance the production of the reservoir as well as the proper strategy for the field management in order to deal with the production decline rate.

An extensive field-data analysis, together with a literature review were carried out to diagnose the problem. Furthermore, an equivalent continuum approach was employed to simulate the injection of cold water into fractured super-heated vapor reservoir. Taking advantage of the numerical simulator, the reason of the negative well-head pressure observed during injection was understood. Accordingly, a suitable injectivity test for vapor-dominated reservoir was proposed by means of numerical simulation. The main issue was found to be that the natural recharge is very low to replenish the extracted steam. Consequently, an injection strategy with the main purpose of heat production enhancement was suggested for the available idle-wellbores. This strategy changed the injection status of PPL-01B to PPL-01A which has a proper location in comparison with the location of the former well. Due to the fact that no injection test at PPL-06 was reported, a fully methodical reinjection test for PPL-06 was proposed by means of field data analysis, knowledge

of other injection test at other vapor-dominated reservoirs worldwide, and the numerical simulation. This injection plan was considered all the possible reservoir responses.

Based on the analysis on the injection test carried out January 12, 2018 at PPL-06, the reservoir properties and the in-situ permeability were estimated. According a numerical model (using equivalent continuum approach), based on this reservoir characterization, was developed to evaluate the effects of the different injection test in the vapor-reservoir. Firstly, the simulation was performed to study the actual injection test and analyze whether the injection test at PPL-06 could improve the production of PPL-02A and PPL-04 whose production were increased during the injection test. The results revealed that with homogeneous permeability and uniform pressure distribution at the reservoir, the improvement could not be supported by the performed-injection test, since a high permeability greater than 15.5 D is required. By this simulation the production decline of PPL-06 after the injection was understood. The pressure decline trend during the injection was simulated.

Simulation of long-term injection test showed that if the injection at PPL-06 lasts long enough (e.g. in the order of 60 days) the production of PPL-02A could be increased up to 20.75 MWe, while no thermal breakthrough was observed. Note that PPL-06 is currently producing less than 1.5 MWe. It seems that PPL-06 could be converted to a successful injector which would improve the production of the system significantly, however, any injection strategy should be monitored and updated over the time to obtain the optimum injection plan; it is due to the fact that the underground fluid paths are complex, and numerical simulations are associated with simplified assumptions, therefore, the numerical simulations and field analysis have to be modified and updated by the actual test results. The results suggested that deep wells seem to be ideal as injection wells at the Patuha field. Finally, the reinjection strategy was proposed to be employed by the field-owner as the proper management strategy instead of drilling of only more production wells (the current strategy at the Patuha field).

Keyword: Reinjection, Vapor-dominated Reservoir, Injectivity Test, Field Data Analysis, Numerical Simulation, Two-phase Flow, Negative Wellhead Pressure, Hydrothermal modeling

Student Number: 2016-22103

Table of Contents

List of Figures

List of Tables

Chapter 1. Introduction

Due to excessive emission of greenhouse gases (GHG), the global warming is considered to be a global concern that earth's residents will face in the next 20 years. (Economic, 2015; KPMG, 2012, 2014). In 2016, International Energy Agency (2017) (IEA) reported that around 66% of the electricity generation is supplied by burning of fossil fuels, and according to the IPCC[1] report (2014), this is the largest single source of global GHG emission. Meanwhile, the global electricity demand has continued to rise at the rate of 1.6% per year, according to the International Energy Agency (IEA) report (Sawin et al., 2016). The exploitation of renewable energies (RE) is necessary to not only meet the increasing global electricity demand, but also mitigate the environmental effects caused by current energy supply (Commission, 2006, 2009). In recent years, the efforts have been put into the transition of the traditional energy supply of the world to RE sources by rapid growth in global investment on and deployment of RE. Solar and wind are being utilized as RE resources with a great potential of electricity generation. However, the intermittent nature of these RE sources makes the electricity output variable and, to some degree, unpredictable (Edenhofer et al., 2011; Skea et al., 2008).

Geothermal energy (the heat from the Earth's crust) is able to supply constant base-load power, and considered as a promising alternative for fossil fuel-based power plants. Although, electricity was first generated from geothermal energy in Larderello, Italy, in 1904 (Barbier, 2002; Fridleifsson, 2001), it has been used for centuries in the form of hot spring for multiple purposes (Cataldi, 1993; Fridleifsson, 2001). Armstead & Tester (1987) estimated that the total heat available in the crust is approximately 2.631×10^{19} J/km^2 (H. Armstead & Tester, 1987). Another estimation was reported by the World Energy Council survey (2013)[2], heat content of the crust is around 540×10^7 EJ[3]. The variations of the reported results are caused by different assumptions and estimation procedures. They all, however, agreed that the amount of the stored-heat in the crust is enormous (Mock, Tester, & Wright, 1997; Sass, 1993; J. Tester, Herzog, Chen, Potter, & Frank, 1994). Harvesting just 1% of stored-heat meets all the energy demand of the planet for 28 centuries (Olasolo, Juárez, Morales, & Liarte, 2016).

The worldwide status of the geothermal power capacity is reported to be about 13.3 Gigawatts as of January 2016 (Matek, 2016). A few countries mainly shared the current capacity, however published-report by the US Geothermal Energy Association (GEA) indicates that the number of countries generating geothermal

[1] The Intergovernmental Panel on Climate Change
[2] https://www.worldenergy.org/ [Accessed May 8, 2018].
[3] 1.055×10^{18} joules (1.055 exajoules or EJ) in SI units.

power is increasing significantly (Holm, 2010; Romitti, 2015). Generally speaking, geothermal energy is being produced from conventional geothermal reservoirs and unconventional geothermal reservoirs. Unconventional energy is expressed as Enhanced Geothermal Systems (EGS). EGS (previously named Hot Dry Rock (HDR)) are considered as geothermal reservoirs created to extract economical amounts of heat from low permeable hot reservoirs by permeability enhancement techniques, such as hydraulic stimulation (J. W. Tester et al., 2006). Karner and Renner (2005) reviewed the stimulation techniques used in EGS. Breede et al. (2013) published a complete review over 31 EGS projects worldwide including different stimulation methods.

Most of the geothermal energy, however, produced by conventional geothermal (hydrothermal[4]) reservoirs. These reservoirs are located in certain geological conditions, occurring predominantly in volcanic regions with abundant groundwater (Tester et al. 2006). Indonesia thanks to its volcanic nature owns the world's largest geothermal potential, which has been characterized by high temperature geothermal resources' concentration. Bina et al. (2018) reported that the geothermal energy potential of Indonesia was estimated 28,617 MW, which is about 40% of the world's geothermal potential. However, only about 4.5% is being utilized as electrical energy supply in this country.

In the following sections of this chapter, firstly the motivation and scope of this study is described, and later a brief review of the conventional geothermal systems, including classification and their energy production, along with the general characteristics of the vapor-dominated reservoirs are reviewed assisting the reservoir characterization of the Patuha geothermal field, as one of the developing high-energy-potential geothermal field in Indonesia.

[4] Hydrothermal systems are geothermal reservoirs which contain fluid, and are classified by the dominant fluid phase contained within the reservoir (Faust, 1976).

1.1 Motivation, Objectives, and Scope of the study

Under the sponsorship of Korean South−east Power Company, Seoul National University in collaboration with Sejong University, INNOGEO, Geo Dipa Energi, and Bandung Institute of Technology, took the responsibility of the engineering aspects of a project titled by "Development of The Business Model of Indonesian Geothermal Power Generation Using Enhanced Geothermal Systems Technology" (Figure 1.1).

The Patuha geothermal field is located in West Java, Indonesia (Figure 2.1). The name of the site is coming from the Patuha volcano close to which Patuha field has been developed. The heat source is coming from the shallow magma; the reservoir consists of a steam zone at the depth of approximately 800 meter to 1600 m with high temperature of T >240 ℃, and low pressure of P <3.3 MPa, a cap rock, and a deep liquid reservoir. The formation permeability is low (order of $10^{-18}\,m^2$), while it is densely fractured. Therefore, since the reservoir permeability is low no fluid can flow from high pressure zones (i.e. the deep liquid reservoir), into the steam zone of low pressure. Thanks to such a strong heat support, the system has a significant potential energy resource (210 MWe), while the current install capacity is 55 MWe. 13 wellbore has been drilled between Kawah Putih and Ciwidey Prospect Area (Figure 2.3), 9 of which are producers, 1 injection well, and the rest did not meet the minimum production, and categorized as non−commercial wellbores, in the present study these wellbores are called "idle wells".

Geo Dipa Energi company, as the main operator at the Patuha field, is trying to enhance the heat production and take the proper strategy management to deal with the high production decline rate at the site. Therefore, the objectives of my study could be summarized as follow:

- Find the reason behind poor production of idle wells and high production decline rate (problem diagnostic)
- Proposing the suitable solution to the identified problem in order to enhance the production of the reservoir and the proper strategy for field management in order to deal with production decline rate.

To obtain the objective of this study, my contribution to the project was divided into 7 tasks represented in Table 1.1.

Table 1.1 Tasks defined for the project of "Development of The Business Model of Indonesian Geothermal Power Generation Using Enhanced Geothermal Systems Technology".

#	Time Status	Task	Method	Output
1	September 2016–March 2017	Finding the most suitable wellbore stimulation	Literature Review of Wellbore Stimulation	Hydraulic Stimulation Thermal stimulation Chemical Stimulation
2	March 2017–May 2017	Reservoir Characterization, Problem Identification (Poor Production)	Data Analysis, Literature Review on Vapor–dominated Reservoirs	Hydraulic Stimulation is not the key solution
3	May 2017–November 2017	Solution, and Injection Design	Literature Review of Similar Injection Design, Numerical Modeling	The Injection Plan was prepared and submitted [injectivity test for vapor dominated reservoirs].
4	November 2017–December 2017	Preparing the Injection Operation	Explaining the problem and solution to the Korean and Indonesian teams	Injection Operation design was fitted into the budget design and available sources.
5	January 2018	Injection Operation [Patuha]	N/A	N/A
6	February 2018–April 2018	Injection Test Analysis	Data Analysis	Insitu Permeability calculation [for the first time at Patuha]. Production Improvement at near producers.
7	May 2018–Peresent	Injection Operation Simulation	TOUGH2 simulator	To analyze the injection effect on the near producers

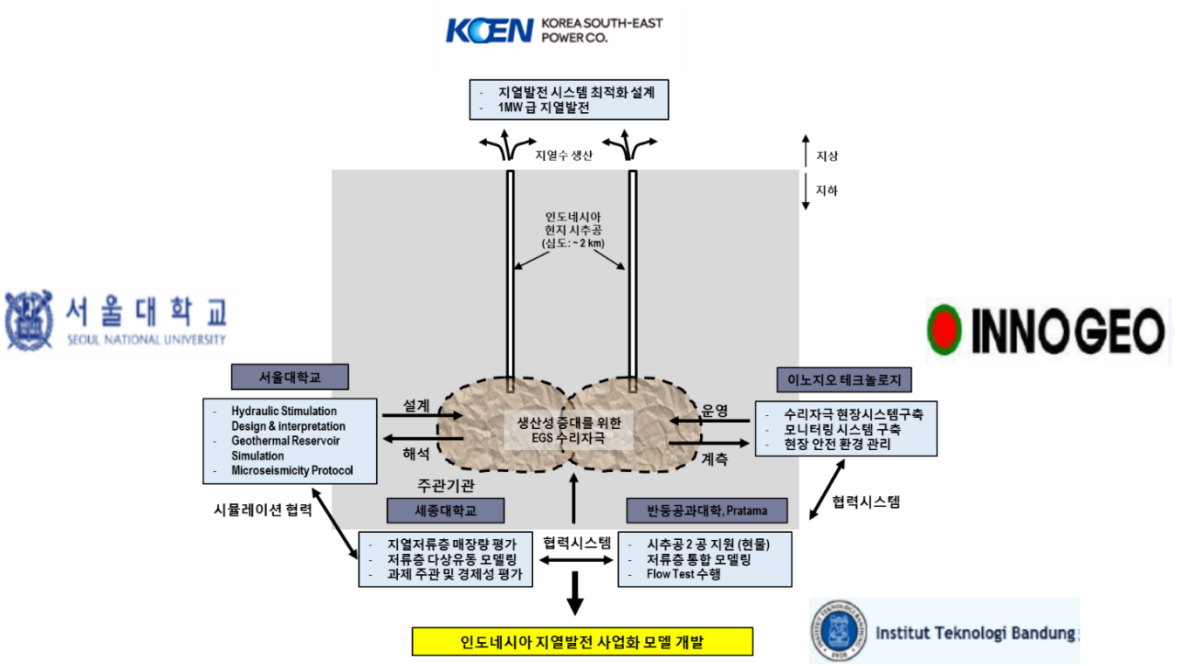

Figure 1.1 Task-chart of the project titled by "Development of The Business Model of Indonesian Geothermal Power Generation Using Enhanced Geothermal Systems Technology"

1.2 Classification of Conventional Geothermal Systems

Conventional geothermal systems, as it was explained in the last paragraph, are located mostly in volcanic regions. Intrusion-related geothermal systems are the connection that link the realms of crustal intrusion, hydrothermal circulation[5], and shallow groundwater flow in which hydrothermal circulation convects the heat from deeper regions to the reservoir zone (Stimac, Goff, & Goff, 2015). This is shown schematically in Figure 1.2 (A), along with the typical temperature and pressure gradients measured in the shallow crust summarized in Figure 1.2 (B and C). A generalized diagram describing conditions within a vapor-dominated and liquid-dominated geothermal systems are shown in Figure 1.2 (E and D). Different researchers tried to classify the geothermal systems. Nicholson (2012) has classified the geothermal systems based on several reservoir properties such as reservoir equilibrium state, fluid type, and reservoir temperature. Kaya et al. (2011), however, made a simple classification based on the reservoir temperature and the production enthalpy, listed in Table 1.2. Taking advantage of such a classification enabled them to assist with the evaluation of energy production of different geothermal systems based on the available data, presented and utilized in this study.

Table 1.2. Classification of conventional geothermal systems[6]

Category		Temperature (T) [℃]	Production enthalpy (h) [kJ/kg]
Hot-water		T<220 ˚C	h<943 kJ/kg
Two-phase, liquid-dominated	Low-enthalpy	22 ˚C<T<250 ˚C	943 kJ/kg<h<1100 kJ/kg
	Medium-enthalpy	250 ˚C<T<300 ˚C	1100 kJ/kg<h<1500 kJ/kg
	High-enthalpy	250 ˚C<T<330 ˚C	1500 kJ/kg<h<2600 kJ/kg
Two-phase, vapour-dominated		250 ˚C<T<330 ˚C	2600 kJ/kg<h<2800 kJ/kg

Source: (Kaya et al., 2011).

[5] Movement of water in the earth's crust resulting from thermal and density gradients.

[6] In the present study, as the main focus is on conventional geothermal energy, the "geothermal reservoir" refers to conventional reservoir.

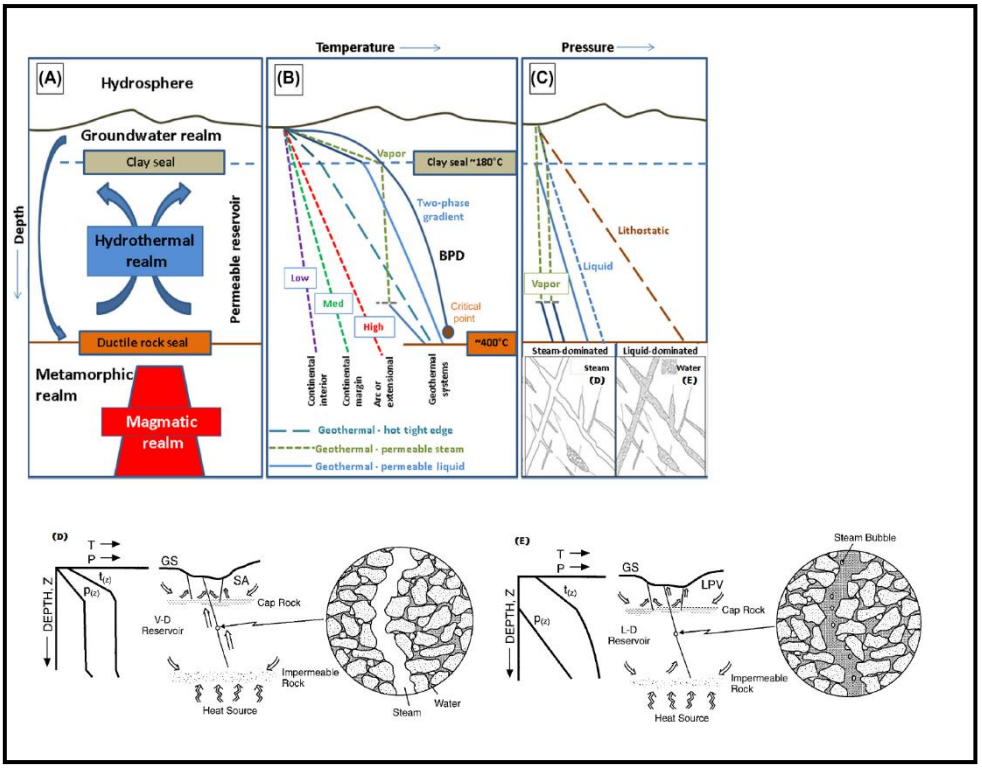

Figure 1.2. Geothermal System

makes the connection of the realms of crustal intrusion, hydrothermal circulation, and shallow groundwater flow. (A) The heat to the system is provided by magmatic intrusion to drive fluid circulation in the hydrothermal realm. The direct communication between these realms is limited by low-permeability seals at the bottom (ductile-brittle transition, brown line) and top (clay cap, dashed blue line) of the hydrothermal zone. The circulation of meteoric waters occur in downward direction, peripheral to the top seal (down-pointing arrows). Hot fluid flows up as a buoyant plume relative to a hydrostatic gradient (up-pointing arrows). (B) Temperature profiles at different depths in the hydrothermal realm. Boiling point is plotted versus depth (BPD)[7]; in the core of the system, temperatures may approach this profile (BPD). At distance away from the upflow[8], temperatures are generally below the BPD but high compared to areas where heat is transported purely by conduction. Vapor-dominated zones might form in the shallowest parts of the system, and the conditions could be observed if it becomes sufficiently isolated from groundwater. (C) Pressure profiles are shown in different locations in a general hydrothermal system. A hydrostatic gradient occurs throughout the hydrothermal regime; however, pressures are commonly sub-hydrostatic relative to surface in high-elevation systems. A lithostatic gradient dominates below the bottom seal of the system. Liquid or vapor gradients may prevail in the system core depending on its history and extent of isolation from groundwater. (D) Schematic model of conditions in a vapor-dominated system where vapor exists in open fractures but liquid water resides in porous rock; GS means ground surface, SA means shallow aquifer. (E) Schematic model of conditions in a liquid-dominated geothermal system where liquid water saturates all the void spaces in the rock; LPV means low-pressure vapor cap. Modified after Stimac et al. (2015).

[7] A temperature–pressure phase diagram for pure water applying hydrostatic depth (weight of a water column to a given depth) as a proxy for pressure. It shows the temperature at which ascending liquid water starts to boil as a function of depth, however is not a strict control on the maximum observed–temperature and –pressure (Stimac et al., 2015).

[8] A buoyant plume of geothermal fluid and contained non–condensable gas that rises from a heat source to a heat sink by advection (Stimac et al., 2015).

1.3 The installed energy capacity of classified conventional geothermal reservoirs.

According to the review by Diaz et al. (2016), the world's installed capacity of the total conventional geothermal energy up to the date of the review was approximately 12,280 megawatts (MWe). By adding the installed capacity of Patuha field (section 2.1), the total installed capacity would be updated to 12,335 MWe. Figure 1.3 represents the installed power capacity in MWe for 125 geothermal systems classified according to table 1.2. 25% of the total installed capacity are being produced by 8 two-phase vapor-dominated developed fields, three of which are located in Indonesia: Patuha, Kamojang and Darajat.

In Figure 1.4, Diaz et al. (2016) analyzed the available production data of 87 geothermal fields to compare the mass production required to generate 1 MWe for each type of geothermal system (refer to table. 1.2); the average mass required to produce 1 MWe at the Patuha field was added according to table 2.1. Since the produced enthalpy of vapor-dominated system is high, it requires less fluid to generate 1 MWe of power than any other system.

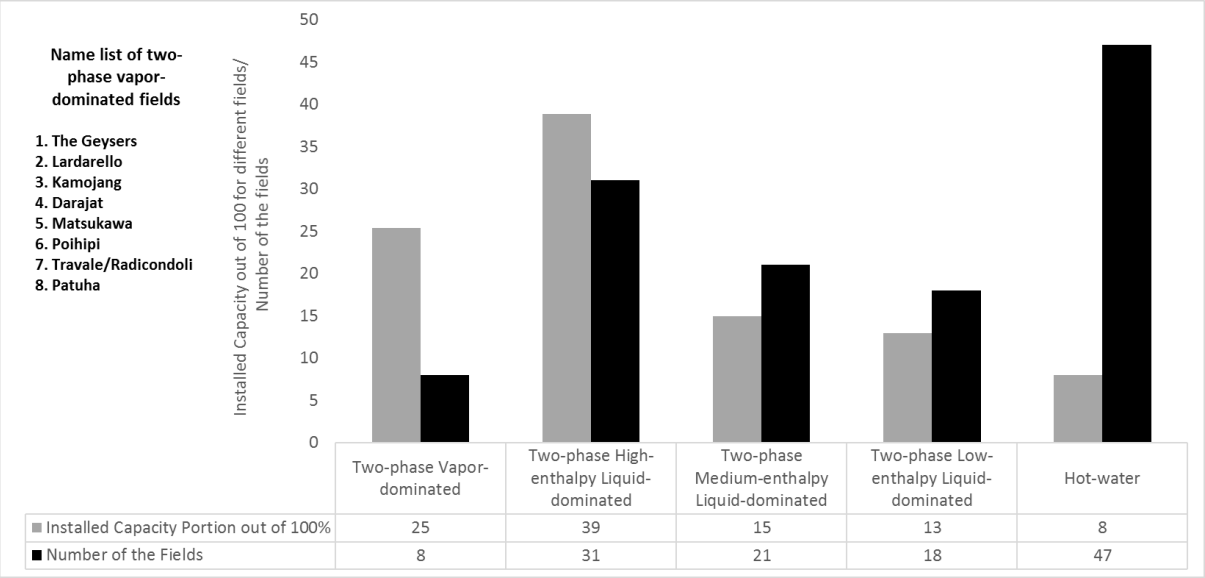

Figure 1.3 The total installed capacity by different types of geothermal systems (refer to table 1.2) for 125 geothermal fields across the world. The name of the vapor- dominated systems are listed (modified after Diaz et al., 2016).

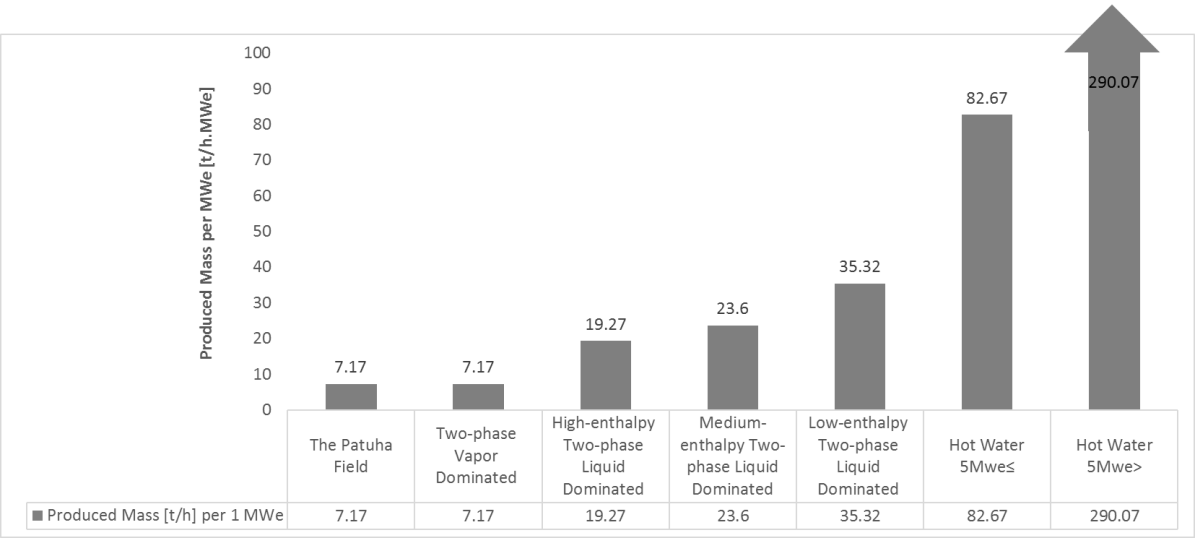

Figure 1. 4 Produced mass (t/h) per MWe for each type of geothermal system (refer to table 1.2), modified based on table 2.1 after (Diaz et al. 2016).

Due to the evolution process and geological settings of the vapor–dominated systems, they own a huge heat sources and play a prominent role in the geothermal industry. In fact, these geothermal systems are highly prized because virtually all their produced fluid could be piped to the power turbines. Hence, the expense of injection wells (less injection is needed since the amount of the fluid to be extracted for 1 MWe is small, see also Figure 5.2/ or 5.3) and phase separation systems could be minimized. Therefore, a proper management strategy is necessary to maintain or even boost the heat production. Knowledge of the characteristics, and the production mechanism of such a system is crucial not only to make a complete analysis on the Patuha reservoir behavior and diagnose the main issues, but also to take the suitable solutions. In the following paragraphs the essential characteristics of the vapor–dominated systems were reviewed.

1.4 The characteristics of Vapor-dominated reservoirs

1.4.1 Temperature

The reservoir zone of vapor–dominated reservoir has high temperatures, in the order of 250–330 °C. These systems are mostly located within active volcanic centers, with elevated–temperature gradients resulting from high heat flow caused by shallow intrusions of magma. Igneous–related geothermal systems are considered as high–potential energy resource; as an example, identified magmatic systems in the United States are thought to contain much more thermal energy than all known hydrothermal[9] systems in the same region (Dobson et al., 2017; Faust, 1976; Smith & Shaw, 1978; J. W. Tester et al., 2006; White, Muffler, & Truesdell,

[9] Hydrothermal systems are geothermal reservoirs which contain fluid, and are classified by the dominant fluid phase contained within the reservoir (Faust, 1976).

1971).

1.4.2 Pressure

Naturally occurring vapor-dominated geothermal systems are rare. Although many reservoirs might have shallow vapor-dominated zones, only a few fields are known to have low pressure (< 7 MPa) vapor-dominated zones extending to below the sea level (e.g. The Geysers, Larderello, Kamojang, Dieng, Darajat, and Patuha). Figure 1.5 Shows the pressure-depth trends in The Geysers, Larderello, Kamojang, Darajat, and Patuha (Allis, 2000; Schotanus, 2013).

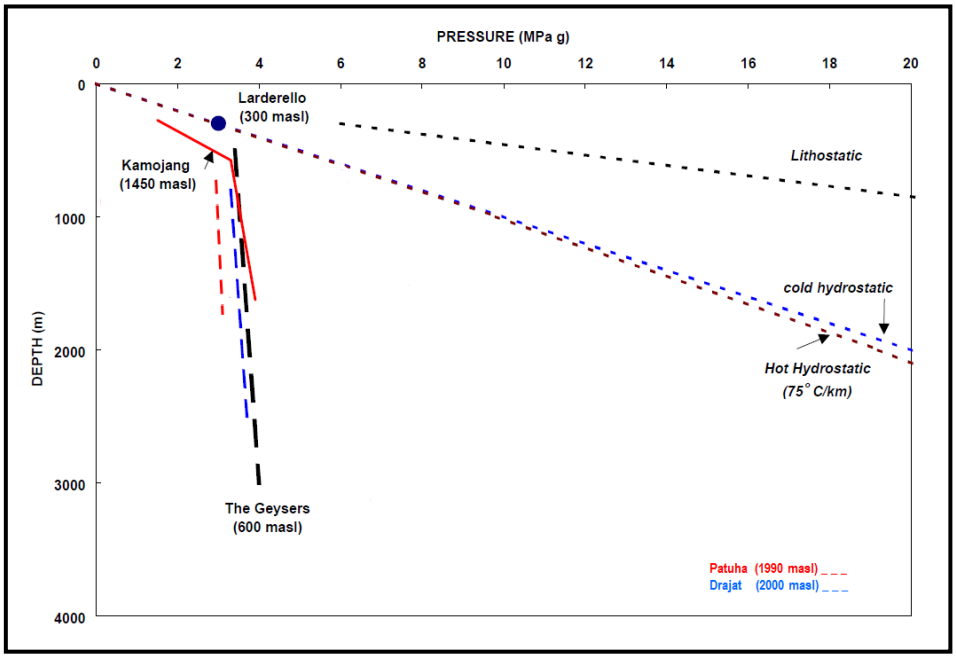

Figure 1.5 Pressure-depth trends in The Geysers, Larderello, Kamojang, Darajat, and Patuha (vapor-dominated systems). Number in parentheses after each name is the ground elevation in meters above the sea level (masl). Modified after Allis (2000).

1.4.3 Permeability

Vapor-dominated systems have low permeability in the reservoir zone (the rock matrix permeability is typically of the order of 10^{-18} m^2) and very low permeability surrounding the reservoir (more explanation is provided in section 1.4.4). Hence, natural recharge, and water movement is very limited from the surrounding rocks; very low permeability of the surrounding rocks is the main reason why the water from high pressure aquifer cannot flow inside the low pressure vapor-zone. Low permeability is also contributing to the production of superheated steam, which is fully discussed in section 1.4.5.

1.4.4 Evolution of vapor-dominated reservoirs

Allis (2000)reviewed the physical characteristics of The Geysers, Larderello, Kamojang, and Darajat, and claimed that The Geysers and Larderello have most

likely evolved differently from Kamojang and Darajat.

Vapor-dominated systems developed gradually from the systems that initially contains hot-water. An increasing heat flux into the system, or a decreasing permeability as a result of self-sealing might cause the initiation of the evolution procedure. In the given condition, it becomes possible that water lost by discharge can no longer be fully replenished by recharge. This phenomenon results in an under-pressured reservoir and consequently a vapor-dominated system starts to evolve.

Geological settings generally assumed to differentiate the evolution process and the consequent properties of such large vapor-dominated systems. The Geysers and Lardarello reservoirs are surrounded by naturally low-permeable rock, consequently limiting the inflow of meteoric waters. The recorded low pressures of these reservoirs are believed to be caused and/or sustained by different reasons such as reservoir dilation and steam loss to the surface. To count the general features of these systems, both The Geysers and Lardarello have large reservoir areas (~100 km^2), low heat flow intensities and long lifespans (>10^5 years) (Allis, 2000).

The Kamojang and Darajat systems are both volcano-hosted. This type of system is assumed to consist of a vapor chimney above the main magmatic plume surrounded by a liquid-dominated geothermal system. The vapor chimney can decay into an under-pressured vapor-dominated system due to magmatic hydrothermal activity and decreasing permeability of the host volcanic formation. The occurrence of this type of system is limited to volcanic arcs where the subduction is perpendicular to the trench/for-arc region, similar to the phenomenon corresponding to the formation of the Sunda and Java Trench (Figure 1.6) where Drajat and Kamojang are located. The heat flow intensity of Darajat and Kamojang is an order of magnitude greater than The Geysers and Lardarello, accordingly, one could imply that the infiltration rate of meteoric waters is much larger and the lifespan of the vapor system is shorter (< 10^4) (Allis, 2000; Hall, 2002; White et al., 1971).

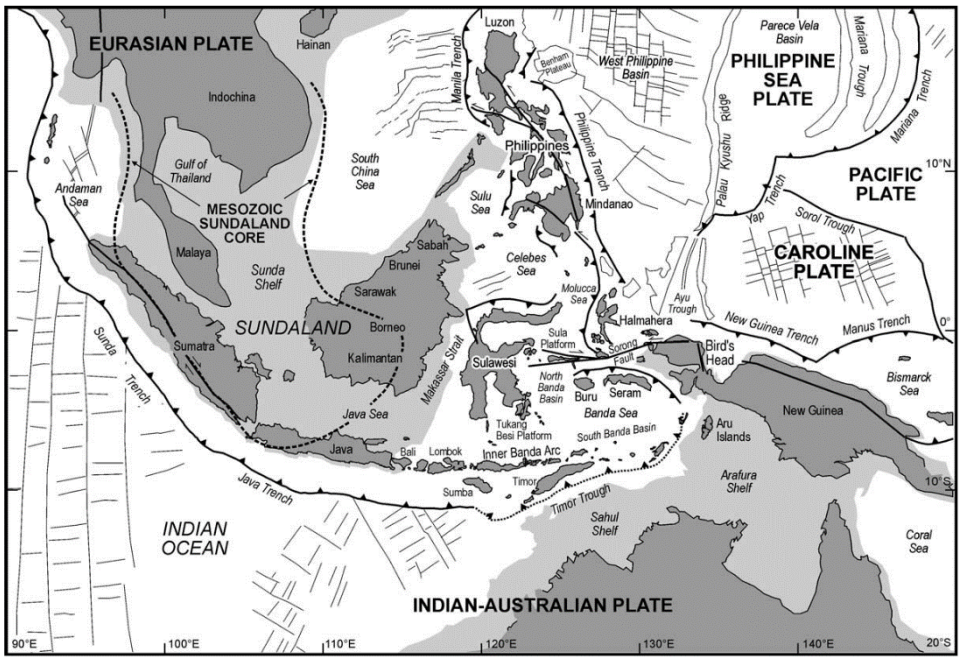

Figure 1.6 Complex tectonic situation of the Java region, the Sunda and Java Trench at where Kamojang, Darajat, Patuha, and Dieng are located. (Hall, 2002)

1.4.5 The presence of immobile water

Generally speaking, vapor-dominated two-phase systems produce dry steam, they, however, contain a large amount of immobile water. According to extensive analysis conducted on the total cumulative production data of Larderello, Italy, and The Geysers, California, in the literature, it was stated that an unreasonably large reservoir thickness is required if the fluids are assumed to be stored in the form of steam in vapor-dominated reservoir (James, 1968; Nathenson, 1975; Weres, Tsao, & Wood, 1977). In other words, even though all the produced fluids of the vapor-dominated system (e.g. The Geysers) have been in the form of steam, the fluid must be stored as liquid in the reservoir (Marconcini et al., 1977). Therefore, the liquid water must paradoxically exist in the vapor-dominated reservoir at a pressure and temperature at which liquid water cannot exist at such an in-situ conditions. For instance, the "paradox of the Geysers" has been investigated by numerous authors (K Pruess & TN Narasimhan, 1982; Thomas, Chapman, Dykstra, & Stockton, 1981; Truesdell & White, 1973), among them Truesdell and White (1973) summarized the early controversy on such a paradox. They proposed that either a separate liquid water source, external to the vapor-dominated reservoir, is responsible for recharge in The Geysers, or storage in the Geysers is accomplished by capillary retained or adsorbed water which, due to vapor-pressure lowering may exist as a liquid form under conditions which would normally specify vapor (for more information about vapor-pressure lowering refer to paper wrote by Pruess (1995)). Subsequent researches have failed to find any evidence of a hidden water source recharging The

Geysers, while a number of studies have supported that the retention of water within the reservoir itself could be the most plausible mass storage source (Hornbrook, 1994; Maria, 1996; Pruess, 1995).

1.4.6. The production mechanism

The production mechanism of the vapor-dominated systems is explained based on the aforementioned fact that the mass produced from the reservoir must be stored as liquid. The production mechanism for these systems was examined along with production data and the thermodynamic properties of water, steam, and rock by Truesdell and White (1973). It was concluded that these systems initially consist of a water and steam filled reservoir (Figure 1.2 D), a water-saturated cap rock, and a water or brine-saturated deep reservoir below a water table. Considering the reservoir as a porous media with permeabilities large enough to be corresponding for the practical field production, Truesdell and White (1973) concluded that most of the liquid water in all parts of the system is relatively immobilized in small pores and crevices (Figure 1.7 A); steam dominates the large fractures and voids (Figure 1.7B, and Figure 1.8) of the reservoir and is the continuous, pressure-controlling phase. With production, the pressure perturbation propagates into the porous media and the liquid water boils, causing massive transfer of heat from the rock and its eventual drying. Passage of steam through already dried hot-rock leads to the production of superheated steam. After an initial vaporization of liquid water in the reservoir, the decrease in pressure produces increased boiling below the deep water table. With excessive production, boiling extends deeper into hotter rock and the temperature of the steam increases.

On the other hand, it could be assumed that the large-scale permeability at vapor-dominated system is provided by networks of interconnected fractures (Figure 1.7 B), while the matrix rock has low permeability typically of order 10^{-18} m^2 (1 microdarcy), or less (Beall, Enedy, & W. T. Box, 1989; Pruess, 1996). Pruess and Narasimhan (1982) argued that in such a reservoir, heat conduction can strongly increase the flowing enthalpy. According to their numerical studies to analyze the amount of the liquid saturation of the vapor-dominated system, it is actually possible to produce superheated steam from a rock matrix with liquid saturation of even ~100%. In other words, K Pruess and TN Narasimhan (1982)concluded that if the matrix effective permeability for the liquid flow (absolute permeability × relative permeability) drops below a minimum value k_{min}, the mass flux of water from the matrix to the fractures will be continuously vaporized by heat transported due to conduction even when liquid water is mobile and flowing. k_{min} depends upon temperature and heat conductivity and is typically of the order of $5\,x\,10^{-18}$ m^2 (5 microdarcies).

Idealized reservoir geometries are shown in Figure 1.7. At the zones vapor, liquid, and rock grains co-exist at the simplified geometries shown with region sign “I” (Figure 1.7, A&B), at where the reservoir has its original temperature and pressure. From region I towards region II (Figures 1.7), the liquid saturation decreases as the temperature and pressure decrease and as heat is transferred to the fluid. Along

surface II the last liquid water disappears and the steam saturation approaches 100%. Further passage through the rock from surface II to the well III is nearly isothermal, however a small amount of additional heat might be transferred and consequently the steam becomes more superheated.

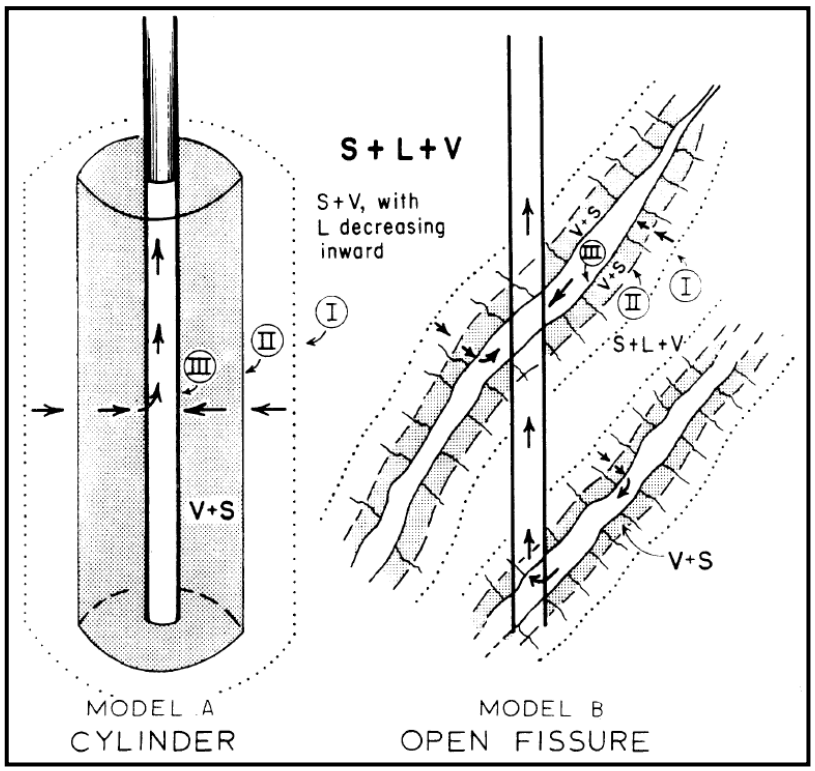

Figure 1.7 Idealized production models of vapor-dominated systems A is for a homogeneous reservoir with initially uniform pressure, temperature, and water content saturation; model B represents a reservoir in which flow is controlled by large permeable fractures in porous rock of low permeability. S: solid, V: vapor, L: liquid. I is composed of S, V, and L. II consists of S, V (more than I), and L (less than I). III is filled with S, and V (Truesdell & White, 1973).

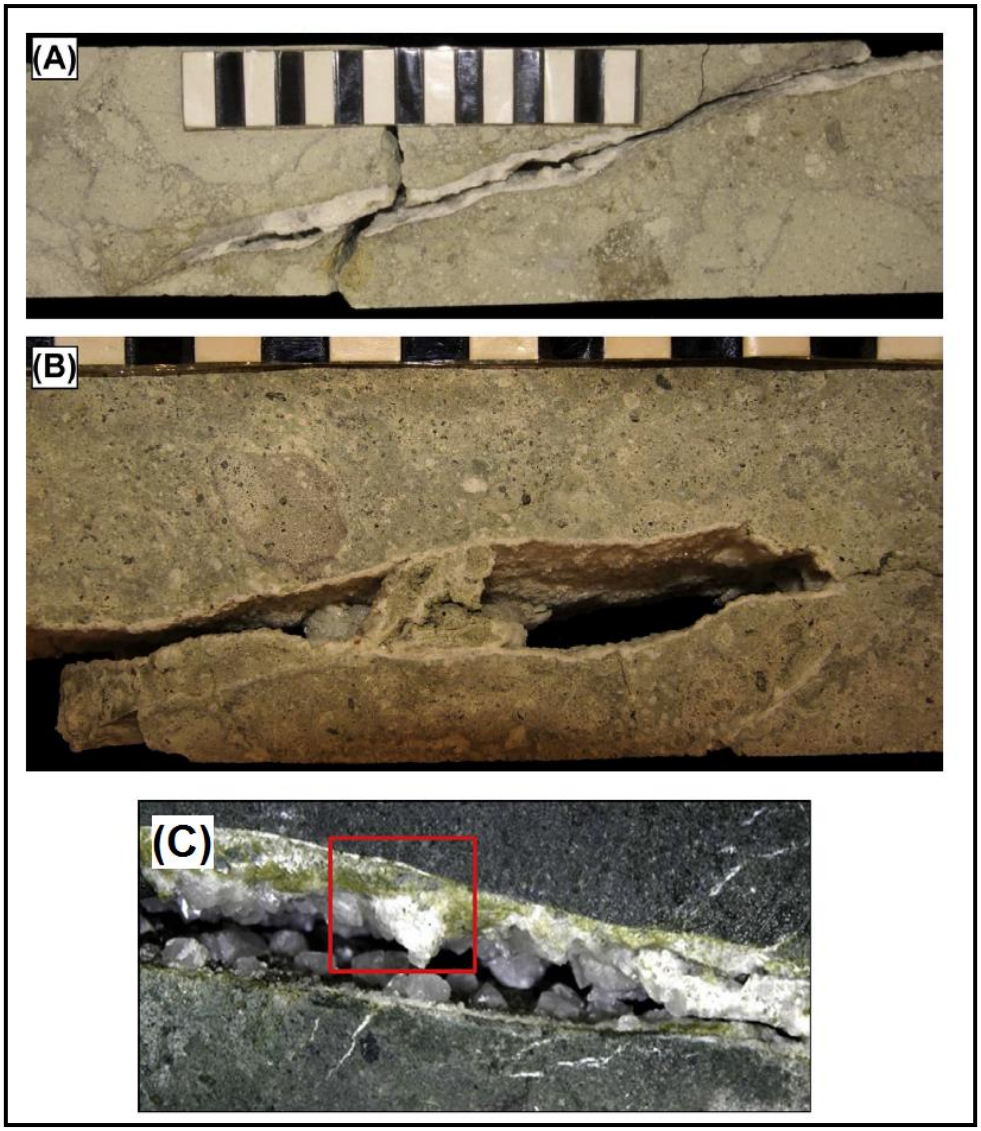

Figure 1.8 The fractures found in hydrothermal systems. These are depicted from core samples of geothermal systems. (A) Brecciated dacite tuff cut by partially filled shear fracture (scale in centimeters). (B) Dacite tuff cut by vuggy open fracture with bridge of cemented rock fragments (scale in centimeters). (C) Andesitic tuff cut by a large open fracture (up to 1-cm aperture) forming part of a fault system. Large calcite and finer epidote crystals are clearly visible (red-box). After Stimac et al. (2015).

Chapter 2. The Patuha Geothermal Field

2.1. Introduction

The Patuha geothermal field is located about 40 kilometers southwest of Bandung on western Java, Indonesia (Figure 2.1). From the pressure and the temperature measurements at depth along with the analysis of the secondary minerals, it has been concluded that the Patuha geothermal system is a vapor-dominated system (as it has been fully discussed by Schotanus based on the studies carried out by West Japan Engineering Consultants Company on Patuha (Schotanus, 2013; West Japan Engineering Consultants (West JEC), 2007). It is believed that this geothermal system consists of a cap rock, an underlying steam cap and a deep liquid-dominated reservoir. The heat flux to the systems is provided by a main heat source below Kawah Putih and the Patuha volcano. The fluid flows through networks of interconnected fractures existing in the low permeable reservoir rock. Although, the potential capacity of this field is estimated to be around 210 MWe, the installed capacity is 55 MWe. According to the field observations and measurements, the reservoir pressure and temperature are reported to be around 3.3 MPa (Figure 1.5) and (higher than) 225℃, respectively (Schotanus, 2013). The precipitation of silica and its consequent problems are very low as well as the amount of the non-condensable gas. 13 wellbore has been drilled in nearby Ciwidey Prospect Area and the Patuha volcano (Figure 2.3), 9 of which are producers, 1 injection well, and the rest did not meet the minimum economical required production and categorized as non-commercial wellbores; in the present study these wellbores are referred "idle wells" (Geo Dipa Energi Presentation Material July 26th 2017-SNU meeting).

Figure 2.1 is representing the installed-capacity of the geothermal systems in Indonesia. The Patuha geothermal system is situated in a similar geological setting as the Darajat and Kamojang systems are (Figure 2.1). The evolution and general properties of geothermal systems are mainly controlled by the geological setting, as stated in section 1.4.6. Therefore, it is reasonable to assume that the Patuha system would have similar properties as the geothermal systems in Darajat and Kamojang have.

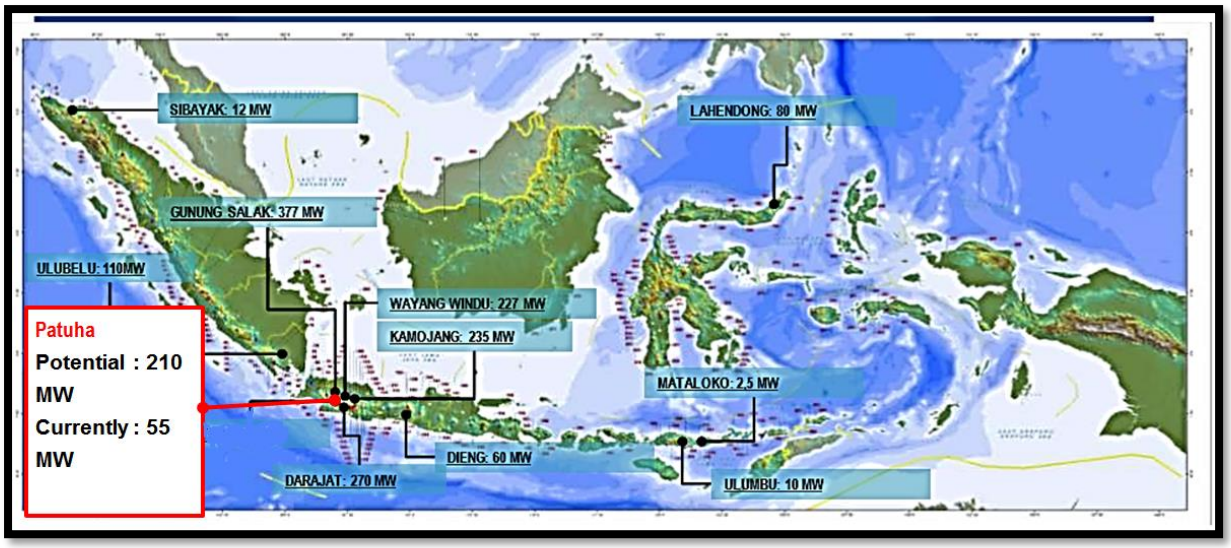

Figure 2.1. Geothermal map of Indonesia (modified after Geo Dipa Energi Presentation Material July 26th 2017-SNU meeting).

Table 2.1 Well status of the Patuha geothermal field, up to November 20, 2017. (Modified after Geo Dipa Energi Presentation Material July 26th 2017-SNU meeting).

Well ID	Total Drilled Depth [m]	Remarks	Temp. [℃]	Tested Output [MWe]	Average Mass [t/h] (based on Fig. A. 2) / Status
PPL-01	1016	Directional	213	12.5	89.625/Production
PPL-01A	2701	Directional	202	N/A	0/Shutin
PPL-01B	1775	Directional	175	N/A	119/ Injection
PPL-02	2089	Directional	228.98	4.5	32.265/ Production
PPL-02A	1760	Directional	227.02	8.4	60.228/Production
PPL-03	1464	Vertical	228.98	8.2	58.794/Production
PPL-03A	995	Directional	228.98	3.2	22.944/Production
PPL-03B	1154	Directional	227.02	13.9	99.663/Production
PPL-04	2172	Directional	262.69	3	21.51/Production
PPL-04A	1628	Directional	212	Non. Comm	0/Blocked
PPL-05	1618	Directional	232	6	43.02/Production
PPL-06	2537	Directional	221	Non. Comm	0/Shut-in
PPL-07	1700	Directional	232.76	12.7	91.059/Cyclic production, injection, shutin

2.2. Structural Geology

The deposition of relatively young volcanic rocks in the Patuha field makes it difficult to identify any structural fault at the surface. Since no remote sensing and seismic survey were conducted, West JEC 2007 estimated the fault-system based on the available data including interpretation of gravity survey, (for more information related to such a technique the reader is referred to Nishijima and Naritomi (2017)), analysis of surface manifestations[10], geothermal-fluid composition, resistivity survey, and temperature distribution survey ; the estimated faults are listed and shown in Table. 2. 2 and Figure 2. 2, respectively. The dip angle of these faults are estimated to be approximately between 75° to 90°, which is believed as a general assumption for the faults in volcanic regions which are related with island-arc systems.

Table. 2. 2 Estimated fault by West Japan Engineering Consultants (West JEC) (2007) at the Patuha Geothermal field, modified after Schotanus (2013).

Fault number	Trending	Dipping to ...	Estimation based on ...
F1	NW-SE	Southwest	Gravity survey
F2	NW-SE	Southwest	Gravity survey
F3	E-W	North	Gravity survey
F4	NE-SW	Southeast	Gravity survey
F5	NE-SW	Southeast	Gravity survey
F6	NE-SW	Southeast	Gravity survey
F7	NE-SW	Southeast	Gravity survey
F8	E-W	North	Gravity survey
F9	NE-SW	Northwest	Temperature distribution
F10	NNW-SSE	East-northeast	Arrangement of volcanic cones

[10] Thermal manifestations: All hot springs, fumaroles, and related features that discharge fluid from underlying hydrothermal circulation systems (Stimac et al., 2015).

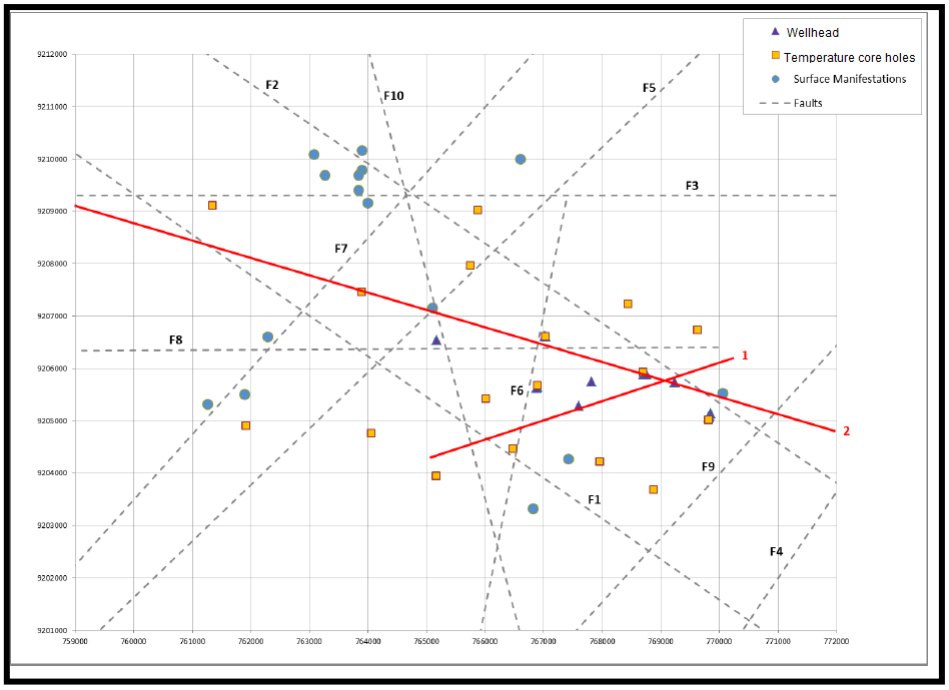

Figure 2.2 Estimated faults map (top view). The faults number is corresponding to the fault number of Table 2. 2 (West Japan Engineering Consultants (West JEC), 2007) modified after Schotanus (2013)

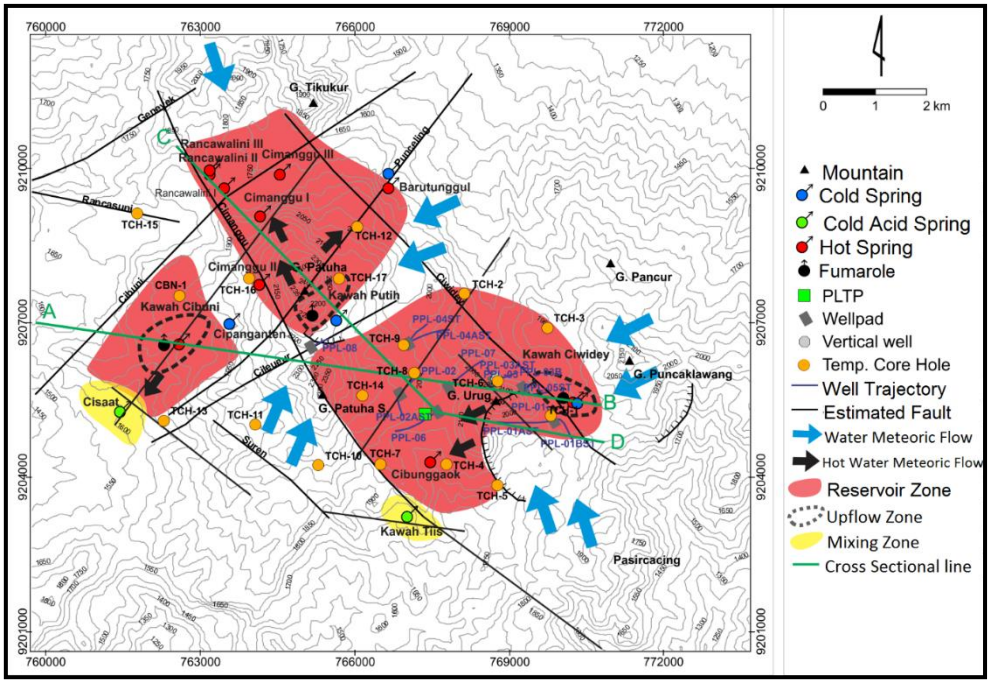

Figure 2. 3 The top view of the Patuha field including the field details such as wellbore trajectory and the meteoric flow[11]paths, temperature hole core[12], and the fault systems (modified after Geo Dipa Energi Presentation Material July 26th 2017-SNU meeting).

[11] Meteoric water: Water originally derived from precipitation (rain and snow) that is the main source of groundwater. Deeply circulating meteoric water is the dominant fluid in most geothermal systems (Stimac et al., 2015).

[12] Temperature hole core are generally both slim and quite shallow, they may reach a few hundred metres depth. Their main purpose is to study shallow temperature conditions (temperature gradient) and estimate heat flow.

Figure 2.3 shows the updated topographic map (top view) of the Patuha field which includes the fault systems, wellbore trajectory and the meteoric flow paths, and temperature hole cores. Engineers at the Patuha field believe that these faults are sealing faults in the direction perpendicular to their strike line (normal to the fault plane). In other words, these impermeable barriers divided the reservoir to a few sub-regions. All the wellbores (table. 2.1) in the Patuha field were drilled in the sub area at which the heat source is supported by both Kawah Patuha and Kawah Ciwidey (section 2.3, Figure 2.4 and 2.5).

2.3. Development of Conceptual Models of Patuha

The conceptual models are representing the system and its basic concepts and features, used to assist the reader to understand the geothermal reservoir. There are three conceptual models developed for the Patuha geothermal field by Layman and Soemarinda (2003), West JEC (2007), and Schotanus (2013). These models are summarized as the following.

The first conceptual model for the Patuha was proposed by Layman, 2003. It can be summarized as below:

- It is a vapor-dominated system.
- It consists of a deep liquid reservoir.
- The size of the reservoir is 20 square Km.
- A single heat source below Kawah Putih which is permanently supporting the system (Refer to Figure 2.3 and 2.4).
- Fumaroles at Kawah Ciwidey and Kawah Cibuni are supposedly the result of lateral flow from the central plume.

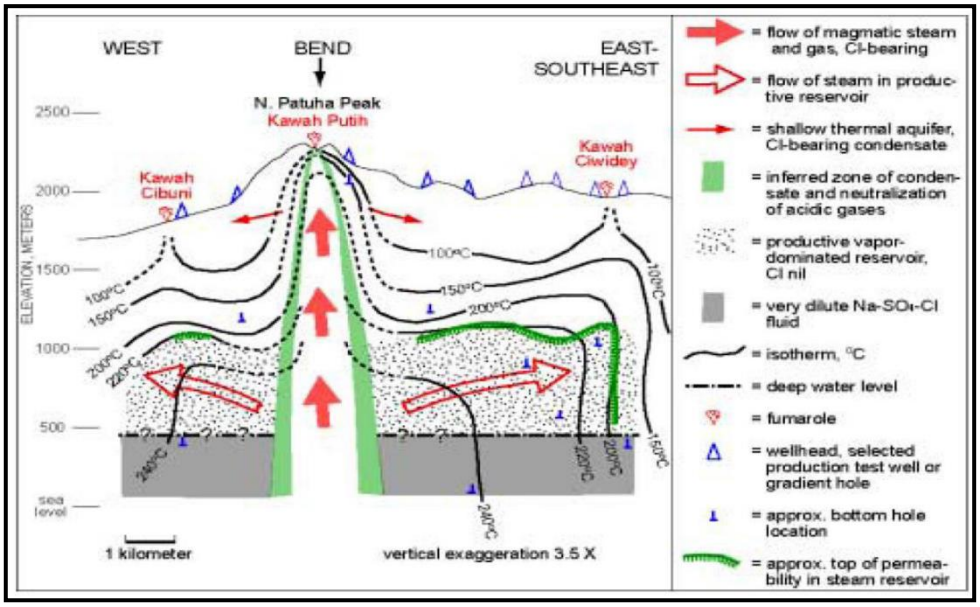

Figure 2. 4 Cross-section view illustrating the conceptual model of the Patuha resource developed by Layman and Soemarinda (2003)

The model was later modified by West JEC in 2007 and the main difference is about the heat source.

- Vapor−dominated system
- The presence of upflow zones near Kawah Putih and Kawah Ciwidey; the upflow zones clearly are associated with the fault zones in the area.
- Presence of Steam cap (500 m.a.s.l ~1200 m.a.s.l, approximate depth of 900 m to 1600 m)
- Presence of deep liquid reservoir in the vicinity of the fault zones
- Heat source is located approximately below these volcanic cones (Convection heat flux by magma) and no lateral heat flow

The last model was suggested by Schotanus (2013) which is basically the same as the two former models but the heat sources are connected with three faults and the one beneath Kawah Putih is the largest heat source. Lateral flow can occur within the reservoir rock Figure 2.5.

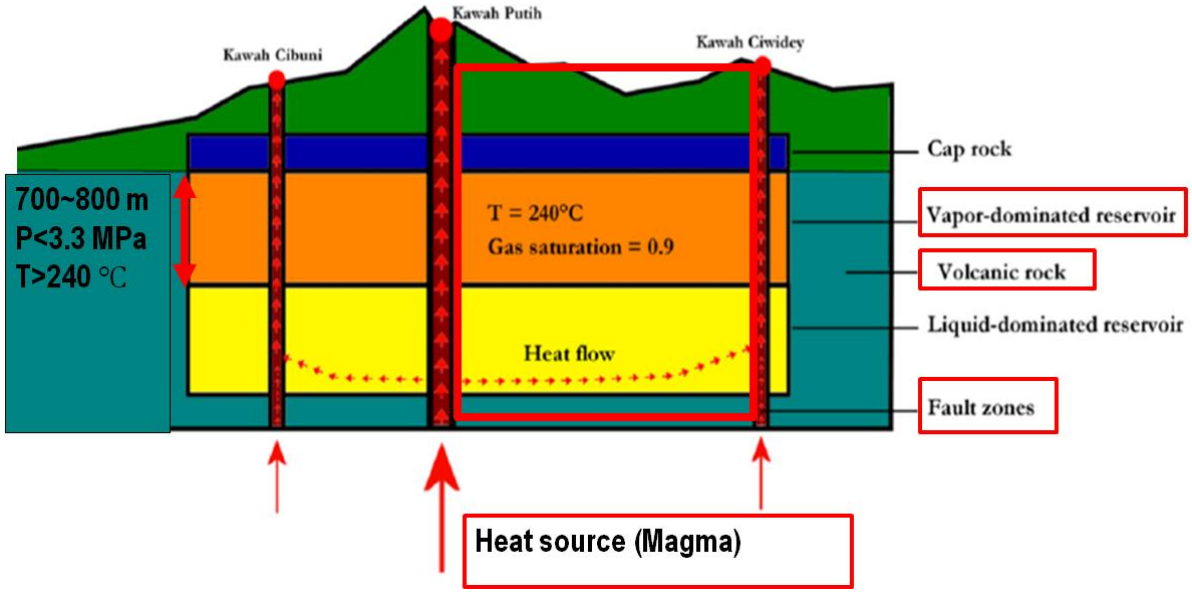

Figure 2. 5 Simple conceptual model of the Patuha geothermal system, after Schotanus (2013).

2.4. Field Data Analysis (Candidate Wellbores)

2.4.1. Data Analysis of PPL-01A

PPL−01A was completed on January 31, 1997, to produce steam from Ciwidey Prospect Area (Figure 2.6, Table 2.3). However, the production test failed to meet the minimum commercial production rate. Since then, the status of the wellbore is shut−in.

Following the drilling completion, the well experienced an injection test for about 25 hours on Feb 26, 1997 at 16:30. Figure 2.7 shows the wellhead pressure (WHP) responses to the injection test. Figure 2.9 shows the pressure and temperature profile along the well in shut−in condition before and after the injection test.

Following the trend of the WHP, one could recognize the unique and different WHP responses to the water injection from the typical geothermal fields, (Figure 4.1); specially, in the case of enhanced geothermal systems (EGS), e.g. Newberry EGS, the U.S. (Figure 2.10). In fact, Figure 2.7 depicts an unstabilized WHP trend vs. time. Except at the minimum rate, the pressure values continuously decrease, as the injection rate increases. The injectivity index (also known as II) values calculated from these data (based on equation 4.1) are represented in Figure 2.8. As it is explained in section 4.1 these injectivity index values are not reliable as the pressure values for each rate failed to reach the stability with respect to the time. The injectivity index obtained is an over−estimation of the permeability of the wellbore (even negative II has been obtained, see Figure 2. 8). Thus, the injectivity test procedure described in section 4.1 cannot be applied to such a reservoir condition.

However, the key point that could be observed in Figure 2.7 is the fact that the pressure at higher injection rates is lower than that at the lesser flow rates. The other key point of such an injection test is that although the II values are not reliable, the injectivity of the wellbore is truly high since we can inject high amount of fluid without any resistance.

Table 2. 3 The General Characteristics and Status of the Idle Wellbores at the Patuha Field.

Well ID	PPL-01A	PPL-01B	PPL-06
True Vertical Depth [m]	2272	1623	2351
Max.Temp. [℃]	202	175	221
Well Head Pressure (WHP) [MPa]	1.530	1.310	2.289
Output [MWe] @ 1.034 MPa	non-comm.	non-comm.	non-comm.

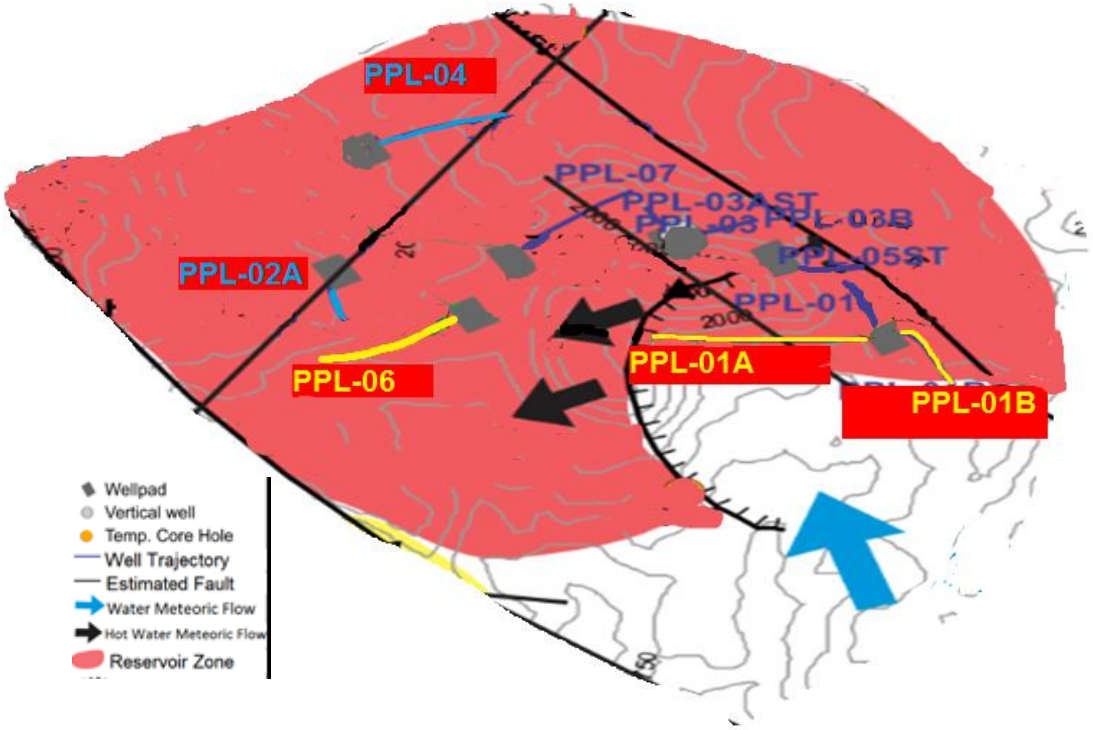

Figure 2.6 All the 13 drilled wellbores at the Patuha (Table 2.1). The trajectory of the idle wells is represented in yellow. PPL-02A and PPL-04 are most likely intersecting the same fault as PPL-06 does.

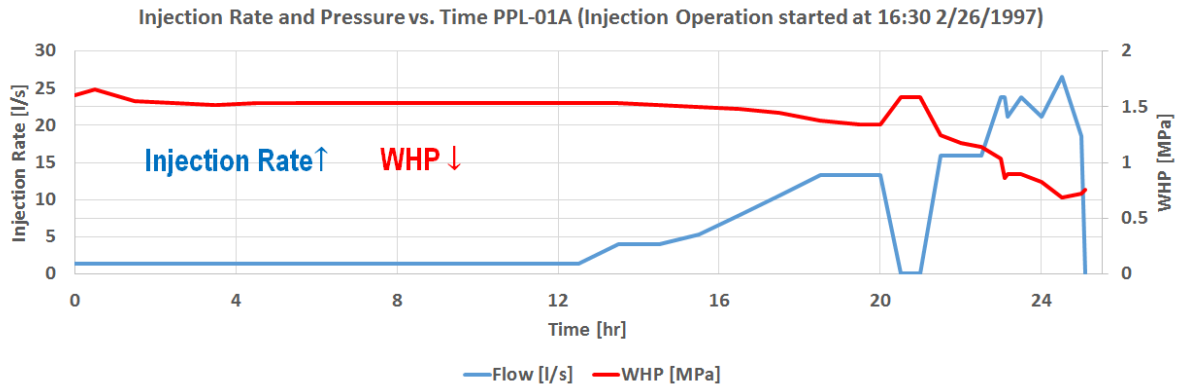

Figure 2.7 Injection test at PPL-01A started at 16:30 on Feb 26, 1997 (0 hour corresponds to the start of the injection operation). The wellhead pressure (WHP) and the injection rate has been plotted versus time.

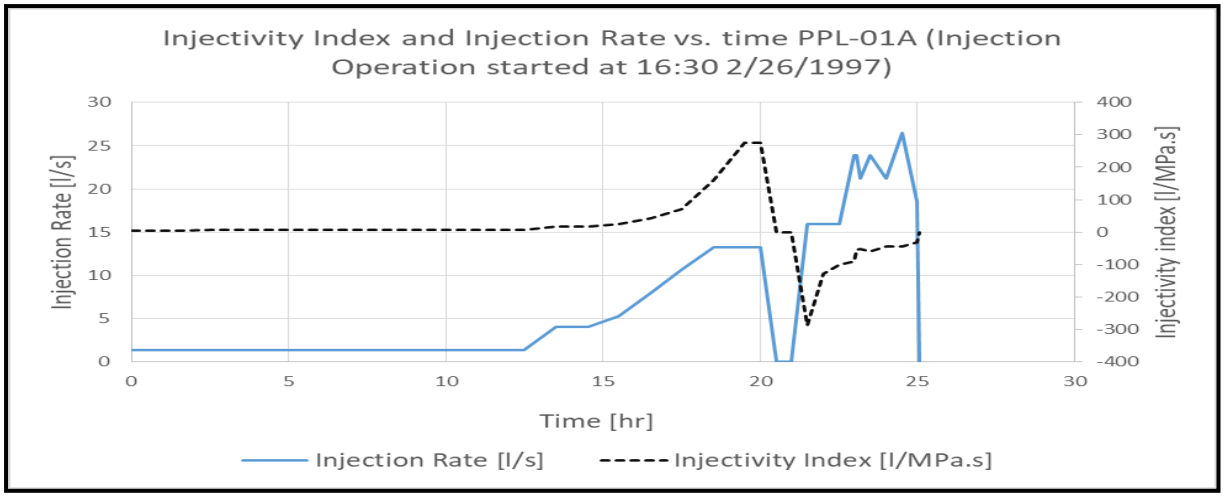

Figure 2. 8 The calculated injectivity index according to equation 5.1 of injectivity test for PPL-01A (started at 16:30 on Feb 26, 1997) has been plotted versus injection time.

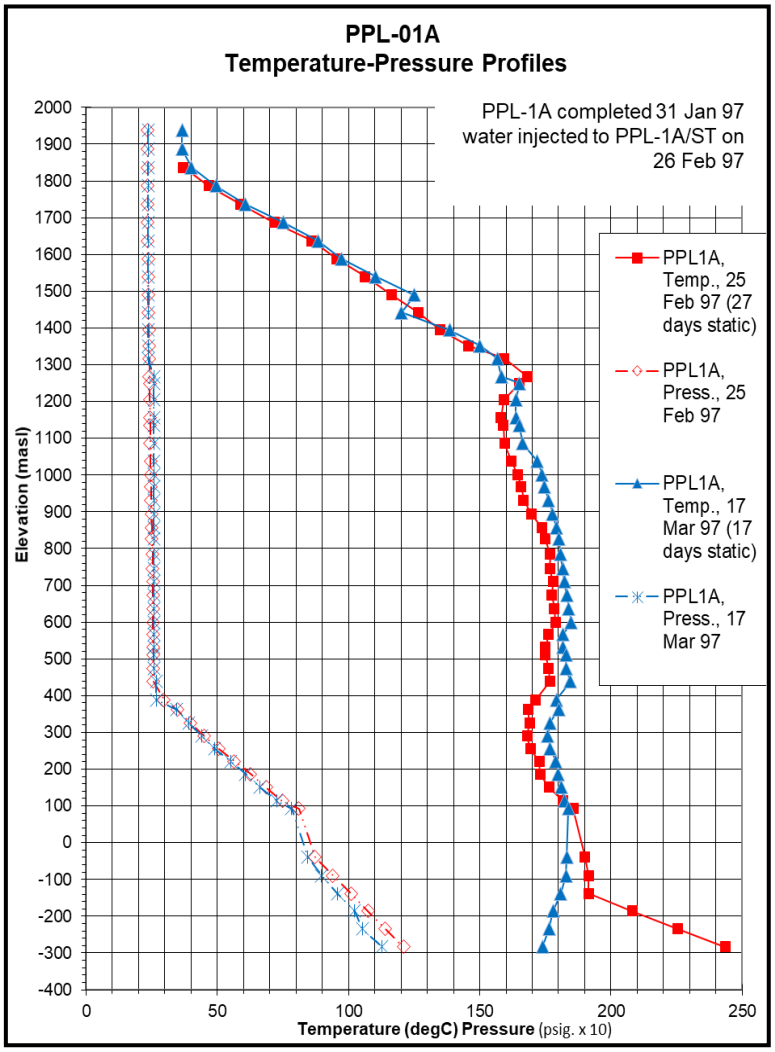

Figure 2. 9 The pressure and the temperature profiles of PPL-01A before and after injection test (injection test performed on 26/02/1997).

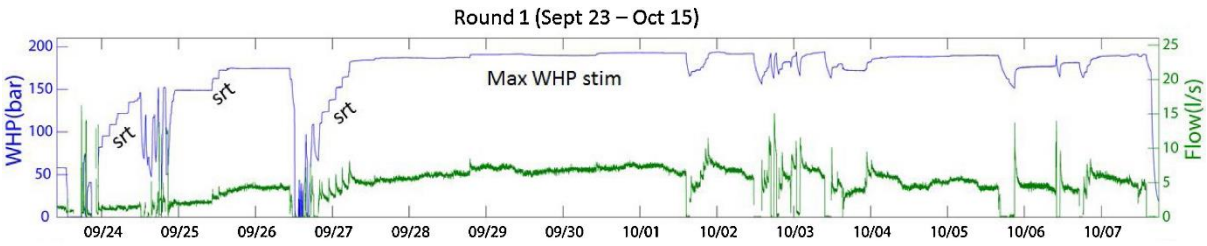

Figure 2. 10 Wellhead pressure and injection rate curves of hydraulic stimulation at Newberry EGS site, the U.S (Srt is representing the Step-rate-test, see chapter 4) (Cladouhos, 2016).

2.4.2. Data Analysis of PPL-01B

PPL−01B has been completed on September 26, 1997 (table 2.3). The production test, similar to PPL−01A failed to meet the minimum commercial production rate. This well also experienced an injection test for around 52 hours with three short shut−in period. The injection rates of the injection test are, however, higher than the rates applied at PPL−01A. The WHP responses to the injection is quite similar to PPL−01A, however, since the injection rate is higher the WHP pressure decreases to a negative value, which is called vacuum pressure at the field.
An interesting point about this graph is the fact that as soon as the negative wellhead pressure is achieved the WHP is almost constant (Figure 2.11 and Figure 2.12).

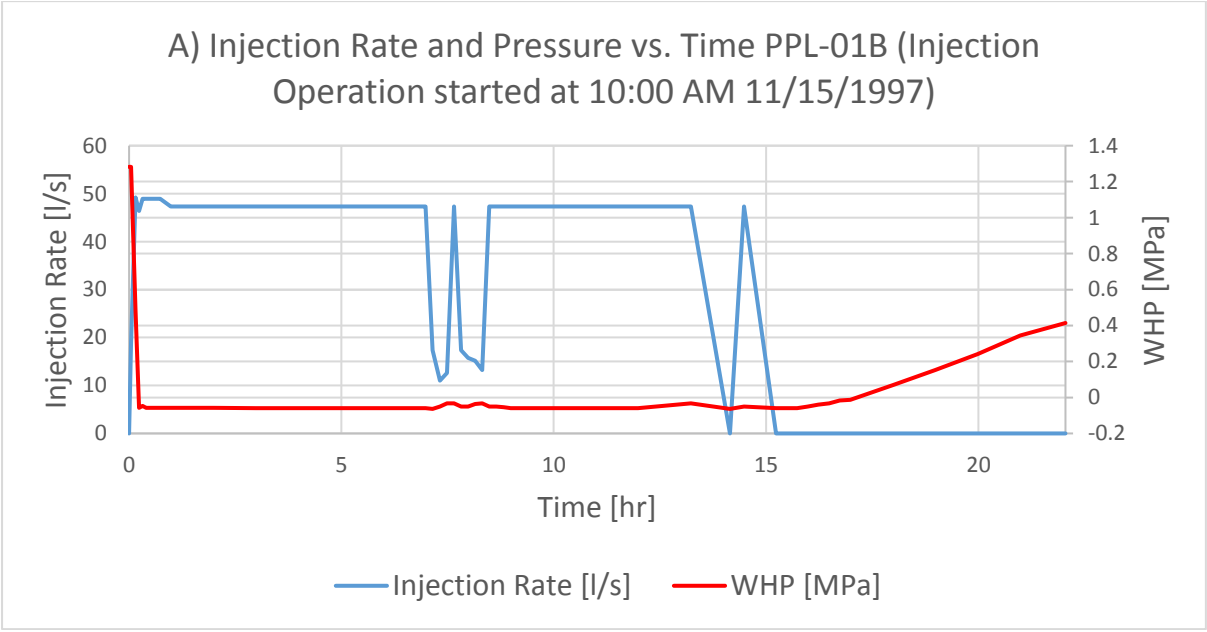

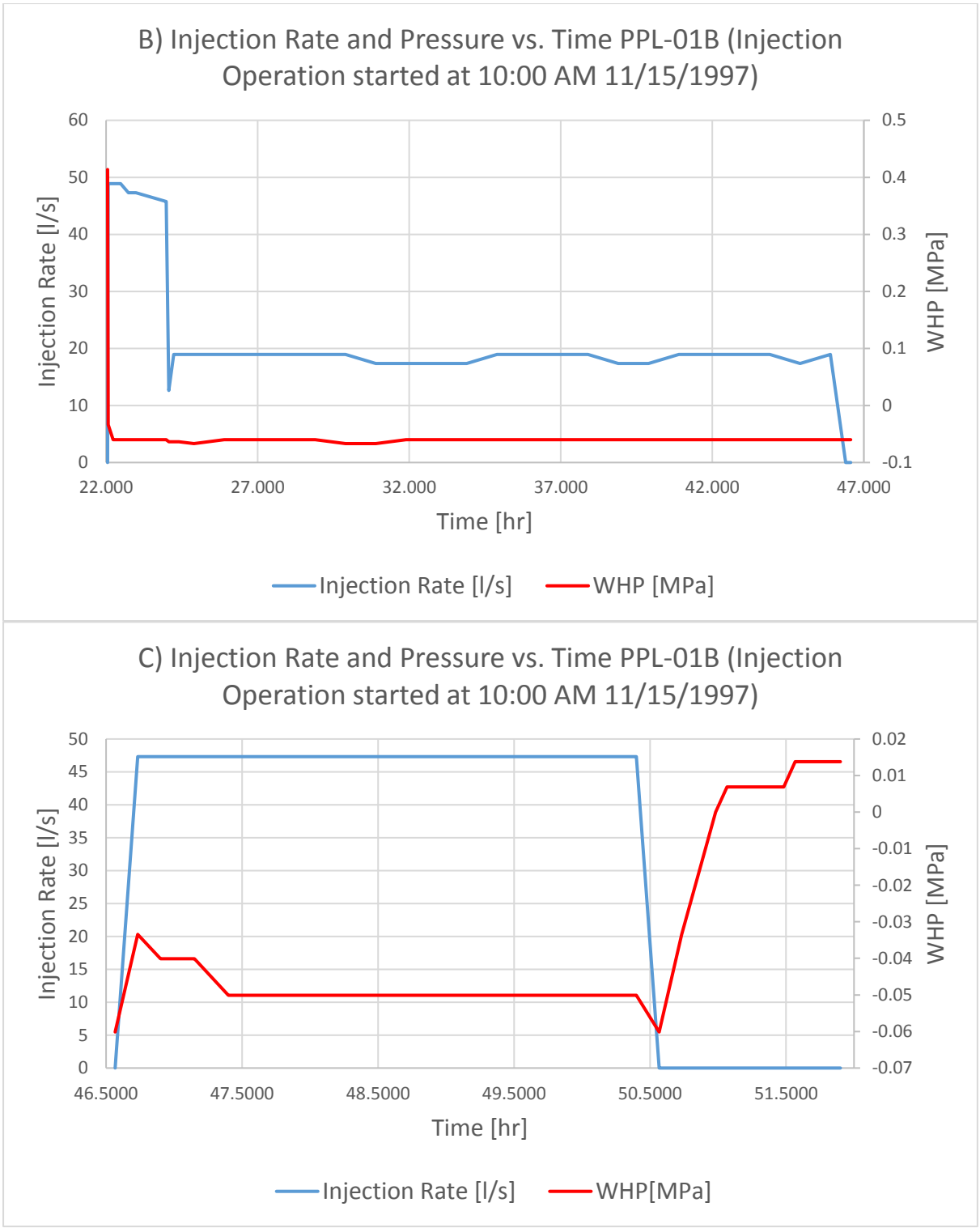

Figure 2.11 Injection test at PPL-01B (the well location is represented in Figure 2. 6) started at 10:00 AM on Nov 15, 1997 (0 hour corresponds to the start of the injection operation). The wellhead pressure (WHP) and the injection rate has been plotted versus time. The injection test includes three shut-in periods; A) The first shut-in B) The second shut-in, and C) The third shut-in.

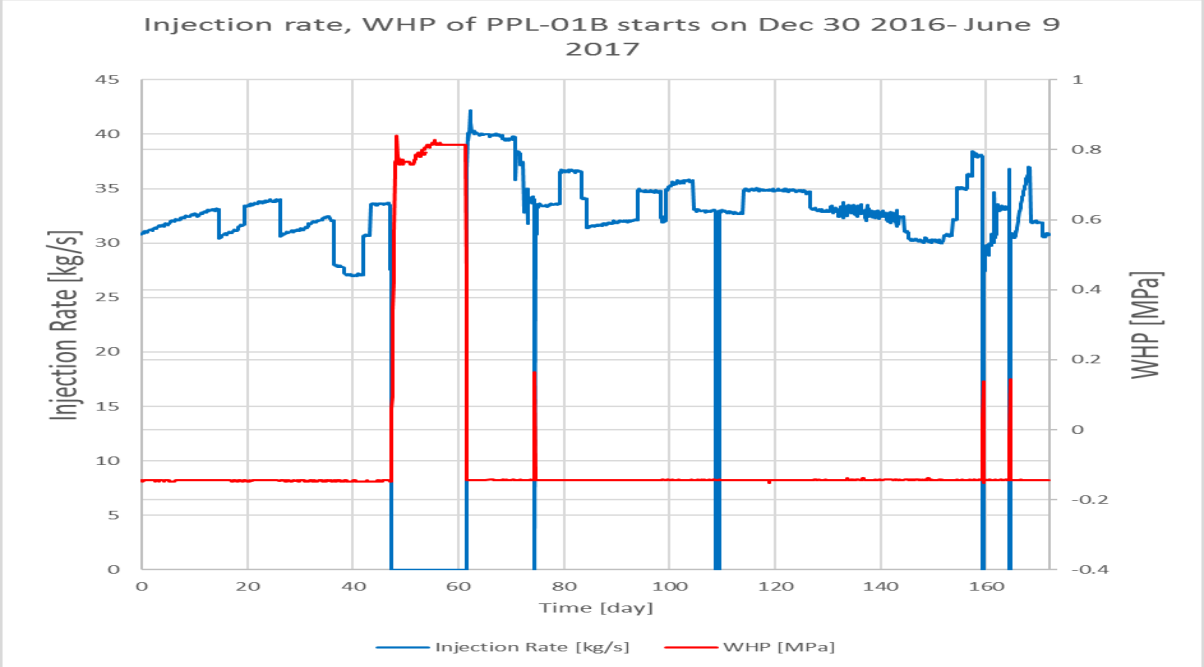

Figure 2.12 PPL-01B is under reinjection since 1998 to late 2017. The graph is representing the WHP at PPL-01B and the injection rate for the period of Dec 30 2016- June 9 2017.

PPL−01B is used as the condensate waste disposal, since 1998. The location of the wellbore relative to the reservoir zone has been depicted at Figure 2.6. As it is shown the PPL−01B is seemed to be drilled at the boundary of the reservoir. According to the drilling reports, this well has intersected with high permeable zones (fractures). The annual cumulative injection mass is around 900,000 ton. Assuming the density of water 1000kg/m^3 and the total injection of 18 years, the amount of the injected condensate is over 16 million m^3. The WHP of PPL−01B is always being reported as vacuum pressure, and there is no evidence of pressure support, or production improvement in the near production wellbores (Figure 2.6).

2.4.3 Insight into Negative Wellhead Pressure (Vacuum Pressure)

Wellhead pressure (WHP) is the pressure at the top of the well (i.e. at its wellhead). It is measured by pressure gauges of the wellhead fittings. The WHP could be reported at static and dynamic conditions. Considering static wellhead pressure is gauged in the shut−in status well and depends on the reservoir pressure, well depth and density of the filling medium (in case of the Patuha it is steam density). Numerically it equals the difference between the reservoir pressure and the hydrostatic pressure of the liquid column from wellhead to reservoir.

Dynamic wellhead pressure is measured in the operating well and depends on the same parameters as the static pressure, and also on the production rate or on the injection rate, since there would be a pressure drop due to friction. In most of the geothermal fields, as the injection starts into the well, the WHP starts to increase (Figure 2.10). Injection at wells in the Patuha reduces the WHP (e.g. Figure 2.12). In this section, efforts have been put to explain such an abnormal phenomenon.

The negative WHP could be due to one, or a combination of the following reasons:

- As the cold water enters the reservoir, the heat transfers from the reservoir to the injected fluid (in-situ fluid and the reservoir rock are in thermally equilibrium condition); such a heat transfer, finally causes part of the liquid to evaporate initially and the prevail temperature decreases continuously (as the required-latent-heat is being absorbed by the cold water); consequently, the in-situ vapor will release the latent heat and condense to liquid. At this stage, the system would be at two-phase, saturated condition. Therefore, the saturation pressure will decrease (following the Clausius-Clapeyron relation, Figure 3.4), as the saturation temperature decrease due to continuous cold water injection. Numerical simulation was performed in this study (Chapter 3, Figure 3.6) to capture such a pressure decline due to injection. Moreover, as the injection at PPL-06 was simulated (section 5.5), such a pressure decline due to condensation of the in-situ steam was observed (Figure 2.13). It is noteworthy to mention that although the WHP is negative the pressure at the depth would not be a negative value.

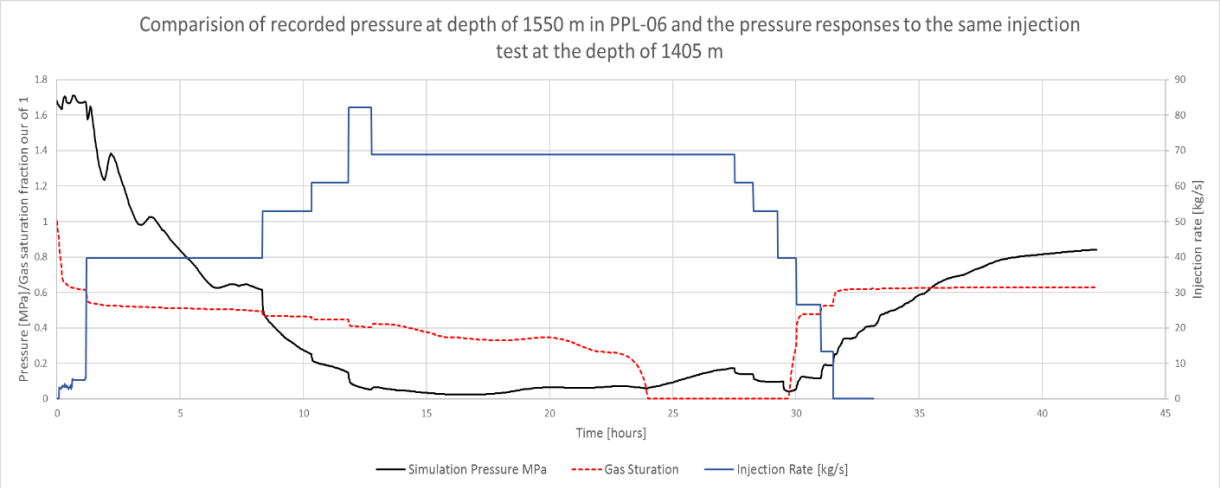

Figure 2.13 The observed pressure decline due to the phase changes at the vapor-dominated reservoir (the results of the simulation conducted at section 5.5).

- After relatively long time of injection (from a few hours to weeks, depends on the injection rate), the cold water injection will cool down the wellbore and the two phase would transit to single-liquid phase (the dominant pressure would be higher than the saturation pressure at the dominant temperature). As it is shown in Figure 2.12, the injection operation is going on for long enough to make sure that the wellbore is under single liquid phase injection. Therefore, the well should be filled out completely by liquid. However, the negative WHP could be interpreted as such the wellbore is not completely filled with the liquid and actually the well is sucking in the fluid; it could be

explained in such a way that the wellbore volume has increased. For instance considering Figure 2.12 at the injection rate of 35kg/s the −0.11 MPa WHP was observed, and as the injection stopped the pressure started to build up. Since after a long time injection the pressure did not build up (PPL−01B is under injection of an average injection rate of 35kg/s for more than a decade), it could be inferred as the injected fluid has not reached any boundary yet. On the other hand, as the negative WHP has not decreased, there is an equilibrium as the injection goes on. The negative WHP could be interpreted as that the volume of the wellbore increased, and the liquid just flows inside a large volume with high permeability (see Figure 2.14). Considering Figure 3.5, by increasing the size of the element the pressure continuously decreases to the saturation pressure and if the volume of the element is large enough the transition to single liquid phase would not happen and the pressure would decrease to the constant saturation pressure at the dominant temperature (see Figure 2.14, the red line). Thus, the equilibrium in pressure would be reached as it was observed in Figure 2.12. As the injection stops the steam starts to flow towards the wellbore and the temperature goes up consequently the saturation pressure would go up (Figure 3.4), and the pressure starts to build up (See Figure 2.12 as the injection rate equals zero, the WHP starts to build up).

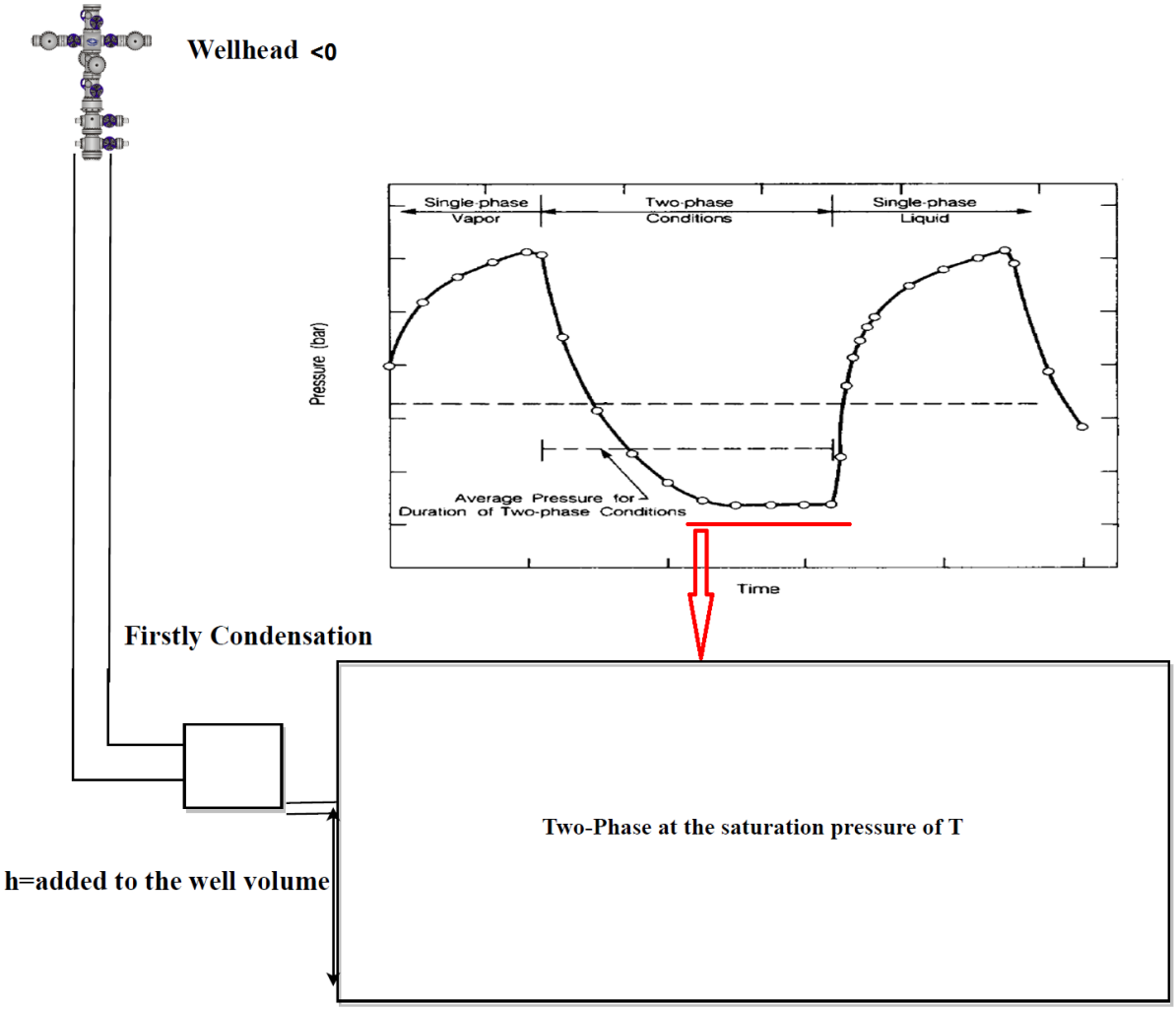

Figure 2.14 The simplified schematic of the injection at a vapor dominated reservoir when the WHP < 0. (See also, Figure 3.5).

One could conclude that the reservoir boundary has not been met yet by the injected fluid at PPL−01B, or the fluid is going out of the system (flowing to the ground by intersected high permeable fault, see Figure 2.6). Moreover, no evidence of pressure support has been reported.

2.4.4. Data Analysis of PPL-06

PPL−06 has been drilled on December 6 1997 (table 2.3 and 2.1), and the wellbore experienced a production test in 2016 (Figure 2.15). Figure 2. 15 (A), shows the production rate plotted versus the WHP. As it is shown for the same WHP, say 1 MPa, the production rate at the second stage (June 04− June 24 2016) has decreased. Recalling Darcy's law, $\boldsymbol{Q \propto \Delta P}$, when $\boldsymbol{Q \downarrow \rightarrow \Delta P \downarrow}$, and (as the WHP is constant at say 1 MPa) $\boldsymbol{\Delta P = P_{Reservoir} \downarrow - WHP}$. Therefore, the reservoir pressure is decreasing (this is also shown at Figure 2. 14 B where for the same WHP, the production rate decreased). This could also be seen in Figure 5.10, where the shut−in pressure has decreased over the years from 1998 to 2018 by the order of 110

Psi (~0.76 MPa). Moreover, the recorded-produced-enthalpy suggests that the steam which has been formed from the stored water inside the reservoir is traveling a relatively long passage to reach the wellbore, thus the steam will heat up more and become superheated (section 2.4.3). In fact, since the maximum produced enthalpy of the vapor-dominated reservoir could be 2800 kJ/kg (table 1.1), while the produced enthalpy of PPL-6 is much higher than the maximum expected value (referring to Figure 2.15 C). Thus, one could confirm that PPL-06 is producing superheated fluid. Consequently, the in-situ fluid near PPL-06 is not sufficient (see section 2.5).

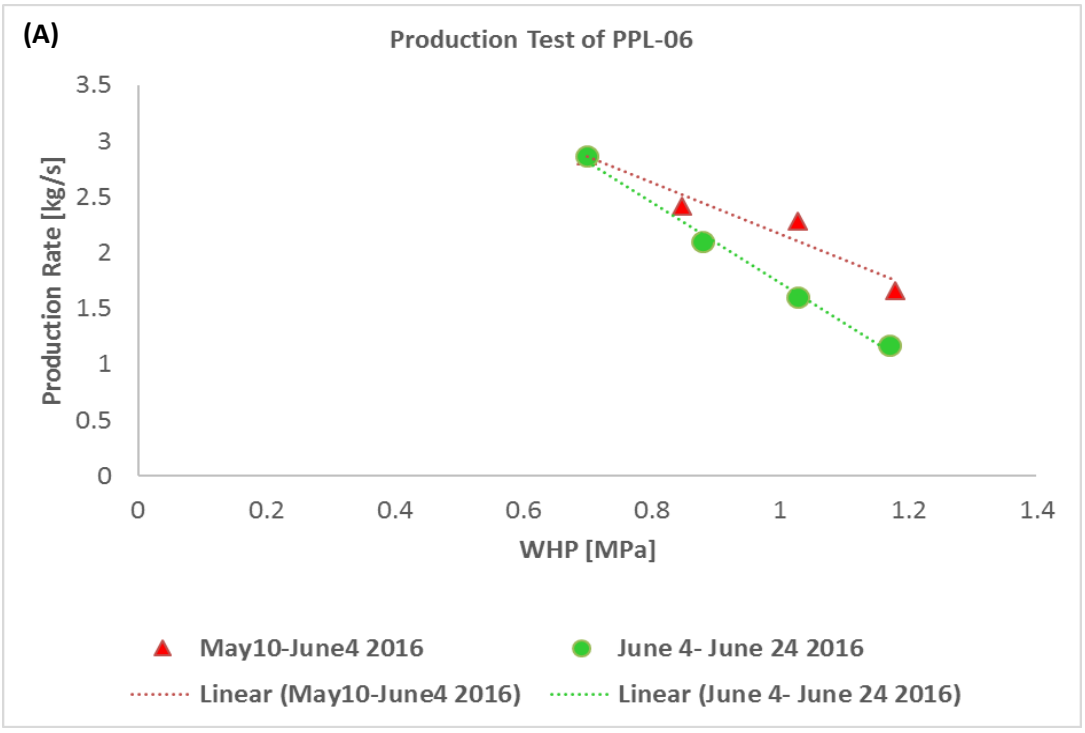

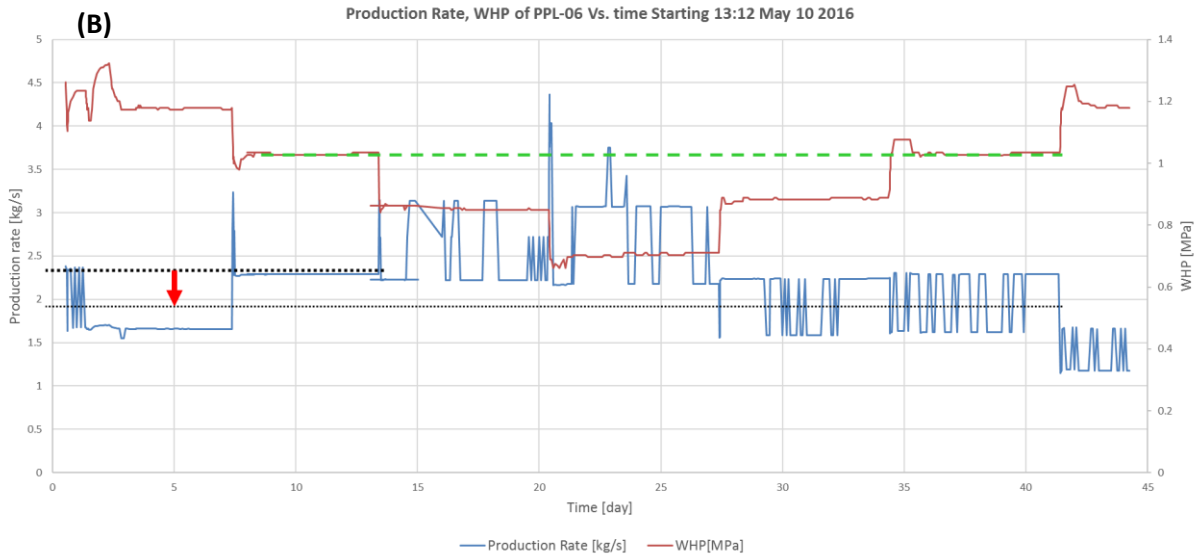

(C)

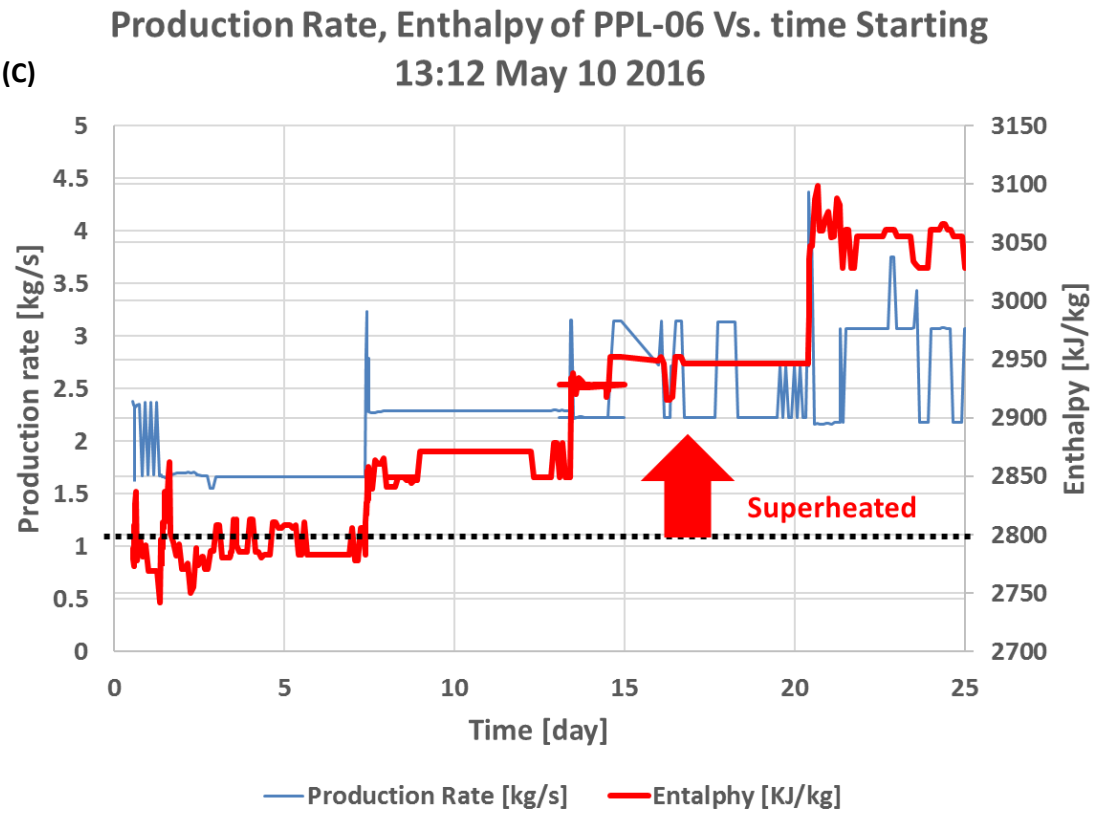

Figure 2.15 The production test of PPL-06 conducted on May 10- June 4 as the first stage, and June 4-June 24 2016 as the second stage. A) Shows the Production rate versus the corresponding WHP. B) It is a full representation of the test plotting the production and the WHP versus the operation time. C) represents the first stage of the production test at which the production rate and the produced enthalpy has been plotted versus operation time (the dotted line is the maximum produced enthalpy for vapor-dominated reservoirs table. 1.1).

2.5. Production Problem Diagnosis

The aforementioned analyses of PPL-01A and PPL-01B show that the permeability of the reservoir might not be the problem of the poor production that could be solved by any permeability enhancement techniques (e.g. hydraulic stimulation), since the wellbores are accepting large amount of fluid without any resistance (i.e. pressure buildup). Therefore, the key reason for the production decline is not the permeability. By reviewing and analyzing the field data, together with the general characteristics of the vapor-dominated reservoirs, as well as reviewing the production behavior of the known-system with the generic similarities with the Patuha field the main problem of the poor production was diagnosed. In fact as it was mentioned in section 1.4.6, by their very nature, vapor-dominated systems have low permeability in the reservoir zone and very low permeability surrounding the reservoir. As the pressure drops to produce the steam, more and more of the water reserves boils to form the steam which then flows towards the production wells. Thus, the water in a vapor-dominated reservoir is not replenished by the natural recharge and, after some years of production, parts of the reservoir may run out of such a water reserve and become superheated. Superheated steam and the reservoir pressure decline has been observed at PPL-06 (section 2.4.4). Figure 2.16 A and B demonstrates the production decline at Larderello and the Patuha vapor-dominated fields, respectively. There are many reports in the literature which prove that in response to extensive steam production, the vapor-dominated geothermal reservoirs at The Geysers (K. P. Goyal, 1999; Khan & Truschel, 2010), U.S.A, Larderello (Arias et al., 2010; Cappetti & Ceppatelli, 2005; Cappetti, Parisi, Ridolfi, & Stefani, 1995; Cappetti & Stefani, 1994), Italy, Kamojang (Tavip Dwikorianto, Zuhro, & Yani, 2010; Saptadji, Artika, & No, 2012), and Darajat (Mahagyo, Molling, & Hidayaturrobi, 2010), Indonesia are beginning to run out of fluid, while heat reserves in place are still enormous (see for example Figure 2.15 C).

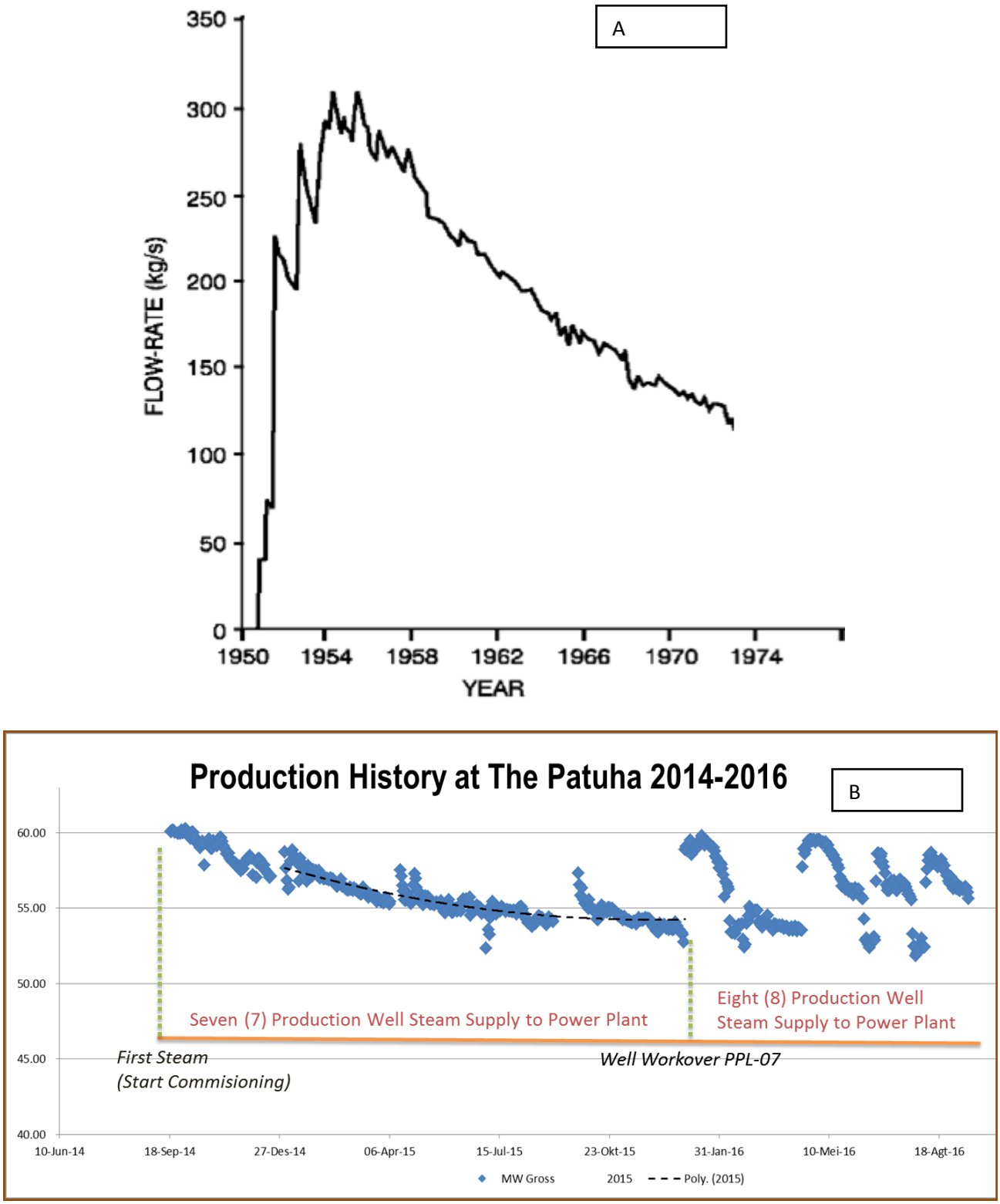

Figure 2.16 The production decline rate at A) Larderello 1950-1974, modified after Cappetti et al. (1995), and B) the Patuha 2014-2016 (Geo Dipa Energi 2017).

Chapter 3. Numerical Simulation of Cold water injection into Super-heated vapor reservoir

3.1. Background and Theory (TOUGH2)

TOUGH2 simulator (Pruess, Oldenburg, & Moridis, 2011) is a fully implicit finite difference code developed to analyze the heat and mass transfer of multicomponent, multiphase fluids in porous and fractured media. Since it was first released to public by Lawrence Berkeley National Laboratory in USA in 1991, TOUGH2 has been applied in different engineering disciplines including geothermal reservoir engineering, nuclear waste disposal, environmental assessment and remediation, and hydrology in saturated and unsaturated media. TOUGH2 provides "EOS" (equation-of-state) modules that contain different fluid properties including water, air, CO_2, brine, salt and hydrogen. Users can select modules for their own needs and purposes.

According to the manual of TOUGH2, TOUGH2 solves mass and energy balance equations written in the following form:

$$\frac{d}{dx}\int_{V_n} M^{\kappa} dV_n = \int_{\Gamma_n} F^{\kappa} \cdot n d\Gamma_n + \int_{V_n} q^{\kappa} dV_n \tag{3.1}$$

The integration is over an arbitrary subdomain V_n of the flow system, which is bounded by the closed-surface Γ_n. The quantity M denotes mass or energy per volume where κ=1 to NK labels the mass components and κ=NK+1 the heat component. F represents mass or heat flux, and q represents sinks and sources. n is a normal vector on surface element inward into V_n.

The general form of the mass accumulation term is

$$M^{\kappa} = \phi \sum_{\beta} S_{\beta} \rho_{\beta} X_{\beta}^{\kappa} \tag{3.2}$$

The total mass of component κ is obtained by summing over the fluid phases β. ϕ denotes porosity, S_β is the saturation of phase β, ρ_β is the density of phase β, and X_β^κ is the mass fraction of component κ in phase β. The heat accumulation term is written as

$$M^{NK+1} = (1-\phi)\rho_R C_R T + \phi \sum_{\rho} S_{\beta} \rho_{\beta} u_{\beta} \tag{3.3}$$

where σ_R and C_R are grain density and specific heat of the rock, respectively, T is temperature, and u_β is specific internal energy in phase β.

Advective mass flux is a summation over phases as below:

$$F^{\kappa}|_{advective} = \sum_{\beta} X_{\beta}^{\kappa} F_{\beta} \tag{3.4}$$

Individual phase fluxes are written in a multiphase version of Darcy's law:

$$F_\beta = \rho_\beta u_\beta = -k\frac{k_{r\beta}\rho_\beta}{\mu_\beta}(\nabla P_\beta - \rho_\beta g) \quad (3.5)$$

where u_β is the Darcy velocity (volume flux) in phase β, k is absolute permeability, $k_{r\beta}$ is the relative permeability to phase β, μ_β is viscosity, and P_β is the fluid pressure in phase β. Heat flux is composed of conductive and convective components,

$$F^{NK+1} = -\lambda\nabla T + \sum_\beta h_\beta F_\beta \quad (3.6)$$

where λ is thermal conductivity, and h_β is specific enthalpy in phase β. Mass transport by diffusion and hydrodynamic dispersion is written as

$$F^\kappa|_{dispersion} = -\sum_\beta \rho_\beta \bar{D}_\beta^\kappa \nabla X_\beta^\kappa \quad (3.7)$$

where $\overline{\boldsymbol{D}}_\beta^\kappa$ is hydrodynamic dispersion tensor.

The integral finite difference method is used in TOUGH2. Space is discretized using appropriate volume averages for volume integrals and a discrete sum over surface segments for surface integrals. Time is discretized as a first−order finite difference. More detailed process for the integral finite difference could be found in the TOUGH2 user's guide (Pruess et al. 2011).

3.2 Hydro-thermal behavior

3.2.1 Modeling approach

Generally speaking, two modeling approaches could be applied to simulate the fractured geothermal reservoirs which are the explicit fracture approach and the effective continuum approach. Modeling fractures explicitly is ideal, this approach, however, requires to add geometric details. An equivalent continuum approach could be applied to estimate the mass and heat transfer in the equivalent fractured medium. Although the continuum approach is easy to deal with, it entails a significant simplification. The continuum approach could be justified when fracture spacing is small enough to allow the thermodynamic equilibrium condition between fractures and matrix. Pruess (1990) stated that the fracture spacing must be less than 2−3 m for thermodynamic equilibrium within a few months. According to a calculation carried out by Armstead and Tester (1986), 26 m is the maximum fracture spacing to apply continuum approach for 20 years of operation in a typical granite reservoir.

Although there are cases (e.g. the East Mesa reservoir, California) in which the fluid flows of the hydrothermal systems occur primarily within a porous (M. A. Grant, Donaldson, I.G., and Bixley, P.F., 1982), most of the hydrothermal systems (e.g. Kawah Kamojang in Indonesia (Wohletz & Heiken, 1992), The Geysers in California, Larderello in Italy, Ahuachapan in El Salvador and Kawerau in New Zealand (M. A. Grant, Donaldson, I.G., and Bixley, P.F., 1982)) are believed to exist in a dynamic state in which fluid circulates within fractured porous rock (Cathles, 1977; Donaldson, 1962; Dunn & Hardee, 1981; M. A. Grant, Donaldson, I.G., and Bixley, P.F., 1982;

Hurst & Dibble, 1981; Parmentier & Schedl, 1981; Wohletz & Heiken, 1992). In the development of a model of such flows, in order to describe the macroscopic flows on the scale of a reservoir, it is essential characterize the microscopic flows through the fractures and pores. The relative resistance to flow through fractures and pores is dependent upon the apertures and spacing of the fractures, and the permeability of the porous matrix. Effects of the fractures on the fluid flow within the reservoir zones are often analyzed and inferred from detailed measurements of pressure and temperature within the wells used for the extraction or injection of fluid (Fradkin, Sorey & McNabb 1981; Goyal & Box 1990; Axelsson & Bodvarsson 1987).

In this work, we adopt a porous flow model to describe the transport of liquid and vapor in a fractured geothermal reservoir. This justified continuum approach provides insight into the flows within highly fractured reservoirs. Therefore, in the current study, I presumed a 2.5 m thickness for the fault system of the fracture zone as continuum porous medium for the simulation of injection into PPL-06. It should be noted that this approach is valid under the assumption that the fracture zone is fractured densely enough to meet the thermodynamic equilibrium condition. Also, there is a possibility that the heat extraction in the early days could be overestimated in the modeling.

Matrix permeability of the unfractured rocks at vapor-dominated reservoirs such as The Geysers and Larderello geothermal fields are reported to be typically of the order of 10^{-18} m^2 (1 microdarcy) or lower. This is considered very small in comparison to the typical permeabilities of the fracture plane which are tens or hundreds of darcies (10^{-11} – 10^{-9} m^2). Thus, rock matrix permeability will have negligible impact on the injection plume behavior over shorter time periods (days), however, vapor adsorption and water imbibition into the rock matrix should be considered since it will affect the injection plume in long-term injection. The current study deals with flow of water injection of relatively short time periods (days); accordingly, matrix permeability is neglected (Hornbrook, 1994; Maria, 1996; Pruess, 1996).

3.2.2 Verifications

Yoo (2018) conducted a verification study to analyze the hydro-thermal responses in TOUGH2 by comparing with a two-dimensional analytic solution for a rectilinear fracture model (Gringarten, Witherspoon, & Ohnishi, 1975). A constant injection rate at one end of a rectilinear 2-D planar fracture model was applied. The transient temperatures were measured at some distances from the injection point along the fracture for a year. The simulation results are in good agreement with the analytical solution as shown in Figure 3.1.

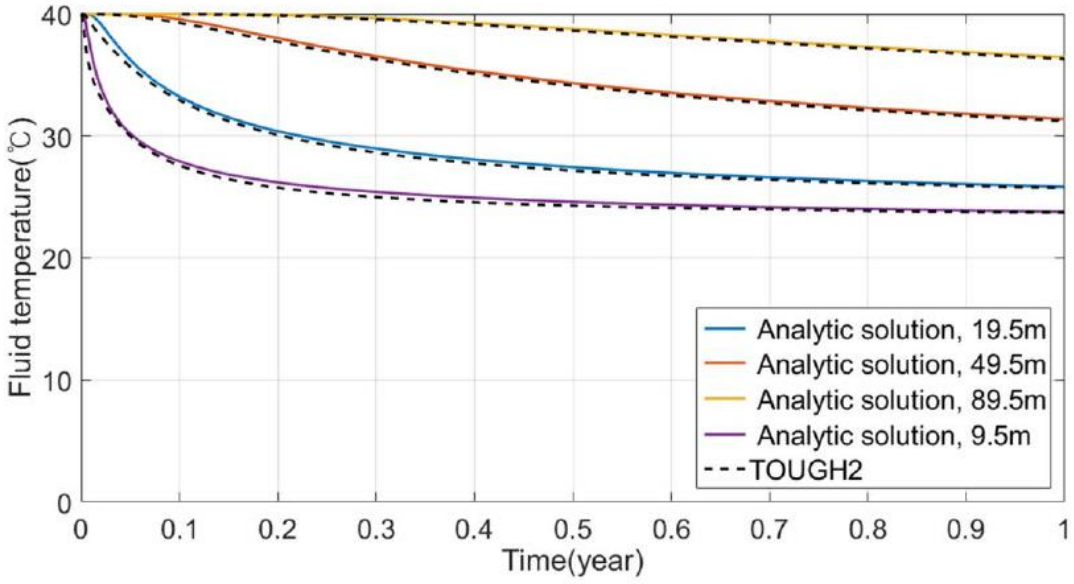

Figure 3.1 Verification of heat transfer in TOUGH2 in comparison with an analytic solution by Gringarten et al. (1975), from Yoo (2018).

3.3 Analysis of Liquid and Vapor Flow in Superheated Porous media

Coupled processes of heat and multi-phase mass transfer in porous media is encountered in injection of cold water into super-heated reservoirs (Figure 3.2). These coupled processes arising from the cold water injection into a super-heated vapor-dominated reservoir are highly nonlinear and can often be quantitatively described only by means of computer simulation. Since these coupled process arising from reinjection into super-heated vapor-dominated reservoirs are complex, it is helpful to describe the thermal condition arising from water injection into single-phase liquid hot permeable rocks.

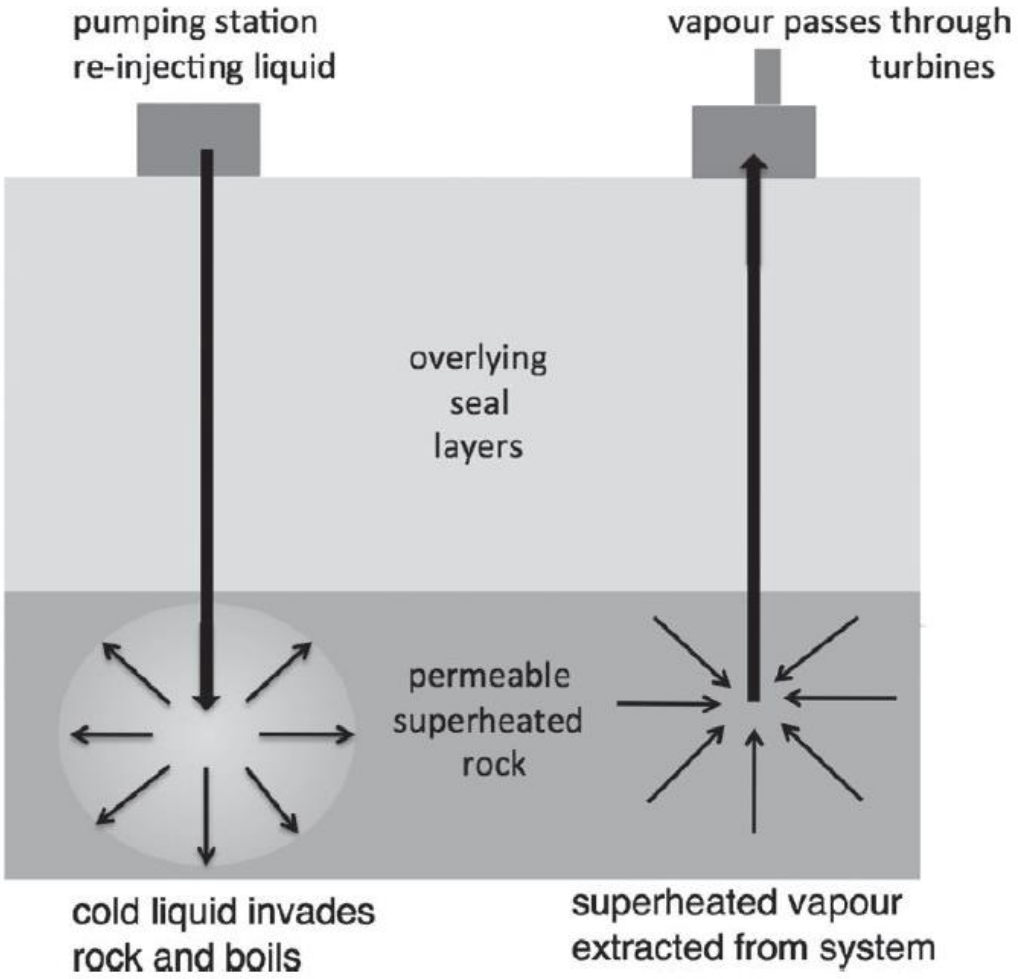

Figure 3. 2 Schematic of the injection of water and extraction of vapor from a geothermal power System (Woods, 2014).

3.3.1 Injection of cold water into hot single-phase-liquid zone

The thermal conditions arising when cold water is injected into a porous medium containing hot single−phase−water are easy to be understood. A cold front with the temperature equal to the injection temperature will advance from the injection point. Due to heat conduction effects, it is expected that the transition from injection temperature to the original reservoir temperature will occur over a finite distance in the direction of the flow; however, in the porous media since the rock−fluid heat transfer occurs over small spatial scales (e.g. grain sizes) with rapid thermal equilibration, the injection front would be sharp. Since thermal fronts (thermal diffusion, thermal diffusivity is in the order of $10^{-6} \sim 10^{-7} \frac{m^2}{s}$) typically travel more slowly than the hydrodynamic fronts (pore pressure diffusion, hydrodynamic diffusivity is in the order of $10^{-1} \sim 10^{-3} \frac{m^2}{s}$), a spatial separation of the leading edge of the injected fluid and the cold thermal front associated with the injected fluid is expected (K. Pruess, C. Calore, R. Celati, & Y. S. Wu, 1987; Schroeder, O'sullivan, Pruess, Celati, & Ruffilli, 1982).

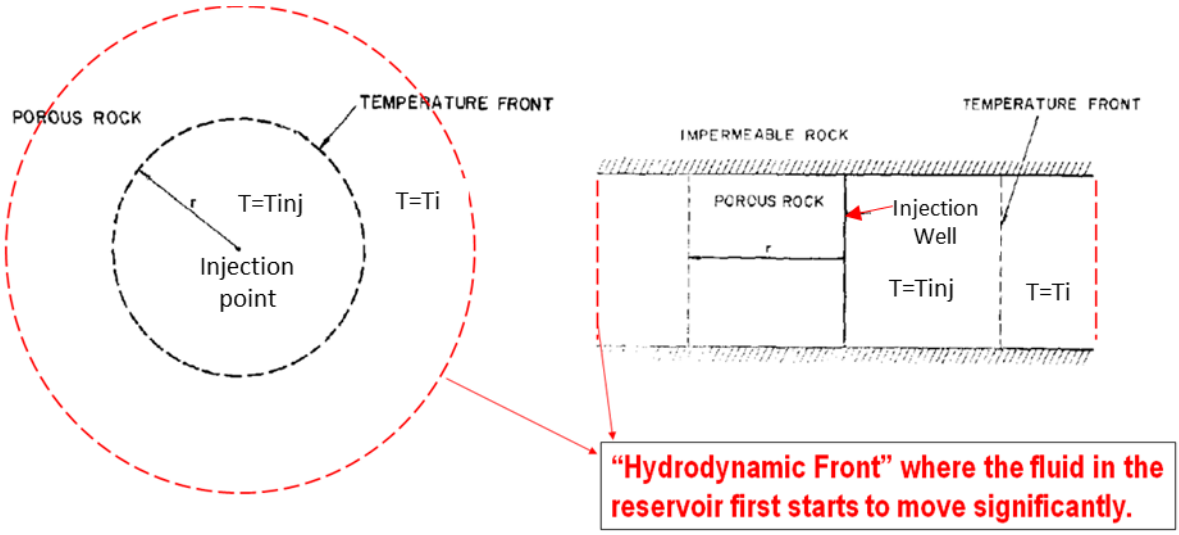

Figure 3. 3. Shows the schematic of thermal front in liquid reservoir (inj=injection, i=initial), modified after G. Bodvarsson (1972).

In a nutshell the injection of cold water into a single−liquid−phase hot porous rock will result in the propagation of two fronts, whose viscosities, temperatures, and pressures are different, while they are both at single−liquid−phase state (see Figure 3.3). The thermally swept volume to the hydrodynamically swept volume could be written as (K. Pruess et al., 1987):

$$\omega = \frac{Cold\_Swept\_Volume}{Totall\_Swept\_Volume} = \frac{\phi C_{l,i}\rho_{l,i}}{(1-\phi)\rho_R C_R + \phi C_{l,i}\rho_{l,i}} \quad (3.8)$$

Where, ϕ is the porosity, ρ is the density, and C is the specific heat capacity (subscripts: i, l, R refer to initial reservoir pressure and temperature, liquid, and rock respectively).

3.3.2 Cold water injection into super-heated vapor-dominated zone

As it was stated before, conditions arising from cold water injection into a porous medium containing superheated vapor are considerably more complex (Figure 3.4). The injection of the cold liquid and heat transfer from the reservoir lead to boiling of the liquid and production of vapor.

Many researchers studied the thermal condition arising from cold water injection into super-heated depleted reservoir, analytically, and numerically (Calore, Pruess, & Celati, 1986; Fitzgerald & Woods, 1995; Kaya, 2016a; O'Sullivan & Pruess, 1980; Pruess, 1995; Pruess, 1996; Pruess & Enedy, 1993; K Pruess & TN Narasimhan, 1982; Pruess & Truesdell, 1980; Schroeder et al., 1982; Tsypkin, Calore, & Marcolini, 2006). To make a summary of these studies conducted on cold water injection into superheated vapor reservoirs, following the injection of cold water into the reservoir, firstly there would be a hydrodynamic front at which pressure is higher than the reservoir pressure and the in-situ reservoir fluid starts to move significantly. This front is the first front traveling away from the injection well. Such an increase in the pressure occurring in the hydrodynamic front could be explained simply as the injection of cold water in the reservoir starts, part of the water would evaporate and heated up to the reservoir temperature, it pushes the in-situ steam; the in-situ steam would be compressed and the pressure goes up. The hydrodynamic front is generated and propagated at a temperature equal to the reservoir temperature.

After the generation of the hydrodynamic front the boiling front will starts propagating away from the wellbore. The pressure and the temperature at the boiling front are in saturation condition, following the Clausius–Clapeyron boiling curve (Figure 3.5). In fact, there is a one-to-one corresponding relationship between saturation pressure and saturation temperature, if saturation pressure goes up, the saturation temperature goes up as well. In order to estimate the fraction of the vaporized injected-water which is leaving the boiling front, it is necessary to find the pressure at the boiling front. Part of the solution to this problem is to the boiling temperature at the front. Preuss et al.(1987)proposed an analytical solution to determine the thermodynamic conditions at the boiling front moving through a porous medium. This analytical solution has been used to verify the numerical model developed in this study to analyze the cold water injection into super-heated vapor-dominated reservoir. The pressure that drives the vapor away from the boiling front could be calculated by equation 3.9:

$$p_{bf}^2 = p_i^2 - \frac{ZRT_i\mu_v q_{vbf}}{2\pi kHm}\exp(\frac{r_{bf}^2}{4\alpha t})E_i(\frac{-r_{bf}^2}{4\alpha t}) \quad (3.9)$$

Where, p_{bf} , p_i , and T_i are the pressure at the boiling front, and the initial reservoir pressure and temperature, respectively. Z , R , k, m, H, t, and r_{bf} are real gas compressibility factor, universal gas constant, absolute permeability, molecular weight of water, formation thickness, time since the injection has started, and radial distance of the boiling front from the injection well, respectively. q_{vbf} is the mass flux of the vapor leaving the boiling front. α is the diffusivity parameter defined as equation 3.10.

$$\alpha = \frac{\bar{p}k}{\phi\mu_v(\bar{p},T_i)} \quad (3.10)$$

Where $\bar{p} = (p_{bf} + p_i)/2$, and vapor dynamic viscosity is a function of the average pressure ($\bar{p}$) and reservoir initial temperature $\mu_v(\bar{p},T_i)$. Considering the fact that the temperature and pressure at the boiling front must be related by the saturated vapor pressure relationship (i.e. $p_{bf} = p_{sat}(T_{bf})$), the temperature at the boiling front could be calculated by equation 3.11:

$$p_{bf} = p_{sat}(T_{bf}) = p_{sat}(T_i - \frac{h_{vbf}\phi\bar{\rho}_l}{(1-\phi)\rho_R C_R(q_l/q_{vbf} - 1)}) \quad (3.11)$$

Where q_l is the injection rate, h_{vbf} is the specific enthalpy of the vapor as a function of initial reservoir temperature and p_{bf} , and average liquid density ($\bar{\rho}_l$) is calculated by equation 3.12.

$$\bar{\rho}_l = \omega\rho_l(T_{inj}) + (1-\omega)\rho_l(T_{bf}) \quad (3.12)$$

Equation 3.11 is valid under the assumptions of steady flow throughout the liquid region (behind the boiling front, which is an excellent approximation because of the small compressibility of the liquid water), neglecting the small difference between enthalpy and internal energy for the liquid phase, and the vapor leaves the boiling front at the original reservoir temperature.

Equation 3.9 and 3.11 are two non-linear coupled equations to estimate the unknowns p_{bf} (equivalently, T_{bf}), and q_{vbf} at the boiling front. These equations can be solved by Newton-Raphson iteration. Note that α , $\bar{\rho}_l$, and h_{vbf} appearing in these equations are a function of front pressure (p_{bf}) or temperature (T_{bf}). By writing a computer program (e.g. in MATLAB) which performs an "inner" iteration on equation 3.11. nested within an "outer" iteration on equation 3.9, once could solve these two equations. However, this program should entails all the saturated-vapor-pressure

relationship as well as all other thermophysical properties of water and steam given in the steam table equations published by the International Formulation Committee (Committee, 1967).

The iteration procedure (solution) starts by picking an initial guess ($n^{(0)}$) for the boiling fraction $n = q_{vbf} / q_l$, by fixing this value and taking $T_{bf}^{(0)} = T_i$ at equation 3.11, $T_{bf}^{(1)}$ and equivalently $p_{bf}^{(1)}$. Obtaining this two new values of the pressure and temperature at the boiling front ($T_{bf}^{(1)}$, $p_{bf}^{(1)}$) for $n^{(0)}$, a second solution for equation 3.11 is generated for $n^{(0)} + \delta n^{(0)}$, where $\delta n^{(0)}$ is a small increment in the order of say $\delta n^{(0)} = 10^{-10}.n^{(0)}$. This is required for numerically computation derivatives in the subsequent Newton–Raphson process on equation 3.9, which generates $n^{(1)} = n^{(0)} + \Delta n^{(1)}$. Consequently, another inner iteration on equation 3.11 obtains the new values of $T_{bf}^{(2)}$, $p_{bf}^{(2)}$, for $n^{(1)}$. This iteration process will be continued until the residuals of equations 3.9 and 3.11 (the difference between right– and left–hand sides) are reduced to a small fraction (10^{-10}) of the left–hand sides.

Generally speaking, at a higher injection rate, the pressure at the boiling front will increase; such an increase of the pressure will result in an increase in the saturation temperature at the boiling front, thus the amount of the heat (transferred from rock to the boiling front due to the temperature differences, i.e. $\Delta T = T_{reservoir} - T_{saturation}$ to be extracted by the boiling front) will decrease and consequently less fluid would be evaporated. The saturation pressure is higher than the reservoir pressure, otherwise no driving force for the generated steam to leave the boiling front.

Finally, as it was explained due to low thermal diffusivity of the rock the thermal front would travel away from the well much slower in compare with other fronts would. At this front the temperature is same as the injection temperature and the pressure is the highest as it drives the fluid inside the boiling front.

The fluid beyond the thermal front and behind the boiling front has higher pressure than the boiling front and lower pressure than the thermal front. It also has equal, or lower temperature than the boiling front and higher temperature than the thermal front. Therefore, the fluid must be liquid (since the pressure behind the boiling front is higher than the saturation pressure at the boiling front temperature, therefore reminding the fact that the maximum possible temperature for the fluid behind the front could be equal to the boiling front temperature, the fluid behind the boiling front must be liquid).

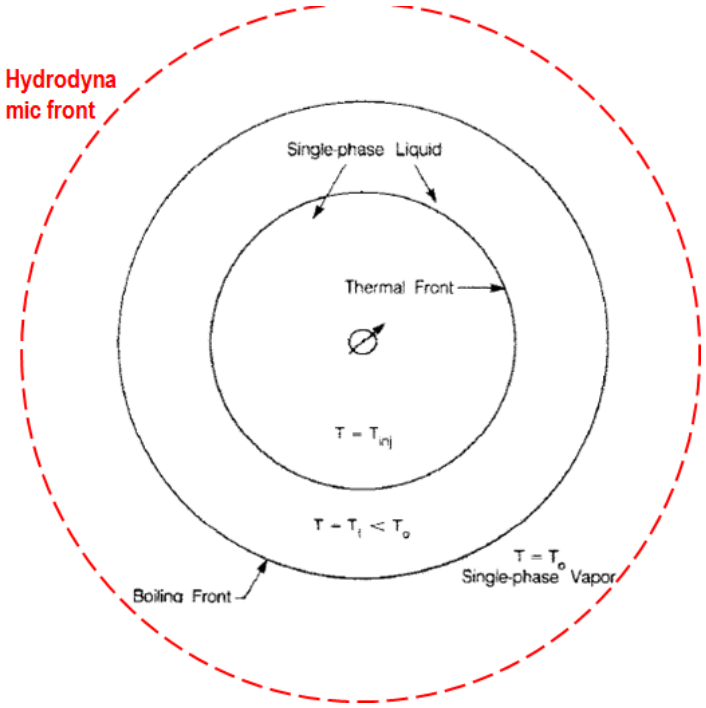

Figure 3.4 Schematic diagram of fronts for cold water injection into a superheated vapor zone modified after K. Pruess, C. Calore, R. Celati, and Y. Wu (1987).

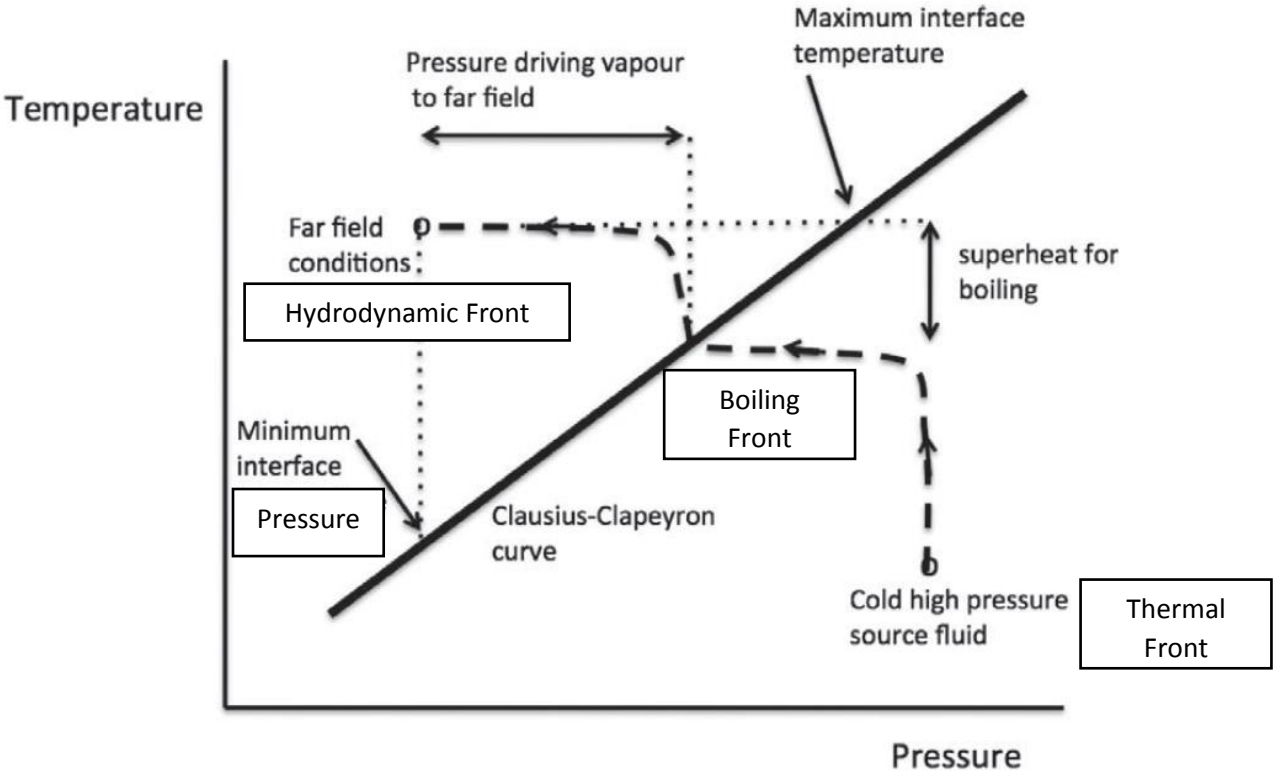

Figure 3. 5 Schematic diagram of the Clausius–Clapeyron boiling curve, illustrating the path (dashed-line) of the injected liquid in P−T space, as it is heated, boils and then adjusts to the far-field superheated steam conditions (arising from cold water injection into super-heated porous rock). Modified after Woods (2014).

3.3.3. Numerical simulation of cold water injection into super-heated vapor reservoir

Verification studies of the hydrothermal behavior of two−phase fluid flow in super−heated reservoir has been conducted by many researchers (Cappetti et al., 1995; O'Sullivan & Pruess, 1980; K. Pruess et al., 1987; Pruess & Enedy, 1993; Pruess & Truesdell, 1980; Woods, 2014). In this study the model which has been proposed by (K Pruess et al., 1987) to analyze the boiling front propagation in superheated porous rock was rebuilt and further studies for the simulation of injectivity test for vapor−dominated reservoir has been conducted, based on this model. The main reason to use this model was the fact that the model was well−developed to avoid any discretization errors that can particularly be severe in problems with coupled thermal and phase fronts, and space− and time−truncation errors were scrutinized carefully so that acceptable results may be obtained (Calore et al., 1986; K. Pruess et al., 1987). Therefore, the model was employed in the way to minimize the aforementioned errors, and accordingly the results would be reliable. A homogeneous, cylindrical, porous media has been discretized as table 3.1, which is schematically depicted in Figure 3.6.

Table 3.1 Numerical simulation discretization (Calore et al., 1986; K. Pruess et al., 1987).

The grid consists of concentric cylinders about $r = 0$ with height $H = 200\,m$. The radii of the grid block boundaries are	
$r_i = 2i$	$for\ i = 1,2,3 \ldots..50$
$r_{i+1} = fr_i$	$for\ i = 51,52,53 \ldots..100$
$and\ f = 1.1607$	$so\ that\ r_{100} = 25000$

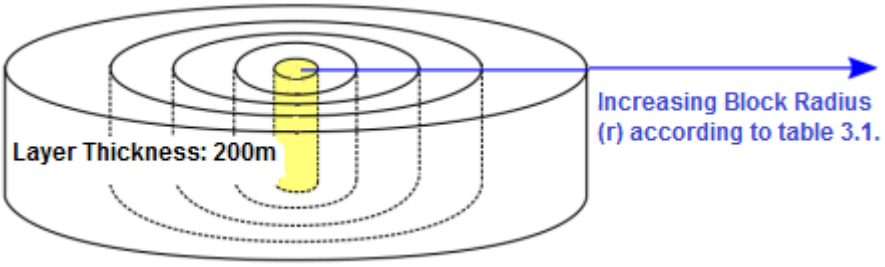

Figure 3.6 Schematic diagram of the geometry of the model used for the injection test. The model was applied by Calore et al. (1986); K. Pruess et al. (1987) to simulate cold water injection into super-heated vapor-dominated low-pressure porous rock. The diagram shows the well block (illustrated in yellow), the thickness thickness of the layer and a representation of the radially increasing grid blocks according to table 3.1. Note: not all the grid blocks are depicted, and diagram is not to scale. Modified after Newman (2018)

The input parameters are the typical values for the upper depleted zones of the Larderello field, table 3.2. However, as it was mentioned in section 3.2.1, in this study the capillary pressure is not being considered.

Table 3.2 The parameter used for the verification and injectivity test design, data from K. Pruess et al. (1987).

Parameter	Value
Permeability	$50 \times 10^{-15} m^2$
Thickness	200 m
Rock grain density	2600 kg m^{-3}
Rock specific heat	920 J kg^{-1} C^{-1}
Reservoir temperature	240℃
Reservoir pressure	6.0 bar
Injection Temperature	29.5℃

A constant injection rate of 2kg/s for a reservoir whose porosity is 8% was applied to the mentioned-built model, to study the boiling front propagation in super-heated porous media. Under this injection condition, with the properties listed in table 3.2, the pressure at the boiling front when it propagates at $r_{bf} \cong 37m$ was estimated to be 9.2 bar (using equation 3.9). The simulated pressure as the boiling front propagates across a grid block is shown in Figure 3.7.

The developed model in this study was able to reproduce the data which was used by Pruess et al., 1987 for the comparison with the analytical solution for the cold water injection at superheated porous medium (equation 3.9 and 3.11).

The relative permeability is a sensitive parameter; therefore, the value similar to the one which was used typically for simulation of cold water injection into super-heated vapor-dominated reservoirs, Corvey's curve 1954 (equation 3.12), has been employed. There was no reported data of residual saturation of steam and water inside the reservoir simulating the boiling front propagation in super-heated reservoir by (K. Pruess et al., 1987). In this study, the residual liquid saturation is considered as 0.3 and the similar parameter for the steam as 0.05, which are the typical values for the simulation of cold water injection in super-heated porous rock. The slightly differences in Figure 3.7 with the simulation model by Pruess et al., might be due to either different residual saturations as the input for Corvey's equations, or the error associated with the old version of simulator used by Pruess et. al in 1987. However, the numerical simulation results and the analytical solution are in the same agreement proposed by them in 1987 (Figure 3.7).

$$\begin{gathered} k_{rl} = \hat{S}^4 \\ k_{rg} = \left(1-\hat{S}\right)^2 (1-\hat{S}^2) \\ where\ \hat{S} = (S_l - S_{lr})/(1 - S_{lr} - S_{gr}) \\ S_{lr}: residual\ liquid\ saturation \\ S_{gr}: residualt\ gas\ saturation \end{gathered} \tag{3.12}$$

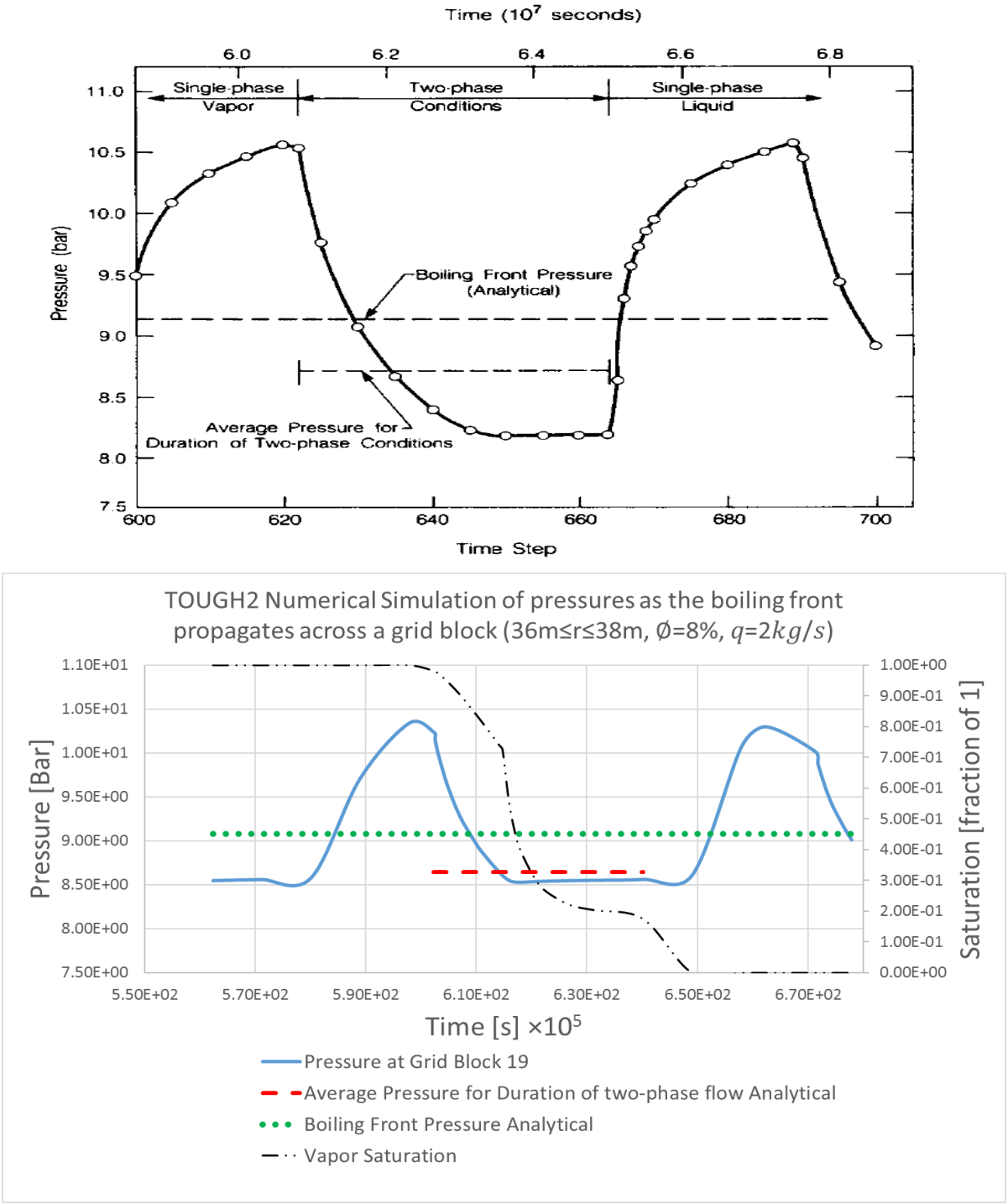

Figure 3.7 Simulated pressures as the boiling front propagates across a grid block (grid block 19 with $36 \leq r \leq 38$ Ø=8%, q=2kg/s), the graph at the top shows the simulation result by MULKOM (K. Pruess et al., 1987), and the graph at the bottom shows the simulation results done by TOUGH2.

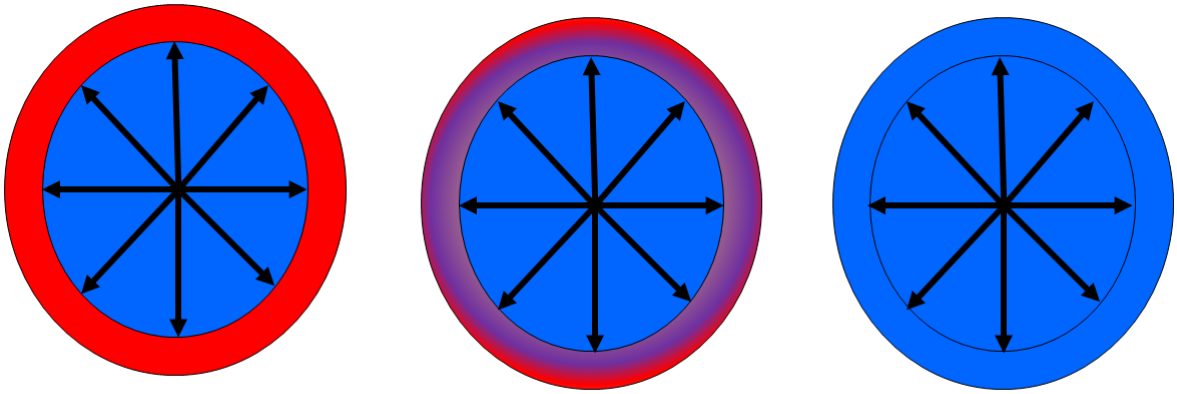

Figure 3.8 schematic diagram showing the boiling front propagation in Figure 3.7.

Before presenting results of the simulations, I wish to discuss how a boiling front is propagating in the finite-difference approximation. Consider a finite subdomain ('grid block') which initially contains single-phase vapor. As liquid water enters the grid block it is vaporized, so that pressure increases while temperature declines (see Figure 3.7, and Figure 3.8). Eventually pressure meets the saturated vapor pressure at the prevailing temperature, at this point the entire grid block makes a transition to two-phase conditions. The liquid flux is continuously entering the grid block, vaporizing in part. The heat of vaporization is being supplied by the porous medium, the temperature of which declines in the process. Pressure must also decline, as in two-phase conditions it is being maintained at the saturation pressure for given temperature. The liquid entering the grid block is vaporized only in part, so that liquid saturation builds up until, eventually, the block makes the final transition to single-phase liquid condition. The process is then repeated at the next downstream grid block.

The model has been used in order to study and analyze the injection water behavior in super-heated vapor dominated reservoir. The front propagation has been observed and analyzed for different porosity values which are possible for a tuff andesite rock Figure 3.10, as the formation rock at the Patuha field is mainly consists of tuff and tuff andesite rock(see figure 3.9, representing the effect of the porosity on the front propagations). The maximum porosity based on the red trend line at the typical depth of Patuha is about 8 %.

As the porosity increase the boiling front saturation temperature and pressure would decrease.

The location of the thermal front and hydrodynamic fronts are affecting by the porosity values in different ways; in the formation with higher porosity the thermal front swept larger area in comparison with the thermal front in rocks with lower

porosity. However, for the hydrodynamic font the effect is more obvious than that on the thermal front, as the porosity increases the hydrodynamic front travel less away from the injection well. This could be also explained by equation 3.8.

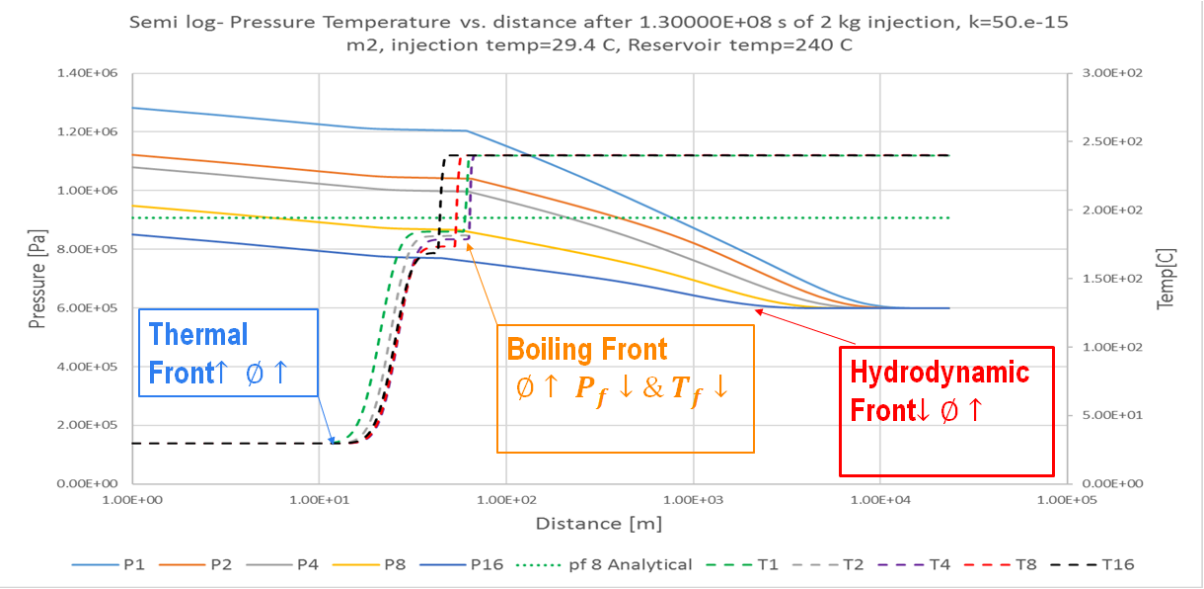

Figure 3.9 The effect of the porosity on the fronts propagation. As the porosity increase the saturation pressure and consequently the saturation temperature increases. The distance of thermal font from the injection point would increase as the porosity increases, contrary the hydrodynamic font distance would decreases at the same condition. The P: Pressure, and T: Temperature, the numbers beside the letter P and T are porosities. This graph follows the equation 3.8.

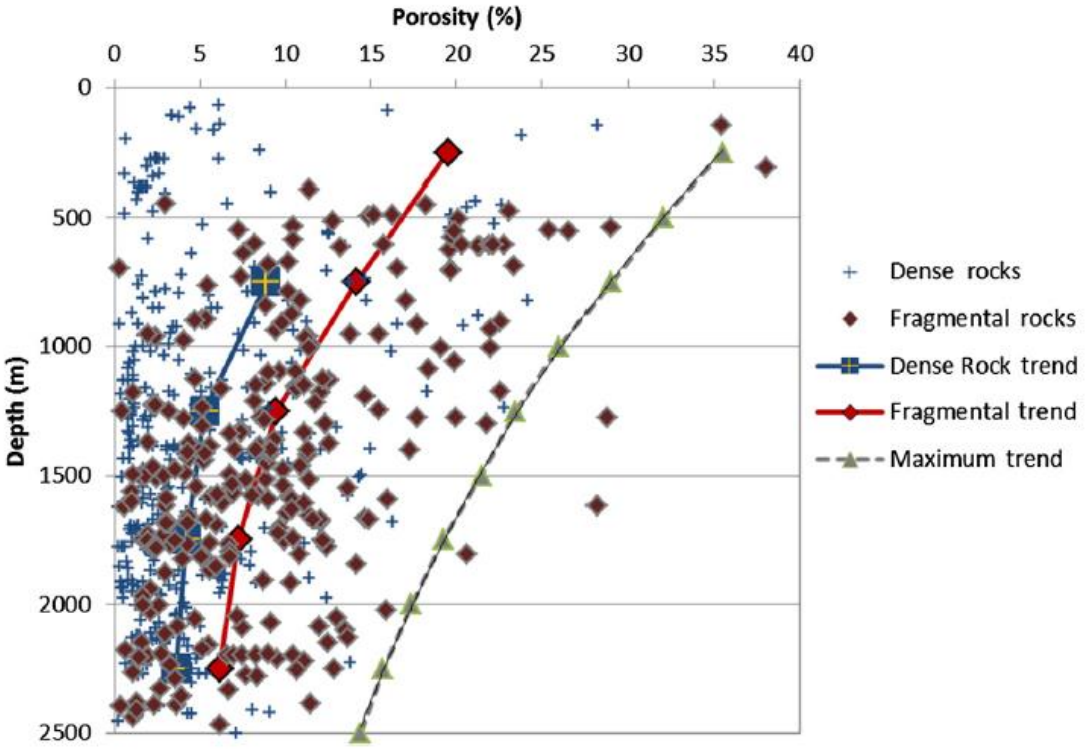

Figure 3.10 Core porosity data from volcanic-hosted geothermal systems versus approximate depth of sample. Rocks are divided into dense (e.g. lava, intrusive) and fragmental (breccia, tuff, volcaniclastic) varieties. The Patuha formation most likely follow the fragmental trend line. The dashed line suggests the maximum porosity that can reasonably be expected as a function of depth (Stimac et al., 2015).

Chapter 4. Injectivity test for Vapor dominated reservoirs

4.1 Injectivity Index

During an injection test, the injectivity index is often used as an estimation of the connectivity of the well to the near borehole reservoir. Injectivity test in vapor−dominated reservoir is a challenging task as the pressure decreases as the injection starts (e.g. see Figure 2.7). Therefore, in this chapter efforts have been put to suggest a method by which the injectvity index could be measured.

In the case of low−temperature production wells by performing a step−rate−test during the fluid extraction a quantified index was defined, termed productivity index (PI). The productivity index could quantitatively describe the production potential of the well and it has been simply defined as the total mass flow rate per unit pressure drawdown. The injectivity index (similar to the productivity index) is a simple relationship, which approximately reflects the capacity of a well, usefully determining whether a well is sufficiently open to be a successful producer, or injector and for comparison with other wells, or monitoring different stage of the well (G. Axelsson, 2013a; Kajugus, 2015). Well testing is a critical component of assessing geothermal resources because it deals with the physical processes occurring inside the well and a portion of the reservoir intersected by the well. A typical well testing in geothermal fields is to perform a step−rate injection test soon after the drilling and completion of the borehole.

During an injection test, the injectivity index, II (see equation 4.1), is often used as an estimation of the connectivity of the well to the surrounding reservoir. In fact, the injectivity index predicts the performance of an injection well and is believed to reflect the success of the well, meaning that the bigger its value, the better the reservoir permeability. It is defined by the ratio of the change of injection flow rate to the change in reservoir pressure measured in the borehole:

$$\frac{\boldsymbol{q}}{\boldsymbol{p_e - p_{wf}}} = \begin{cases} Productivity\ Index,\ PI & if)\ p_e > p_{wf} \\ Injectivity\ Index,\ II & if)\ p_e < p_{wf} \end{cases} \tag{4.1}$$

II: injectivity index [(L/s)/bar],
q: volumetric flow rate (if $q < 0$: injection) [L/s]
p_e: reservoir pressure (at no−flow boundary) [bar]
p_{wf}: bottomhole flowing pressure [bar]

Well injectivity is tested by injectivity test; a method applied to establish the rate and pressure at which fluid can be injected into a well over a prolonged period

(i.e. steady−state conditions are observed) without fracturing the formation. Injectivity test could be performed during a step rate test (see Figure. 4.1(a)). Water is injected into a well at a constant rate until a stable pressure (downhole, or wellhead pressure) is recorded; it is also common to record the temperature during injection, in particular inside the wellbore, which such a data for example the fluid and the flow condition inside the wellbore could be better understood. It is important to achieve a relatively stabilized pressure during the injection at each step in order to obtain an index value which truly represents that of the well and to also be able to calculate the II (using equation 4.1, the change in pressure could be compared with any base pressure, e.g. reservoir pressure, or initial pressure). In fact, the slope (determined by linear regression) of the plot of the stabilized representative pressure data at each flow rate versus the flow rate is termed II (Figure. 4.1 (b)). The injection test usually causes an increase of the pressure in the well, e.g. figure 2. 10 Such a pressure response to the injection has been frequently reported in the literature (G. Axelsson, 2013a; Malcolm A Grant, Clearwater, Quinão, Bixley, & Le Brun, 2013; Kajugus, 2015; Park S et al., 2018; Rutagarama, 2012; Yoshioka, Pasikki, Suryata, & Riedel, 2009).

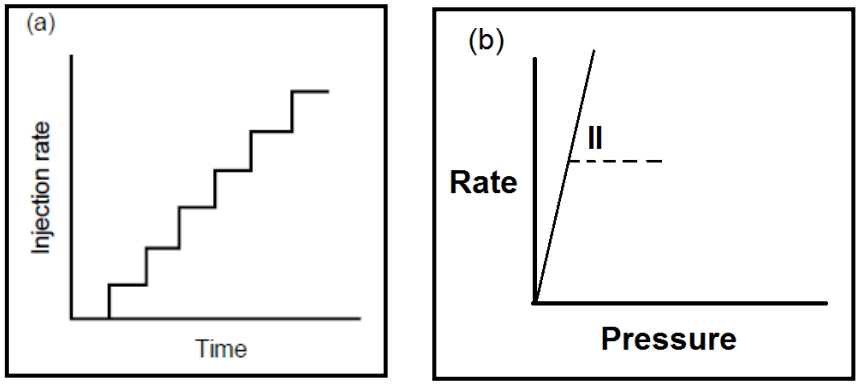

Figure. 4.1 The schematic (a) of the injectivity step-rate test (b) of injection rate vs. changes in pressure equation 4.1

Geothermal wells are often stimulated following drilling, either to recover the permeability reduced by the drilling operation itself, or to enhance the near−well permeability and to open up connections to permeable structures not directly intersected by the well. Moreover, in Enhanced Geothermal Systems (EGS) the main tool to evaluate the result of the stimulation operations is the injectivity index (II); by comparing the injectivity (or productivity) indices estimated before, during and after stimulation operations, one might evaluate, quantify, and estimate not only the success of the operation, but also the most possible mechanism associated with the stimulation. The stimulation operations often result in well injectivity being improved (refer to Appendix B) by a factor of 2−3 (Aqui & Zarrouk, 2011; Malcolm A Grant et al., 2013; Portier, André, & Vuataz, 2007; Paul A Siratovich, Sass, Homuth, & Bjornsson, 2011; Yoshioka et al., 2009).

4.1.1. The relationship between injectivity index and productivity index

The injectivity test can estimate the production characteristics of the well (i.e. production characteristics are deduced from the injectivity index). For most of the wells, however, different values of injectivity and productivity were recorded. Grant (2013) compared injectivity and productivity of wells from different geothermal fields and found that injectivity is on average 3.5 times higher than the productivity (as Grant stated the average varied between geothermal fields but the geometric mean of the ratio of injectivity to productivity is 3.5). Rutagarama (2012) also found that injectivity indices were roughly three times higher than productivity indices by studying data from several wells at the Reykjanes high-temperature geothermal field. Rutagarama (2012) plotted injectivity indices (II) versus productivity indices (PI) of wells from several high temperature geothermal fields worldwide (see Figure 4.2). Two upper and lower limits are represented by two linear relationships between productivity and injectivity (the blue line representing PI = II/3 and the orange line represents PI = II) in Figure 4.2 (the plot showed a great deal of scatter). No attempt was made to identify the reasons accounting for the scatter, as there is insufficient information about the well conditions and the surrounding reservoirs characteristics. Grant and Bixley (2011) suggested that injectivity is usually higher than productivity, where injectivity is either 3 or 5 times higher than productivity (Malcolm A. Grant & Bixley, 2011). However, there are reported cases where the productivity indices are higher than injectivity indices, as would be expected for viscosity effects (Gudni Axelsson, Thórhallsson, & Björnsson, 2006; Garg & Combs, 1997; Malcolm A Grant et al., 2013). All these investigations suggested that one should be careful about using II instead of PI, or vice versa. This is also noteworthy to mention that II neglects transient changes and turbulence pressure drop at high flow-rates as well as the temperature dependent viscosity. Therefore, in order to partly explain such a difference in the magnitude of the injectivity and productivity indices, the effects of the injection temperature has been investigated in the following.

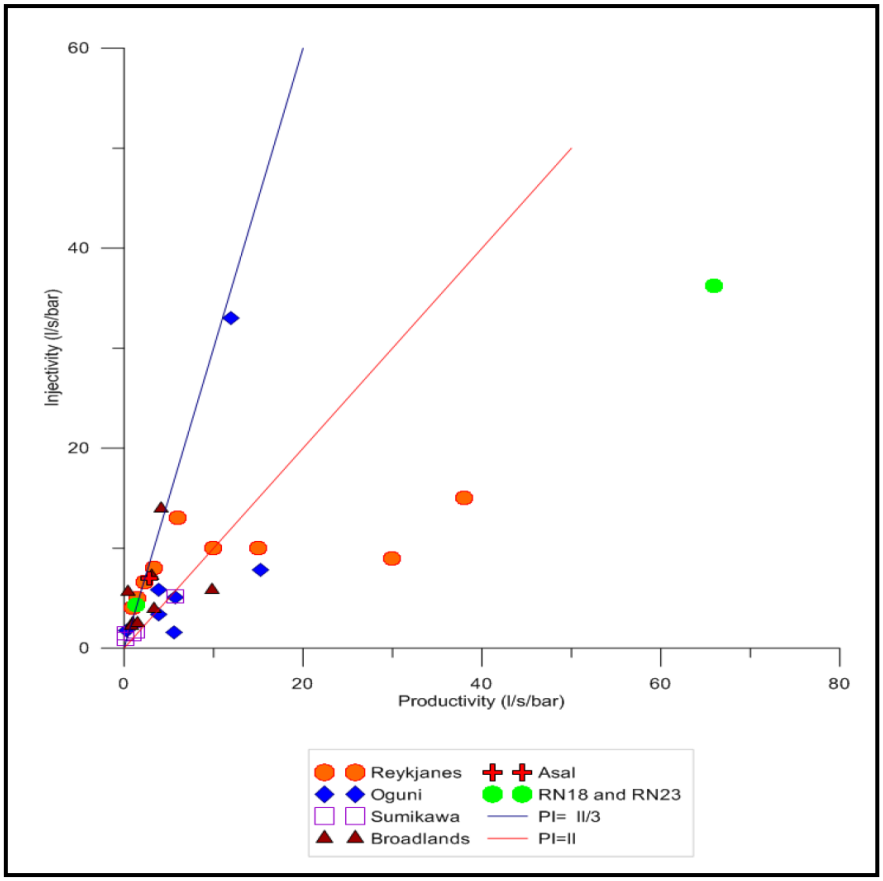

Figure. 4.2 Comparison of productivity and injectivity index for several high temperature geothermal fields worldwide (Rutagarama, 2012).

4.1.2. The effect of the injection temperature on the injectivity index

In fact, injection of cold water into the hot reservoir imposes thermal stresses on the constrained reservoir formation, this affects the stress state near the wellbore (refer to Appendix B equation B.1). Following such a change in the stress state, the injectivity (permeability) might enhance (refer to Appendix B, table B.1). This enhancement of the permeability could be either reversible, or irreversible depending on the dominating mechanism caused by the thermal effects (so-called thermal stimulation).

To understand the temporary and permanent II improvement, the mechanism of thermal stimulation has to be briefly reviewed. The mechanism of the thermal stimulation has been investigated by many authors in the literature analytically and theoretically (Clifton, Brown, & Wang, 1991; Dusseault, 1993; Elsworth, 1989; Ahmad Ghassemi, Nygren, & Cheng, 2008; A. Ghassemi, Tarasovs, & Cheng, 2003, 2005, 2007; Kurashige, Furuzumi, & Kamijo, 1997; Perkins & Gonzalez, 1985; Slevinsky, 2002; Stephens & Voight, 1982), experimentally (Finnie, Cooper, & Berlie, 1979; Geyer & Nemat-Nasser, 1982; Paul A Siratovich et al., 2011), numerically (Bruel, 2002; Chun, 2013; Jansen & Miller, 2017; Kohl, Evansi, Hopkirk, & Rybach, 1995; Tarasovs & Ghassemi, 2011). As a conclusion based on the

literature, the main mechanisms that can improve the permeability, followed by the application of the thermal stimulation or the injection of cold water into the hot reservoir could be categorized as fracture opening (mode−1), fracture shearing (mode−2), micro−cracking (due to Thermo−elastic properties mismatch in grains expansion, see for example (Paul A. Siratovich, Villeneuve, Cole, Kennedy, & Bégué, 2015)). Therefore, if the improvement of II is reversible, one could conclude that the fracture opening (mode−1) has occurred. Needless to say that in the case of irreversible II improvement the other two mechanisms or a combination of them occurred. All in all, the difference between injectivity index and productivity index could be partly explained by the concept of thermal stimulation and the injectivity improvement during the injectivity test.

In order to review, the effect of the injection temperature and its consequent changes in viscosity and permeability, Gunnarsson, et al. (2011) conducted a controlled experiment on three injection wells at the Húsmúli reinjection site of the Hellisheiði geothermal field[13] in Iceland. Three injection tests using different temperatures (120°C, 90°C and 20°C) were performed on three wells, HN−09, HN−12 and HN−16 (i.e. nine tests in total). Natural reservoir temperature at the depth of feed zones in the wells (1755 m to 2220 m) was reported of the order of 260°C. All the tests were performed in the same manner: first, the maximum attainable flow of fluid at the appropriate temperature was injected into the well for a week. After that a temperature and pressure sensor was fixed at the depth of the main feed zones of each well, and the injection rate was decreased in three steps (each step was approximately 3 hours). The injectivity index prevailing at the end of each test was estimated from the step−response for each test (i.e. the slope of the linear fit of plotted flow versus measured pressure of each step).

The order in which the injections at different temperature were performed is not mentioned in the paper. The paper however states that changes in the permeability of the feed zones of the wells occurred during the cold water injection tests. This provides evidence suggesting that the temperature−related permeability enhancement observed in the injection tests is partly reversible (however the degree of reversibility is not clear). If the injection of cold water was firstly conducted, then the permeability change is reversible since it would decline with the following injection test where hotter fluid was injected. Alternatively, if the sequence was from

[13] The Hellisheiði Power Plant was commissioned in 2006. It is located in the southern part of the Hengill Volcanic System. The geothermal reservoir is water dominated and the average enthalpy of the produced fluid is 1750 kJ/kg (see table. 1). The install capacity of the power plant is 303 MW in electricity produced in six high 45 MW pressure units and 33 in low pressure unit, and 133 MW of thermal energy (Gunnarsson & Energy, 2011; Gunnarsson, Kristjánsson, Gunnarsson, & Júlíusson, 2015).

hot fluid injection to cold, then repeated hot−water injection test could show whether the permeability enhancement was reversible or irreversible (i.e. results from a 120°C injection cycle after a 20°C cycle would show whether the permeability declined or not).

Figure 4.3 shows an example of the steps performed at the decreasing trend of the injection test on well HN−16 conducted with 120°C fluid. Figure 4.5 represents the location of the wells and faults of the Húsmúli reinjection zone. For each of the three wells, the injectivity indices derived from the tests performed with the three different fluid temperatures were plotted versus the fluid temperature for the three wells (Figure 4.4). The test results revealed that the II of all three reinjection wells were highly dependent on the temperature of the injected fluid, and increased with colder injection temperature.

As shown in Figure 4.5, all these three wellbores are intersected with the same fault. Let's assume that the injected fluid flows through a simple single fracture (considered as two separated plates). Then the laminar flow along such a fracture can be explained by:

$$q = \frac{d^3 h}{12\,\mu L}\Delta P \qquad (4.2)$$

where d is the width of the fracture, μ is the viscosity of the fluid, L is the length (parallel to the flow) of the fracture, h is the height (perpendicular to the flow), and ΔP is the pressure difference driving the flow.

Viscosity is dependent on temperature. 20°C water has five times higher viscosity than 120°C hot water. Thus, according to Equation 1.2 the injectivity for the 120°C should be five times higher than for the 20°C water. The measured injectivity for 20°C water is, however, 3−8 times higher than for 120°C water (Figure 4.4). Thermal effects working on the feed zones in the wells must explain the increase in injectivity, either through mode−1 opening or shearing of pre−existing fractures in the reservoir. In fact, the reason for this lies in the width of the fractures. The changes in the width of the fractures due to thermal expansion/contraction are big enough to compensate for the viscosity effects and more. A rough estimate reveals that the width of the fractures has to triple from 120°C to 20°C in order to explain the difference in the injectivity for those temperatures. The effects appear to be at least partly reversible. For HN−09, an earlier test where colder water was injected following a period of 120°C water injection was accompanied by an increase in injectivity, although steady−state conditions were not reached to allow the effect to be quantified. Nevertheless, the observation that qualitatively the same behavior is observed in two tests indicates it is partly reversible. Thus, mode−1 opening of fractures is the favored explanation.

Since the changes occurred after only 3 days of injection, the feed zones must be supporting relatively low effective normal stress under ambient conditions, so that they open in response to the cooling effects. However, significant numbers of earthquakes located near the wells were recorded during the injections, indicating that shearing was also occurring somewhere in the reservoir (Gunnarsson & Energy, 2011; Gunnarsson et al., 2015; Witherspoon, Wang, Iwai, & Gale, 1980).

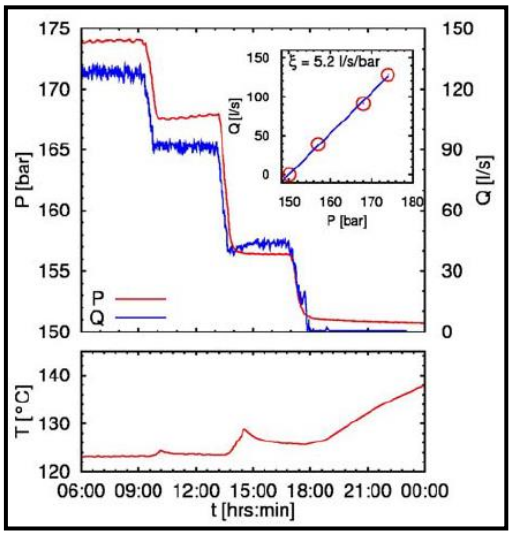

Figure 4.3: Injection test in well HN-16, using 120°C water (Gunnarsson & Energy, 2011). Upper part: pressure and flow versus time of injection, and the inset shows flow vs. pressure in steps, the slope gives the injectivity in (l/s)/bar. Lower part: temperature versus injection time Figure from Gunnarsson and Energy (2011).

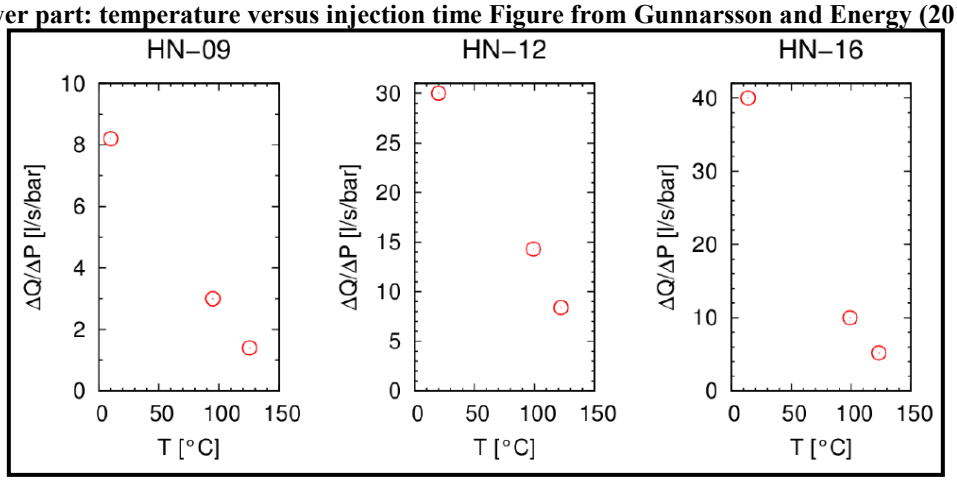

Figure 4.4. Injectivity (attained from injection tests of different fluid injection temperatures) shown for wells HN-09, HN-12 and HN-16 (See Figure. 4.5). Note that the injectivity values for the lowest temperatures in well HN-12 and HN-16 are not very accurate. Figure from Gunnarsson et al. (2015).

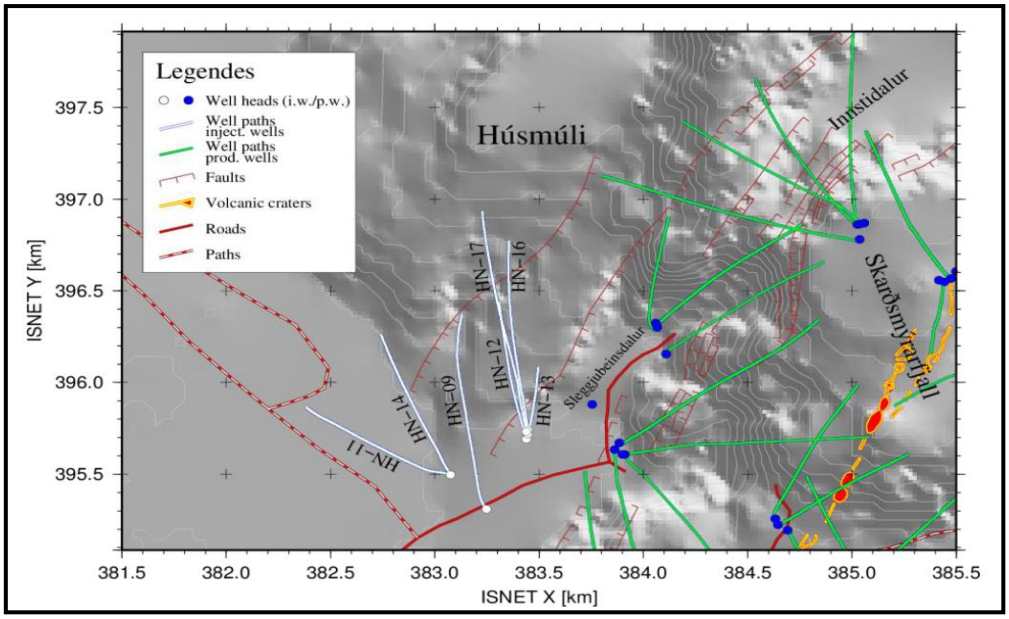

Figure. 4.5 The location of injection, and production wellbores in Húsmúli reinjection zone. NH-09, NH-12, and NH-16 are well-connected with the fault system. (NH-14 & NH-11 have low injectivity and poor connection with the faults). Figure from Gunnarsson et al. (2015).

4.2 Injectivity Test in Vapor Dominated Reservoirs

One of the first challenges in this study which had to be dealt with was the injectivity test for vapor-dominated reservoir in order to be able to measure the injectivity of the wellbores and quantify any possible improvement. The injectivity test for a vapor-dominated reservoir is much more complicated than a typical geothermal field. As the data are complicated by various factors (wellbore effects, non-isothermal effects, two-phase flow, and fractured rocks) the applicability of conventional injectivity test analysis methods is questionable. Considering the pressure responses to the injection test at PPL-01B. As it was fully discussed in section 2.4.3, one of the following or the combination of them could cause of such a decrease in pressure by injection:

1. The condensation of the gas due to high flow rate cold water injection not only makes more space for the fluid to be sucked in, but also there is a drop in pressure due to temperature drop in saturated-condition (the numerical simulation for PPL-06), see section 2.4.3, 3.3.2, and 3.3.3.

2. The injection into the fracture network, as injection goes by the fracture aperture may increase more; for example, mode 1 due to hydro and thermal effects (or permeability enhancement- due to thermo-hydro-fracturing mode 1/thermo-hydro-shearing mode 2 fracture opening/dilation), as it was explained in section 4.1.2

3. It could also be due to injection at a high permeable fault which is extended to the surface, or has a large volume (section 2.4.3).

For example, assuming that during injection, the well has been filled with just liquid water (in fact, the water has been injected long enough to cool down the wellbore and flow inside the wellbore has been totally changed from two-phase flow to liquid-single-phase flow), the hydrostatic pressure of the water column inside the wellbore at the depth of 1.7 km (assuming the density of the water 1000kg/m^3, and the gravity acceleration as 10 m/s^2) would be 17 MPa, and the maximum typical vapor-dominated reservoir pressure is 3.3 MPa (see section 1.4.2, Figure. 4.6 and 1.5). Thus, apparently due to such a huge pressure difference and the intersection of the wellbores with the fractures of high permeability (in the order of hundreds of mD), large amount of the injected fluid can be easily gravity fed into the reservoir.

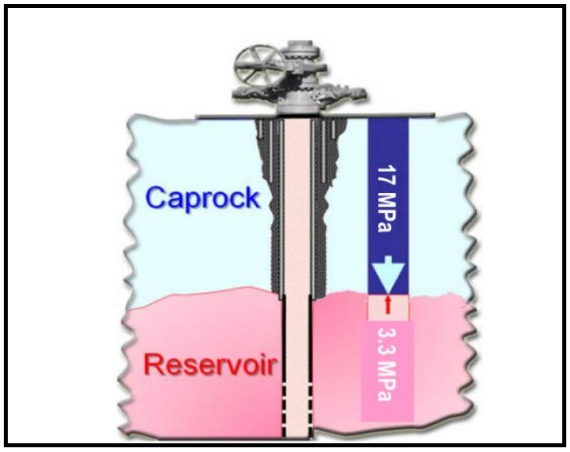

Figure. 4.6 The schematic of the water injection into a hot vapor-dominated reservoir which has a feed zone at the depth of 1.7 km. The hydrostatic pressure of the water is calculated, assuming the well is filled completely with single-phase liquid water of the density of 1000 kg/m^3. Modified after Khan and Truschel (2010).

4.2.1 Vapor-dominated injectivity test design

Taking advantage of the developed model for studying the cold water injection into vapor super-heated reservoir, which was explained in section 3.3.3, the injectivity test has been designed. Analyzing the thermal and boiling fronts propagating into a hot porous rock, the sinusoidal (Figure 3.7) pressure responses due to phase changes and condensation is being transferred by the continuous liquid to the wellbore through the boiling and thermal fronts (Figure 4.7, the first 30 days of injection).

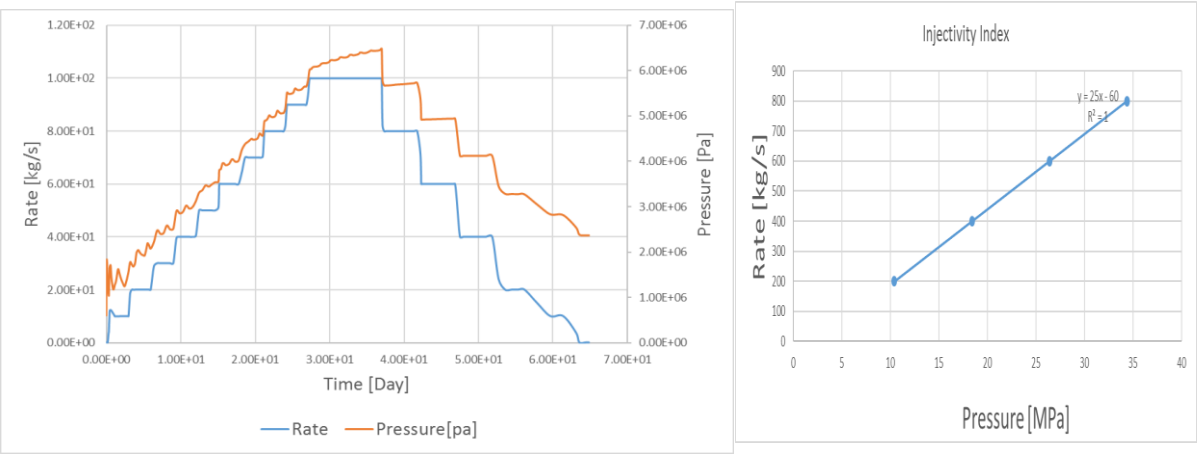

Figure 4.7 Left: The injection test at vapor-dominated reservoir the model parameters and size are same as Table 3.1 and Table 3.2. The pressure has been monitored at the injection element. Right: calculated injectivity index explained in section 4.1.

As figure 4.7 shows the pressure responses during the increasing rate is not stabilized and therefore the injectivity index may not be achieved, while the pressure at the decreasing trend reaches the stabilized status and the injectivity index might be measured using the equation 4.1.

How the decreasing trend of injectivity test for vapor-dominated reservoir is working?

In order to answer this question, we should take a look at the front propagation and pressure distribution within the reservoir. Figure 4.8 shows the front propagation at the increasing trend for three different time, 11, 14, and 17 days after injection started (Figure 4.7, Left plot). As the graphs show the thermal front and boiling front are propagating inside the reservoir and since the injection rate increases the pressure support would be similar to the phenomenon explained in section 3.3.2 (i.e. the pressure at the thermal front > the pressure at the boiling front > the initial pressure). The red arrow in figure 4.8 represents the pressure declining gradient. Hence, during the injection the pressure at the thermal front pushes the fluid to the boiling front and the front propagates further away from the injection point and the similar sinusoidal pressure responses due to phase changes would be observed continuously (see Figure 3.7 and 3.8).

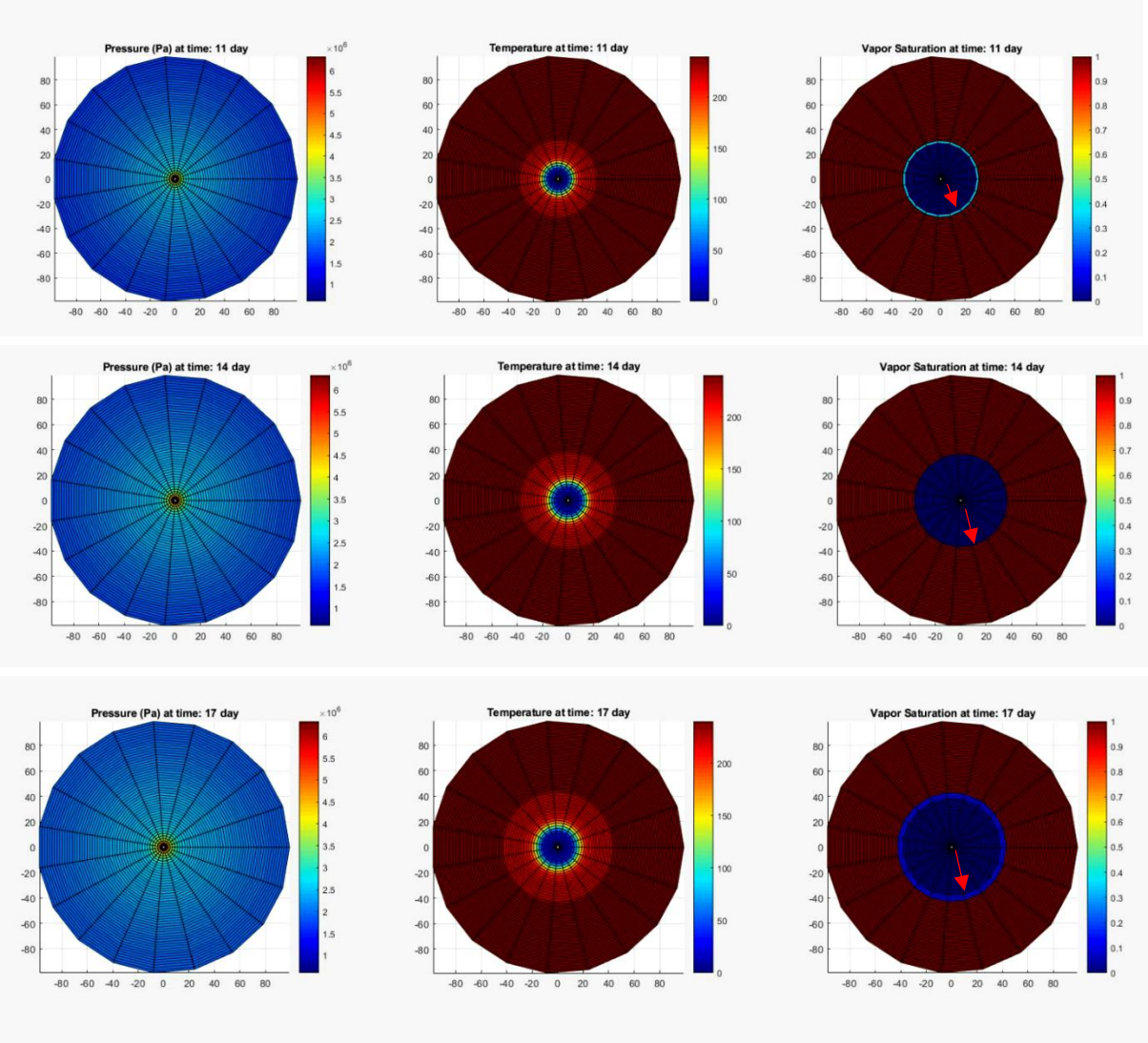

Figure 4.8 This figure shows the pressure, temperature and vapor saturation distribution in all over the reservoir when the injection follows the time according to Figure 4.7. The red arrow shows the pressure gradient. Note: the grid blocks are as shown in Figure 3.6.

One the other hand, considering the front propagation during the decreasing trend (see Figure 4.9, which is representing the reservoir condition 25, 27, 34 days after injection started), since the injection rate decreases and the pressure support to the boiling front reduces (lower injection rate), the required pressure to increase and pass the saturation–pressure at two–phase condition (i.e. the transient from two–phase to single–liquid–phase, Figure 3.7) would not be supported as strong as it was before by the thermal front. Additionally, since there would be a lower injection rate the pressure would decrease at the thermal front while the liquid beyond the thermal front has higher pressure due to the earlier injection at higher rate (Figure 4.9, and 4.10); therefore, there would be a decreasing pressure gradient inwardly (directed to the injection point, see Figure 4.9 red arrows). The boiling front would change to a two phase zone, and start extending and propagating as two–

phase condition (since the additional pressure support to pass the two−phase zone to single−phase−liquid zone is not supported, therefore the pressure and temperature condition would remain at the two−phase saturated condition as it is shown in Figure 3.7 by a the minimum section of the pressure curve), thus no sinusoidal pressure response due to phase change could be seen at the monitoring element (injection element) as the pressure would be almost constant at the saturation pressure of the dominant temperature (see figure 4.9 middle graph, also see Figure 3.5, 3.7, and 3.8).

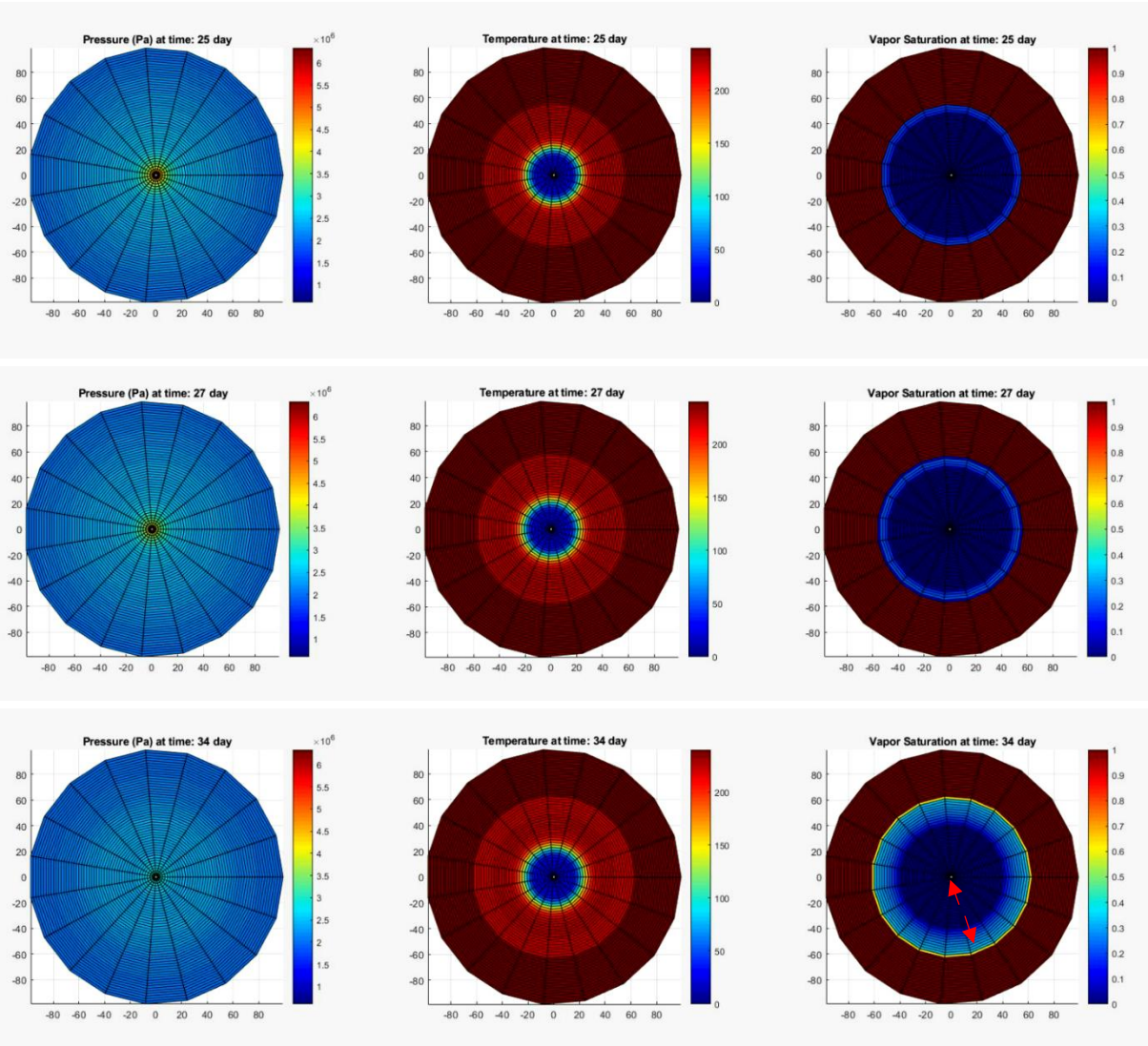

Figure 4.9 This figure shows the pressure, temperature and vapor saturation distribution in all over the reservoir when the injection follows the time according to Figure 4.7. The red arrow shows the pressure gradient. Note: the grid blocks are as shown in Figure 3.6.

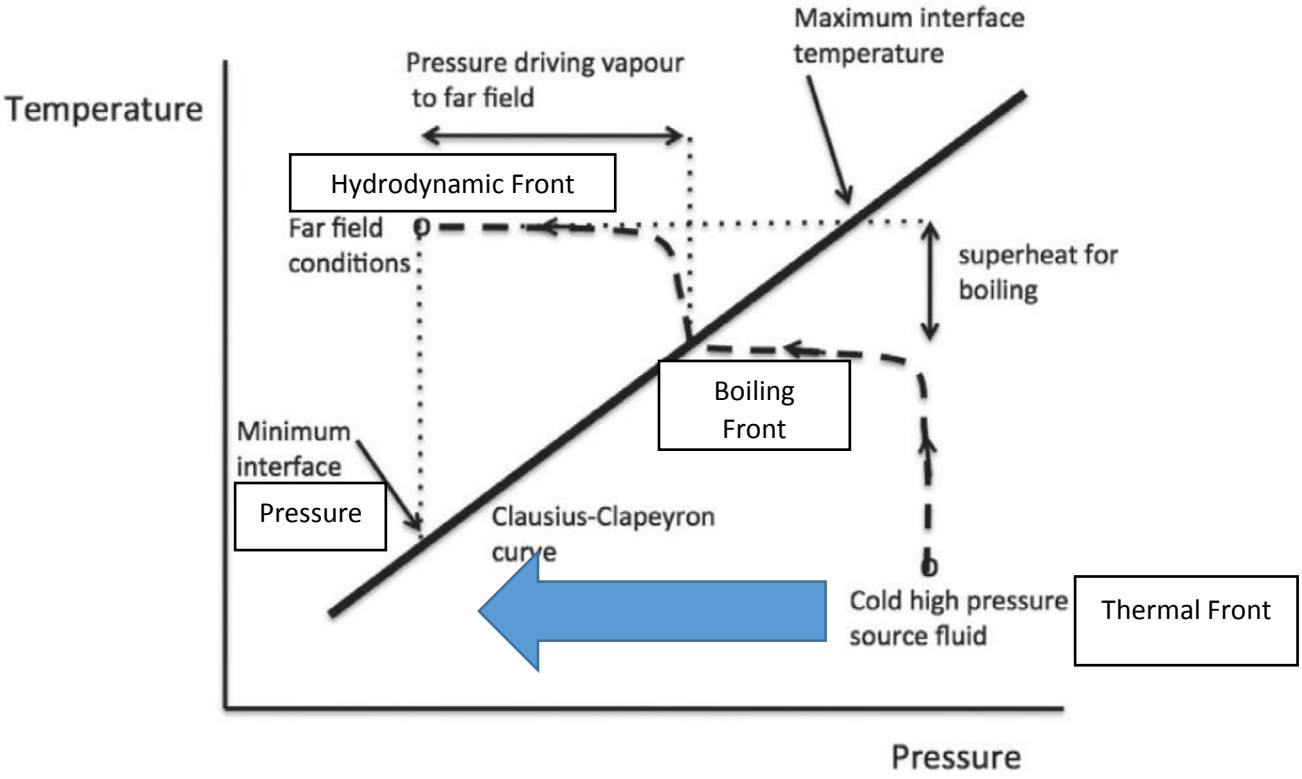

Figure 4.10 shows the new location of thermal front, although it keeps its own temperature but due to lower injection rate the pressure will decrease while the pressure at the boiling front was not changed yet. Modified after Woods (2014).

4.2.2 The injectivity test concept for vapor-dominated reservoirs

To summarize, in order to be able to obtain reasonable pressure data from vapor−dominated systems, one way is to create a single−phase liquid region close to the wellbore during injectivity test. The goal of this single−phase liquid region is to eliminate the effects of condensation of steam during cold water injection. To do so, injectivity test should be done by two flowrate trends, including increasing and decreasing. During the increasing flowrate, steam condensation is expected and the single phase will be created near the wellbore. The data from decreasing flowrate trend might be used to obtain injectivity index.

Chapter 5. A Solution for Production Decline at a Vapor-dominated Reservoir

5.1. Reinjection Strategy

As it was mentioned in section 2.5, the reason behind the production decline of vapor-dominated reservoir is not the permeability, but the in-situ fluid. Since, the natural fluid recharge is not sufficient, the key solution is to reinject the fluid to enhance the heat production. In fact, field experiences at other vapor-dominated reservoirs show that water injection may have very beneficial effects, e.g. increasing the reservoir pressures and flow rates of offset steam production wells (Beall et al., 1989; Cappetti et al., 1995; S. Enedy, Enedy, & Maney, 1991; S. L. Enedy, 2014; K. Goyal & Box Jr, 1992; Keshav P. Goyal, 1995; K. P. Goyal, 1999; Hanano, Ohmiya, & Sato, 1991; Khan & Truschel, 2010), Figure 5.1. Effects of water injection are not always favorable, however, because thermal degradation (temperature decline) or water breakthrough may occur at neighboring wells (Barker, Gulati, Bryan, & Riedel, 1992; Khan & Truschel, 2010). Efforts have been taken to summarize the reinjection experiences worldwide by some researchers, e.g. Diaz, Kaya, & Zarrouk (2016), Kaya et al. (2011), and Stefansson (1997). These review papers are considered as great sources to assist the design of the reinjection operation, because although the design of reinjection is most often empirical and site-specific, there are some generic similarities depending on the characteristic of the system.

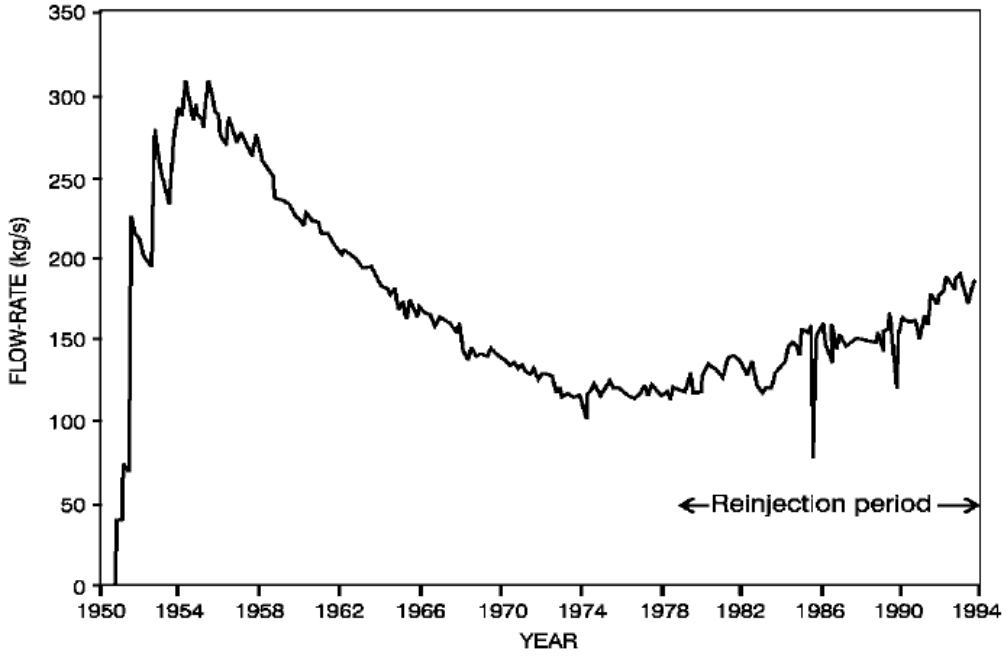

Figure 5. 1 The steam flow rate decline not only has been successfully stopped, but also improved at the Larderello field (Capetti et al., 1995).

Lessons from other Reinjection Experiences

Firstly reinjection was applied as a method of waste water disposal (R. N. Horne, 1985; Stefansson, 1997), but now it has become an important tool for field management. It is a key issue, which can be controversial. It should be dealt with in the early stage of the development by deciding whether to inject infield[14] or outfield, deep or shallow, or possibly some combination of all of these options. In an attempt, Diaz et al. (2016) gathered the available total reinjection mass data of 78 geothermal fields (including 5 vapor-dominated systems). They plotted the average required injection mass rate per generation of 1 MWe energy for each type of systems Figure 5. 2. As it was expected since lower amount of fluid is extracted in vapor-dominated systems to generate 1 MWe energy (Figure 1.4), lower amount of water is required to be reinjected. However, it is essential to point out that the condensate is not enough and external sources of water is necessary for vapor-dominated systems since only 10% to 25% of produced fluid is available as the accumulated condensate (Cappetti et al., 1995; Hanano, 2003; Sanyal & Enedy, 2011).

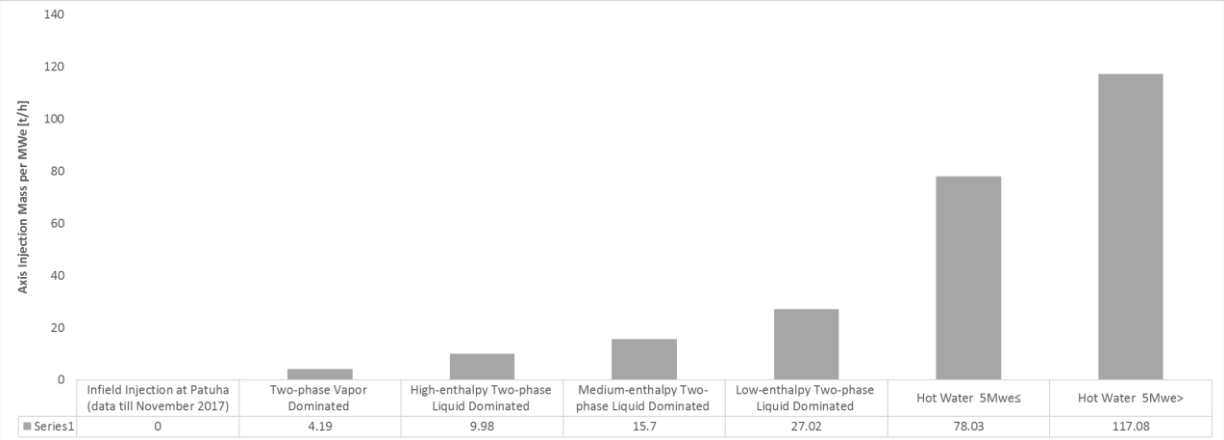

Figure 5. 2 Injected mass rate(t/h) per MWe for each type of geothermal system. Modified after Diaz et al. (2016).

Later, simply by comparing the total produced and reinjected mass data Diaz et al. plotted the average necessary injection (Figure 5.3) for each type of reservoir systems (according to Table 1.1). The available data of the Patuha field according to table 2.1 was used to modify the graph; it is necessary to mention that the injection at PPL-01B is considered as outfield reinjection, therefore infield reinjection at the Patuha field is zero, which should be around 60% according to the reported data available for other vapor-dominated reservoir in which the reinjection operation is being practiced. As it was stated before, although the design of reinjection is most often empirical and site-specific, the recorded observations and responses to injection into other geothermal systems is a treasure source that can be very useful

[14] which means in the vicinity of the producers (less than 1~2 km)

in the designing stage of the reinjection for the system with some generic similarities (e.g. similar geological settings, reservoir type, see table 1.1).

Experiences have shown that reinjection should be planned as early as possible in the field development process and it should be flexible, as it is likely to change with time (e.g. the reinjection at The Geysers as the universally largest vapor-dominated system dated back to April 1969, and electric power generation started in 1960, Enedy 2014). An optimum reinjection strategy should balance the requirements of sustaining the reservoir pressure and preventing early thermal breakthrough of reinjected water. The effects of reinjection on the natural hot recharge and, therefore, on energy recovery from the system may also be important (Diaz et al., 2016).

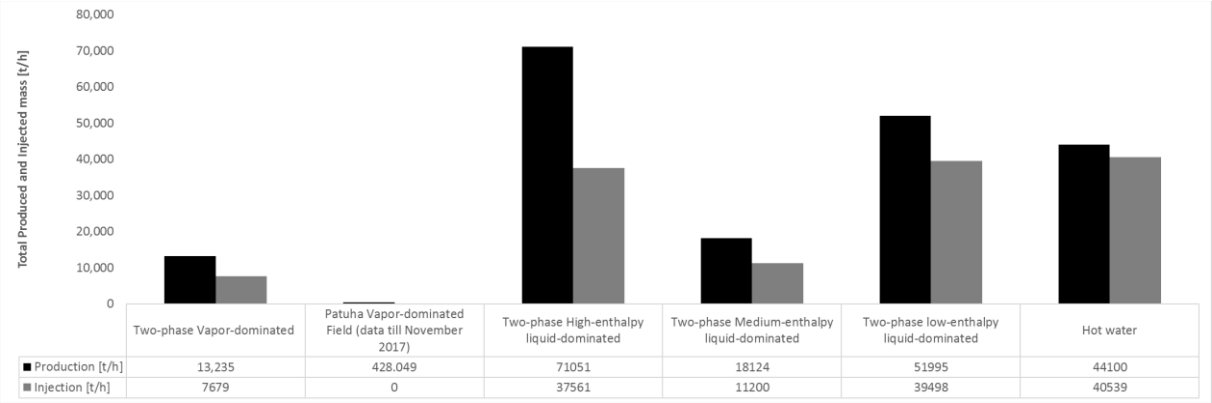

Figure 5. 3 The total produced mass flow rate (blue bars) compared to the total injected mass flow rate (orange bar) per type of system, table 1.1 modified after Diaz et al. (2016).

Reinjection has the following advantages (G. Axelsson, 2012; Diaz et al., 2016; Khan & Truschel, 2010):

- ✓ It is an environmentally friendly method for the disposal of the separated geothermal brine and steam condensate, specially when compared with the surface discharge of the waste geothermal fluid, which can result in thermal and chemical pollution of shallow ground water and water pathways.
- ✓ Reinjection may assist with the recharge of the reservoir and may support the reservoir pressure, thus reducing reservoir pressure drawdown.
- ✓ Reinjection also helps in reducing and managing the consequent ground subsidence that might arise from large scale fluid withdrawal.
- ✓ Reinjection provides the reservoir with low-gas working fluid compared to the higher gas content in the natural deep fluid. This can result in improved plant efficiency with less gas in the geothermal steam going through the turbines (e.g. reduction of these gases in Larderello, Italy (Diaz et al., 2016)).

Reinjection also has the following disadvantages and difficulties (G. Axelsson, 2012; Diaz et al., 2016; Kaya et al., 2011; Khan & Truschel, 2010; Stefansson, 1997):

- Difficulty and expenses of siting suitable reinjection wells.
- Cooling of the production zones and quenching of steam wells.
- Dealing with large reinjection pressures.
- Groundwater contamination and leakage of reinjected fluid to the surface.
- Ground inflation.
- Change of chemistry in production wells. For example, a change in chloride concentration and pH will change the solubility of solids and may trigger corrosion or scaling.

Due to different response of each field to a particular reinjection strategy, a sound monitoring plan needs to be in place to provide early warning and to help in formulating and designing an appropriate steam field management strategy, in order to decrease the unfavorable effects of the reinjection. During the reinjection, cold water breakthrough occurring at the neighboring production wells is one of the most important unfavorable reported effects. Underground flow paths are complex and a distance above ground is not necessarily representing the distance below ground. Tracer testing is, therefore, one of the most important tools assists the geothermal reservoir engineers in order to design a more reliable reinjection plan, by mapping the underground flow paths (G. Axelsson, 2012, 2013a, 2013b; Ayling, Hogarth, & Rose, 2016; T Dwikorianto, Abidin, & Kamah, 2005; FUKUDA, KUWANO, & ITOI, 2013, 2018; R. N. Horne, 1985). Needless to say that it is not yet clear whether the full effects of reinjection water breakthrough are detectable through just tracer test unless full-scale, field-wide test is in progress. Therefore, reinjection schemes should likely be designed conservatively in the meantime, and up-to-dated by a robust monitoring plan.

5.2. Reinjection Plan for PPL-01B and PPL-01A

Calling the analysis performed at sections 2.4.1 and 2.4.2, considering the fact that during 18 years of injection at PPL-01B no pressure support has been observed at the Patuha field and the trajectory of the well is relatively outside of the reservoir zone (Figure 2. 6), it has been suggested by the current study to stop the injection at PPL-01B and instead start to reinject at PPL-01A which is drilled inside the reservoir zone, at least it might be intersected with the same estimated-fault as intersected by PPL-07 (Figure 2. 6), and finally the injection at PPL-01A may support the hot meteoric flow (Figure 2. 6). Therefore, the current status of PPL-01A and PPL-01B is as table 5.1.

Table. 5. 1. The current status of PPL-01A & B.

Well ID	PPL-01A	PPL-01B
True Vertical Depth [m]	2272	1623
Max.Temp. [℃]	202	175
Average Mass [t/h] (based on Fig. A. 2) / Status	119/ Injection (Since 24/11/2017)	0/Shutin (Since 24/11/2017)

The data to study and analyze the effect of the injection mainly to production history of the near wellbores (Figure 2. 6) has not been received yet. However, considering the average production of the Patuha geothermal reservoir (table 2. 1), the cumulative mass production is around 430 ton/hour (PPL−07 is producing most likely the injected fluid heated up during the shut−in period), while the reinjection at the current injection wellbore (PPL−01A) is approximately 119 ton/hour (see Figure 5.4). The ratio of the injection to the production is 36% which is much less than the average value of 58% proposed by Diaz et al. (2016) (Figure 5. 3), or the effective injection/production ratio at The Geysers, Figure 5.5. Therefore, other injection wells are needed. In the literature there are successful experiences of reinjection at poor producers in for example The Geysers (Khan & Truschel, 2010), Kamojang (Tavip Dwikorianto et al., 2010), and Lardarello (Cappetti & Stefani, 1994); therefore, considering the poor production of PPL−06 (section 2.4.3), reinjection has been planned for this well, which will be discussed in the next section. It is noteworthy to mention that since the injection at PPL−01A is the total produced condensate of the system, an external water source is needed. External water was used for the injection at The Geysers, and Matsukawa (Diaz et al., 2016; Keshav P. Goyal, 1995; Hanano et al., 1991).

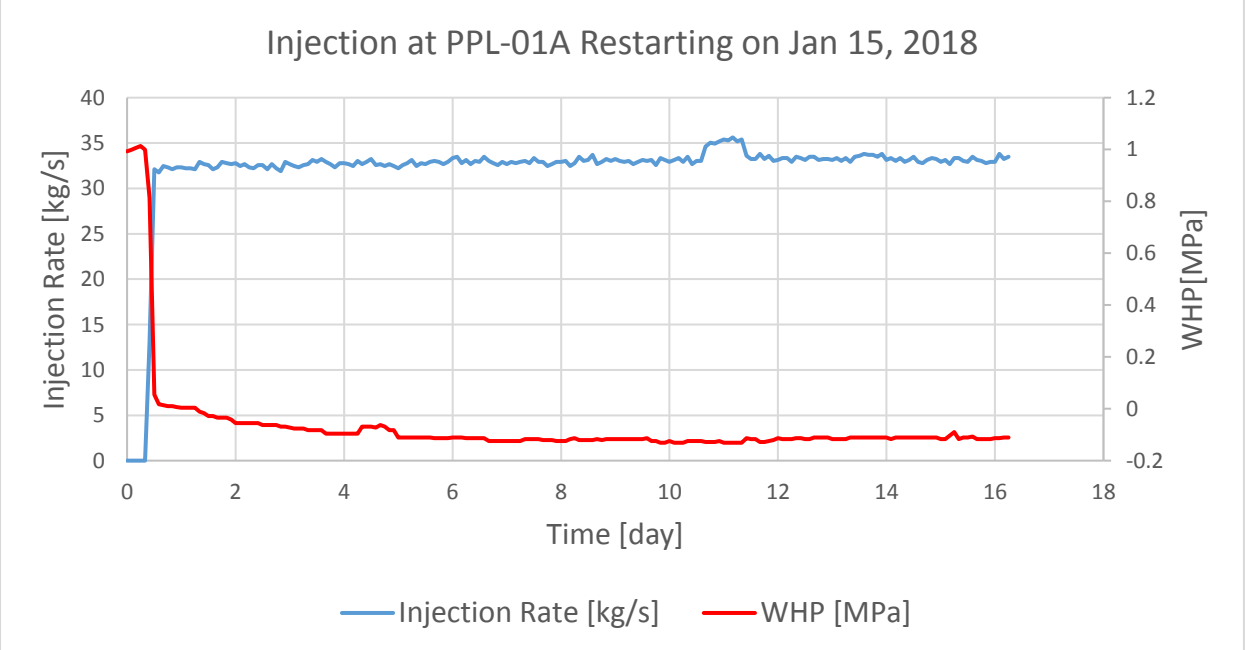

Figure 5.4 The WHP response to reinjection at PPL-01A, the reinjection has been started after a shut-in period.

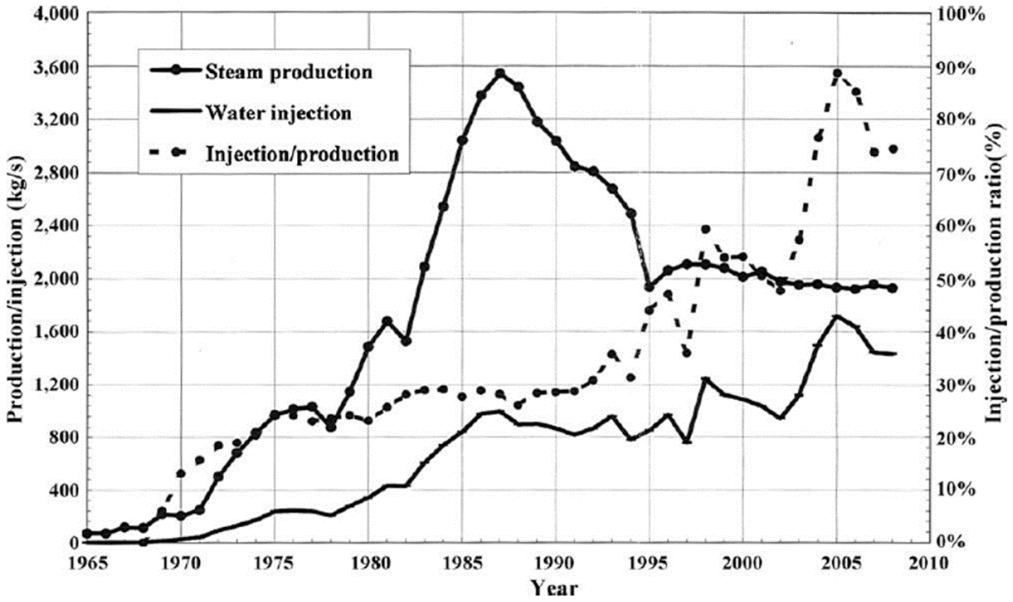

Figure 5.5 Steam production and water injection history of the Geysers,USA, the injection/production ratio has been increased to more than 40 % since 1998 (Goyal and Conant, 2010).

5. 3. Reinjection plan for PPL-06

Considering the data analysis of PPL−06 (section 2.4.3) and the production mechanism of vapor−dominated reservoirs (section 1.3.6) one could conclude that the poor production of PPL−06 could to be caused by one, or a combination of the following factors:

- Lack of in−situ immobile water to replenished the produced−steam
    - Increases in the produced−enthalpy and decline in steam production are believed to be caused by this issue.
- Small fracture network or lack of a pre−existing fracture network (no enough connection with low−permeable porous rock which is the main fluid supplement for the steam production, section 1.3.6).
- Poor connection between wellbore and the pre−existing fractures (due to for instance reservoir damage during the drilling stage).

Therefore, an injection test (Figure 5.5) has been designed to not only ensure the cause of the poor production of PPL−06, but to pursue the following purposes as well:

- Injection characterization
    - Observation of the reservoir response
- To check the difference with somewhat higher injection rate

- Test reservoir seismic responses during injection and shut-in period
- Possible measurement of Injectivity index
- To map any possible underground connection to near producers (Figure 2. 6)
- Identification of the most impermeable zone and possible calculation of in-situ permeability
- Implement and test traffic light system of seismic risk management
- Establish amplitude-ML relationship to be used for traffic light system

Hence, based on this injection test the best appropriate injection plan as the second stage might be planned.

Expected Scenarios upon Reinjection at PPL-06

Since there was no data related to any injection test for PPL-06, a complete injection plan considering all the possible reservoir responses to the injection was designed. The injection starts, based on the contribution of the most permeable interval(s) one of the following scenarios is expected:

I. Injection into the vapor zone

a. Due to low pressure, the injected-water will go mainly to this zone and if this scenario is the case, then the wellhead pressure is continuously decreasing; due to phase change of hot steam to water there would be void space and there would be a suction into the wellbore (section 2.4.3). The fracture network is large enough, and/or the matrix is accepting the water. In this case, the fluid will either flow towards the producers, while it is heating up, and improve the overall production of the field, or by replenishing the produced-fluid, and after a temporary period of shut in and heat up in addition to the preexisting steam the amount of production will improve. We may confirm the interval of flow contribution by spinner log/pressure/temperature logging.

II. Injection into vapor zone saturating the small fracture network or filling the porous medium and reaching the impermeable boundaries

a. If this is the case, the wellhead pressure may increase after a while of continuous decreasing; in this case, once WHP starts increasing, by doing a step rate test we might measure the minimum principle stress, and tune the injection rate of the second injection stage in order to design a thermo-hydro-shearing stimulation. It also has to be confirmed, which interval is contributing to the fluid flow dominantly by spinner log/pressure/temperature logging.

III. Injection into vapor zone, due to poor connection with the well, is not possible.

a. In this case, the injection may just happen into the liquid zone and the wellhead pressure will increase from the first moment; if this is the case, then the use of packer to isolate the liquid zone from the vapor zone is proposed. Similarly, due to limitation of budget and the expenses of the proppant agent in high environment, by doing a step rate test we may measure the minimum principle stress, and tune the injection rate of the second injection stage in order to design a thermo-hydro-

shearing stimulation. The importance of application of spinner log/pressure/temperature logging is apparent.

However, based on the previous injection experiences in other vapor-dominated fields including kamojang, as well as the injection experiences in other wellbores at the Patuha field(section 2.4.1 and 2.4.2), the possibility of the first scenario is high.

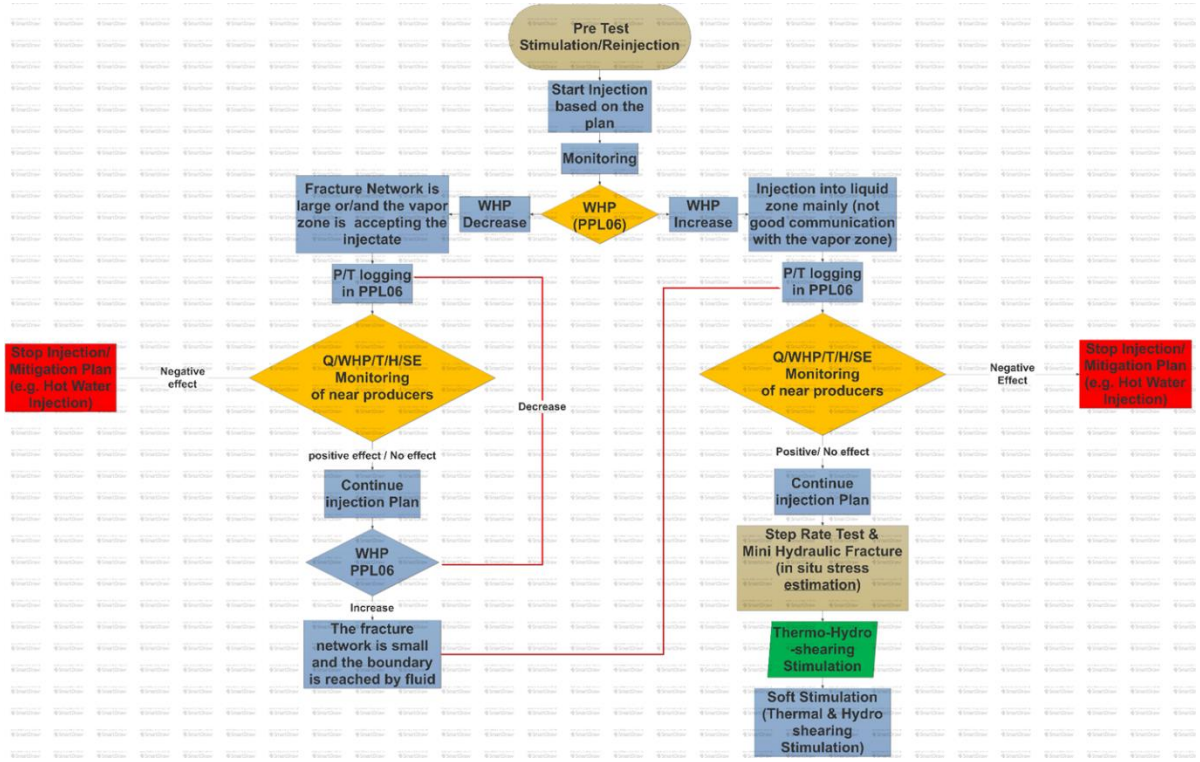

Figure 5.6 Flow chart of all possible reservoir responses to the injection, this algorithm could be applied to any unknown well for an injection test.

Therefore, all the scenarios where implemented with an algorithm represented at Figure 5.6 which could be applied for any unknown well for an injection test.

The full design of the injection test has been implemented as Appendix A.

The reinjection experiences of other vapor-dominated reservoirs such as Kamojang, The Geysers, Lardarello, Matsukawa have been considered as a treasure source guideline. Figure 5.7 shows the final modified-version of the injection test designed for PPL-06, based on the lessons from the injection experiences in other vapor-dominated reservoirs, and the numerical modeling of cold water injection into super-heated porous media (Chapter 3).

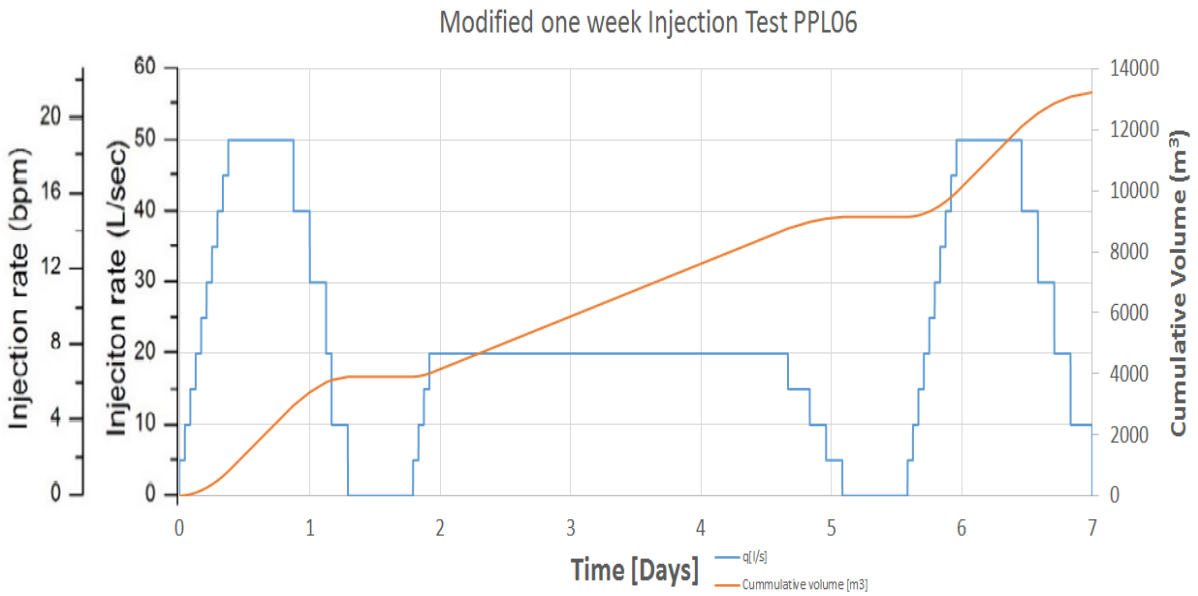

Figure 5.7 The proposed injection test for PPL-06.

Figure 5.7, includes three injectivity test concept which was developed within this study for the vapor dominated systems (chapter 4). The first injectivity test and the last injectivity test are designed to compare the possible injectivity index improvement during the cold water injection into hot reservoir (a mechanism known as thermal stimulation, chapter 4, and Appendix B).

Therefore, the results of this test will be used in order to find the best optimum reinjection strategy. Carrying out an injection test in PPL-06 is believed to have promising effects on the field management strategy development and production of the fields. The response of the reservoir must be observed carefully by an exact monitoring plan to formulate the most appropriate field strategy management. Although, there is a temporary halt in production of PPL-06 due to a short injection test, an overall improvement in production is expected. It is worthy to mention that in other vapor dominated systems, also the poor producer has converted to a successful injector in a way that the reinjection practice is designed for a longer period in the order of years and the overall improvement in production is positive (refer Appendix A).

Overall, the reinjection plan is suggested as above, this injection is started with a relatively smaller injection rate in compare with the pre injection test since the distance of the bottom holes of PPL-06 and the nearest production well PPL-02A is 351.65 m (Figure 2.6). This injection experiment requires continuous monitoring of production rate and temperature of all the producers since the underground flow paths are complex. For example, in Matsukawa vapor-dominated system in Japan (Hanano et al., 1991), although there was a closer producer to the injection well, it

was not affected by the injection, instead another wellbore which was located at longer distance from the injector was affected by the reinjection.

5.4 Injection test at PPL-06 January 2018

The injection test at PPL−06 was finally modified as Figure 5.8 shows; the plan has been shortened to fit in the available sources at the field. The effort has been taken to follow the concept of injectivity test developed in this study for geothermal field (chapter 4).

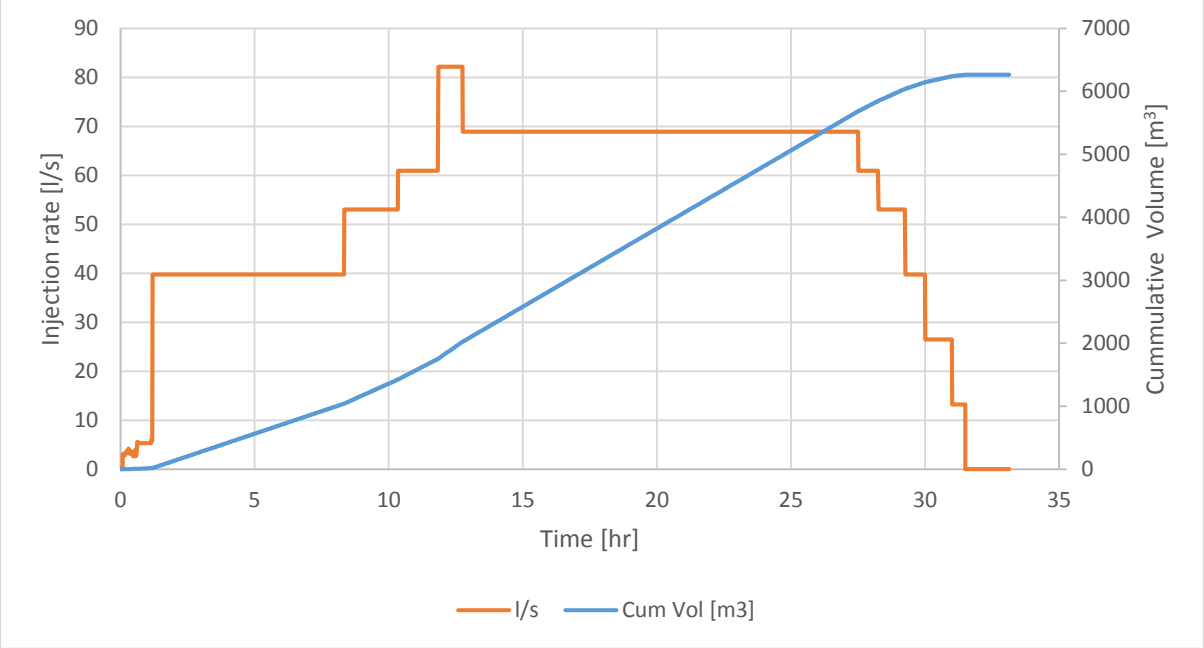

Figure 5.8 Modified injection test for PPL06 (0 hour corresponds to 7:00 am on January, 12 2018).

5.4.1 Injection Test Analysis at PPL-06

The primary aim of the well testing measurement interpretation is to analyze the behavior of dynamic fluid inside the wellbore, and to quantify the properties of the reservoir around the well. Ideally, a complete interpretation provides a complete model of the well, including:

1. Location and thickness of permeable zones
2. Permeability of these zones
3. Reservoir pressure at each zone (This could be found in Figure 5.10)
4. Reservoir temperature over the entire well depth (This could be found in Figure 5.9)
5. Reservoir temperature or enthalpy of fluid at each permeable zone (This could be found in Figure 5.9)

Location and thickness of permeable zones

The available data to find the location and thickness of permeable zones are Pressure/Temperature/Spinner (PTS) Logging data, and the drilling reports.

Considering combination of the data (figures 5.9, 5.10, 5.11 & 5.12), it could be concluded that there is a vapor feed−zone of high permeability at the interval depth of ~1370 to 1550 m (placed in the low constant pressure section[15] of the well Figure 5.10). Figure 5.10 also supports the observation of the reservoir pressure decline explained in section 2.4.2.

Figure 5.9 is showing the temperature distribution of PPL06 during the shut−in period in different time (note that the drilling has been finished on December 8, 1997). Considering the sudden increase in temperature (see Figure 3. 7 ~1340 to 1550 m in vapor interval) during the well logging in January 2018 (which has higher resolution in terms of measurement in comparison with other well logging data do) shown in Figure 5.9, it could be interpreted as a sign of a vapor−feed−zone.

Figure 5.11 presents the spinner[16] log data along PPL−06 during the injection of 15 barrel/min (39.75 l/s). This graph shows the presence of high permeable feed−zone at the depth interval of around 1370 m to 1550 m.

Figure 5.12 shows the schematic of PPL06 including the recorded−depth of the drilling fluid circulation lost. As it shown there is a total lost around 1350 m depth. Note that the depth measurement could be erroneous specially during drilling operation.

Therefore, one could conclude that the wellbore has a simple model as Figure 5.13 with one feed−zone located at the depth interval of 1370~1550 m.

In geothermal wells usually the permeability is being measured by the injectivity test as it will be explained in chapter 4. However, based on the injection and pressure responses one could estimate the permeability based on Darcy's law for steady state of vapor flow.

Using the spinner log data (Figure 5.11), constant pressure and temperature within the dotted−red−box (Figure 5.14), the permeability of the high permeable zone was calculated using the below equations and assumptions:

The fluid injected at feed−zone in the reservoir is steam.

The injected water density is assumed to be 1000 kg/s.

The molar mass of water is 18.015 g/mol (assuming pure water injection).

The standard condition at the surface is P=0.1 MPa, T=288 K.

Assuming homogenous porous media.

The constant recorded pressure (dotted−red−box, Figure 5.14) is assumed to be the pressure gradient between the bottom hole and the reservoir initial pressure, which drives the fluid into the reservoir zone(i.e. $P_{wf} - P_r = 0.544\,MPa$, wf: wellbore (bottom−hole) flowing pressure, r: reservoir).

[15] The constant pressure at Figure 3. 8 from depth of 0 to ~1650 m is the vapor section of the well.

[16] A spinner is an impeller which is used to measure fluid velocity

The reservoir pressure is 2.36 MPa (Figure. 5.10).

The thickness of the high permeable zone is 76 m based on the spinner data, Figure 5.11 (i.e. h=76 m).

Gas viscosity within the dotted−red−box pressure and temperature, is $\mu_v = 0.0003\ Pa.s$.

Equation of State for the vapor:

$$\rho_v[kg/m^3] = \frac{P[Pa]m[g/mol]}{R\left[\frac{Pa.m^3}{mol.°K}\right]T[°K]} \tag{5.1}$$

Where P is the bottom hole pressure, P_{wf} ,the universal gas constant $R = 8.3144598\left[\frac{Pa.m^3}{mol.°K}\right]$

Based on equation 3.1, and the constant pressure and temperature at the dotted red box $\rho_v = 17.56\ \left[\frac{kg}{m^3}\right]$. Now considering a cylindrical porous media of height of h=76 m and porosity, $\phi = 10\%$, and the total injected−mass of 5,692,000 kg water (Figure 5.8), The gas volume would be 324,145 m^3 the radius of the injected fluid would be then approximately 116 m, (i.e. $r_2 \cong 116\,m$)

The steady−state radial−flow equation for the gas at pressure lower than 2000 psi:

$$q_g = \frac{\pi khT_{sc}\Delta p^2}{\mu_g p_{sc} T \ln(r_2/r_1)} \tag{5.2}$$

Where, T_{sc}, p_{sc}, are standard temperature and pressure at the surface, and $\Delta P^2 = P_{wf}^2 - P_r^2$, $r_1 = 8.89$ cm wellbore radius

If we multiply both side of Darcy's equation (eq. 5.2) by ρ_v, the permeability could be written in the form of mass flux, $\dot{m}_v$, as:

$$k = \frac{\dot{m}_v \mu_v P_{sc} T \ln(r_2/r_1)}{\rho_v \pi h T_{sc} \Delta P^2} \tag{5.3}$$

Using eq. 5.3, the permeability of the 76 m thickness of the PPL−06 is estimated to be $1.227 \times 10^{-12} m^2$. This in−situ permeability is measured for the first time at the Patuha field. This value has been implemented in the numerical simulation to analyze the injection test at PPL−06 (section 5.5).

Figure 5.9 The temperature profiles along depth of PPL06 during different shut-in periods (LU: Logging Up, LD: Logging Down in the wellbore and the numbers are the speed of the tool [m/min], these two tests were carried out on January 2018).

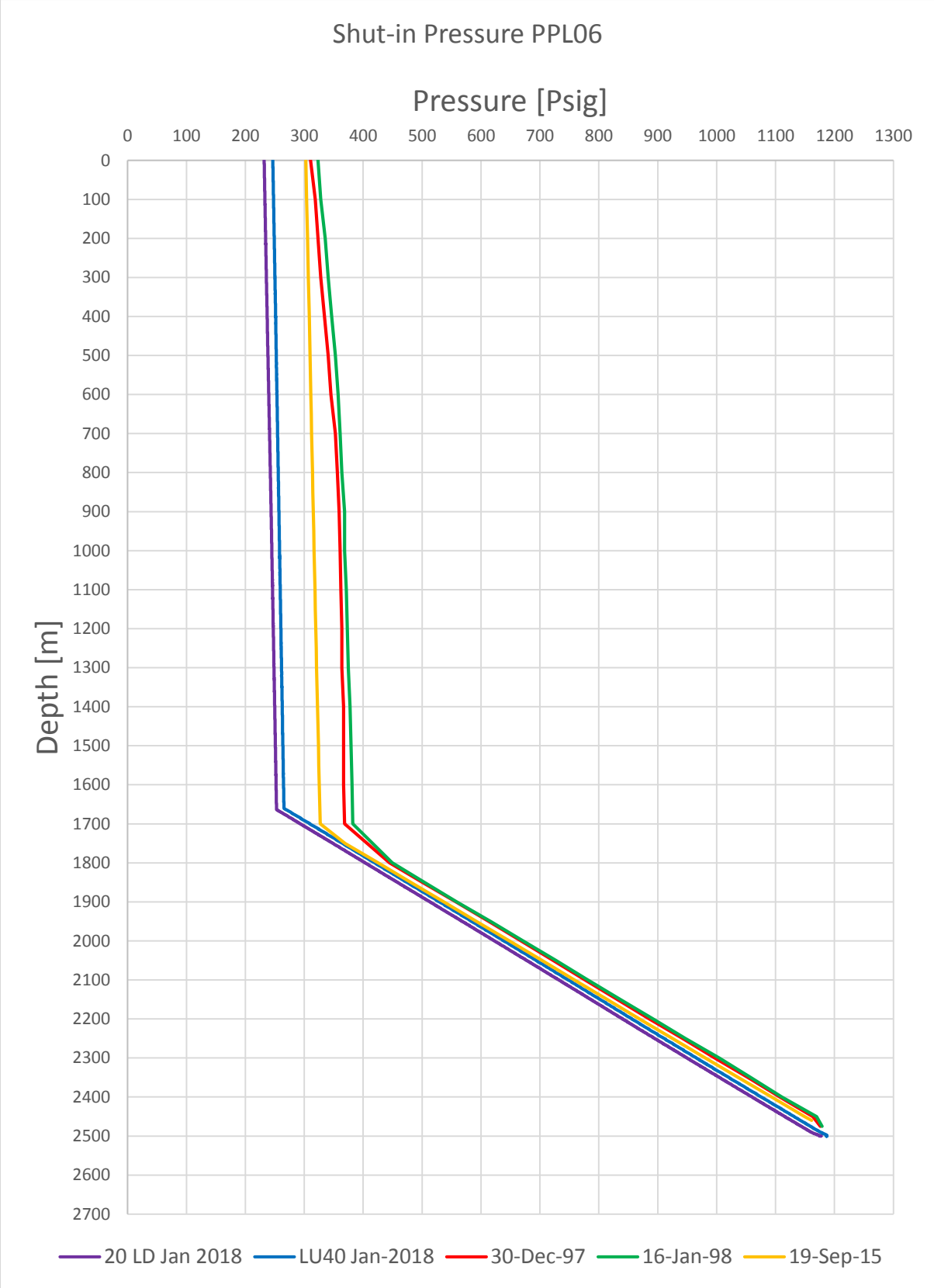

Figure 5.10 The pressure distribution of PPL06 during different shut-in periods (LU: Logging Up, LD: Logging Down in the wellbore, and the numbers are the speed of the tool [m/min]).

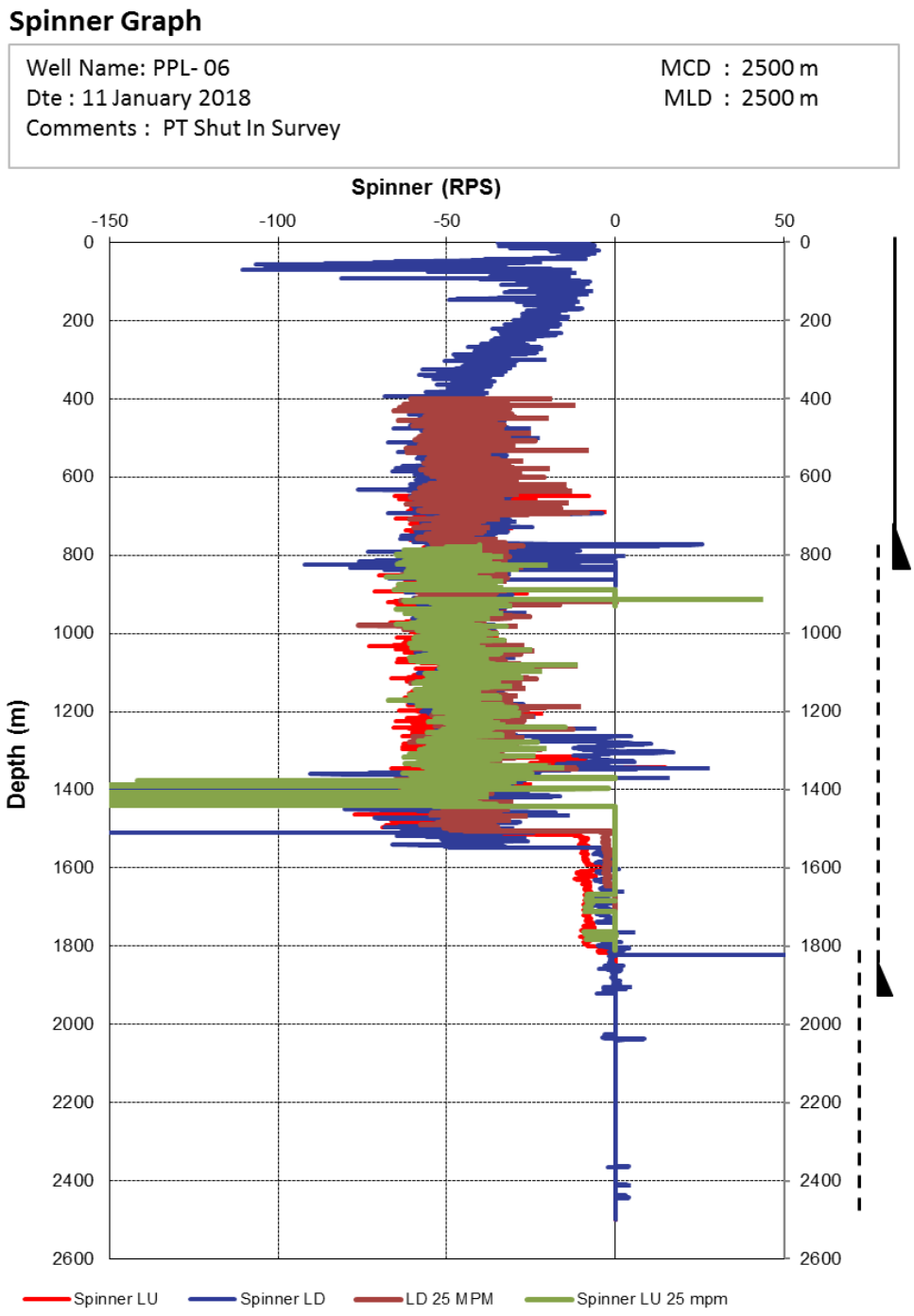

Figure 5.11 The spinner log data at PPL06 during injection of 15 barrel/min (39.75 l/s). To obtain a reliable fluid velocity profile requires up and down passes at two different tool velocities (LU: log up pass, LD: log down pass, and RPS is the spinner speed in revolutions per second, and the values of RPS appear on the horizontal axis, with values positive for down runs and negative for up runs.).

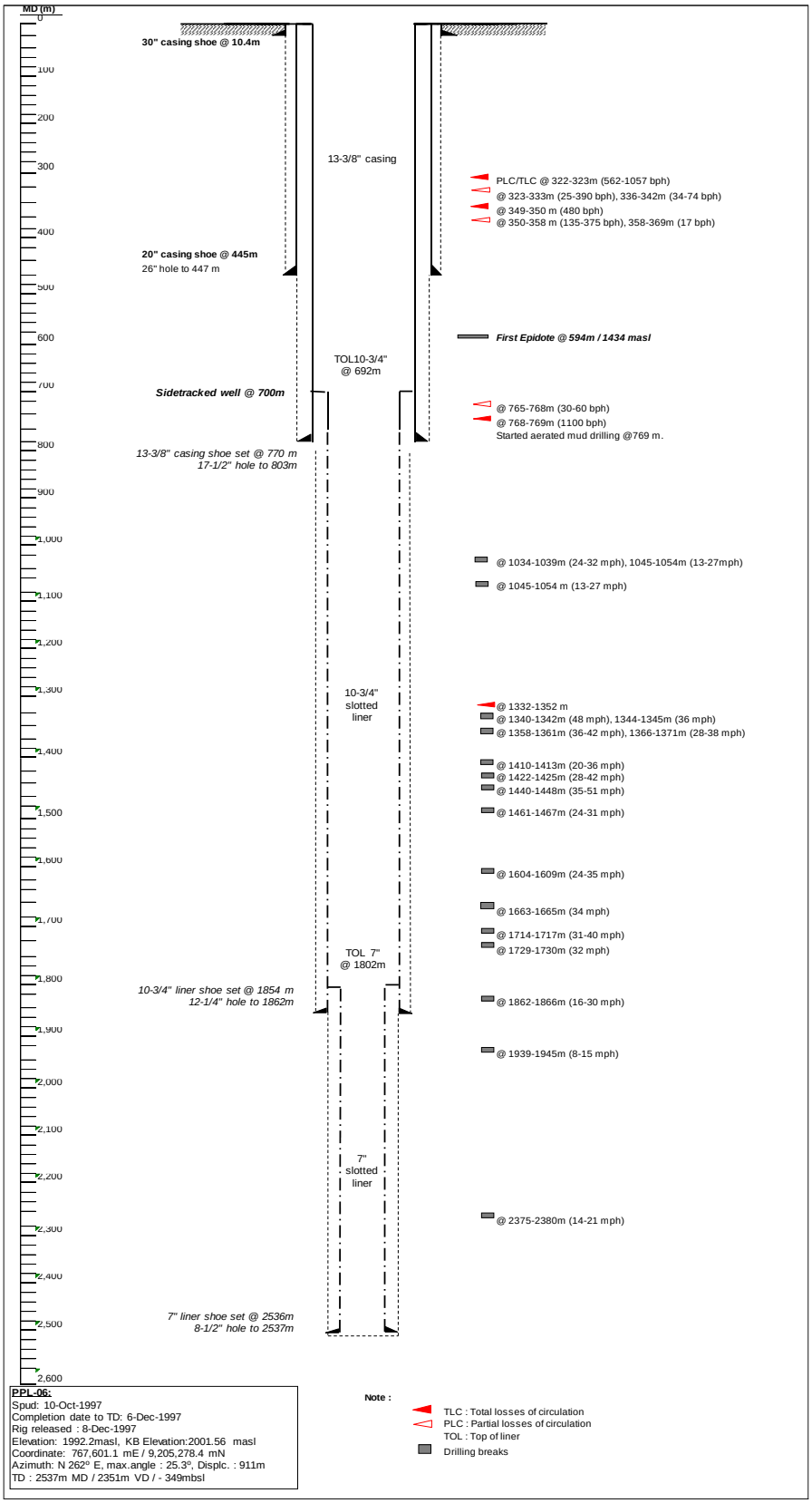

Figure 5.12 The schematic of PPL06 including the drilling report data.

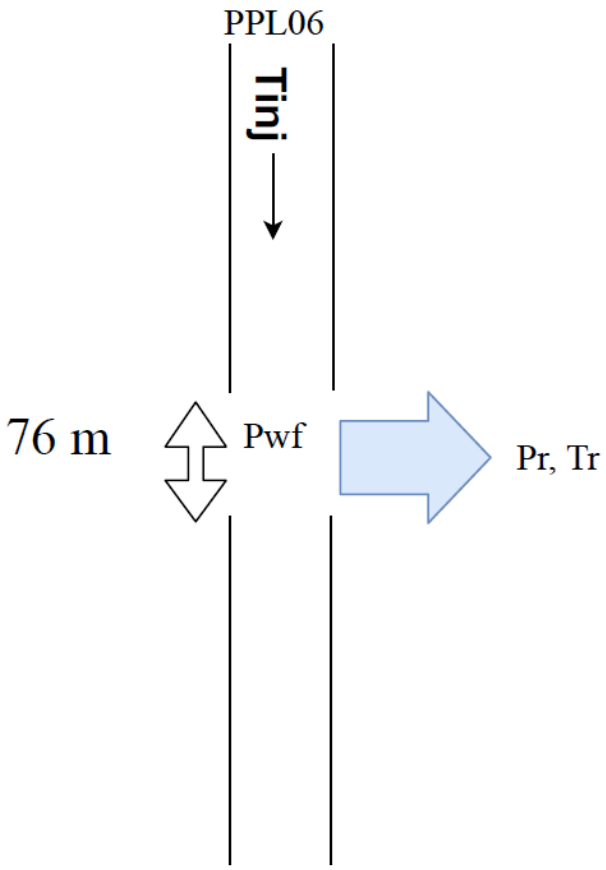

Figure 5.13 the simplified model of one feed-zone proposed-model for injection operation started January 12, 2018 for PPL06.

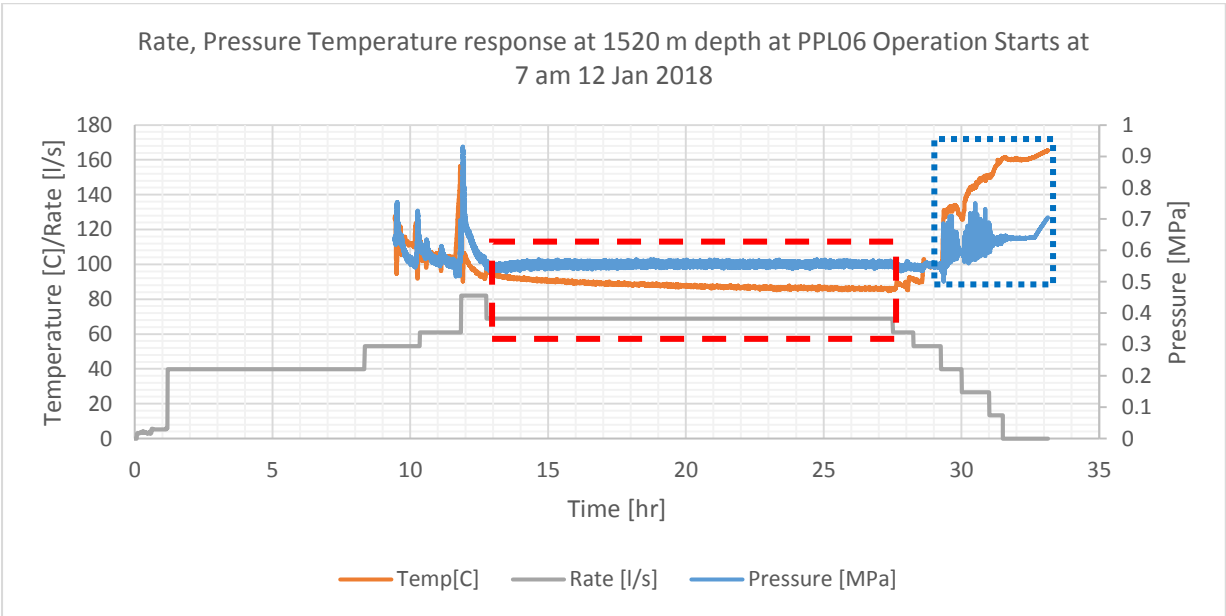

Figure 5.14 The total injection at PPL06 starting 12 January 2018, 7:00 am, the pressure and temperature has been recorded at depth of 1520 m.

5.4.2 The Reinjection effect on the production of PPL06

PPL06 has been operating as one of the producer wells since July 2017 (figure 5.15), although the production test conducted on the time period of May10−June 24 2016 (Figure 2.14) shows a poor reservoir pressure support due to production, considering the hot meteoric flow in Figure 2.6, it could be inferred that the fluid has been recharged naturally; this amount is not huge as the production data shows (in comparison with other producers Table 2.1). The overall production trend for any constant wellhead pressure is declining (red dotted−arrows in Figure 5.15) which means that the reservoir pressure is declining as the well keeps producing. This has been also observed in Figure 5.10 by comparing the pressure distribution along the depth at PPL06 in different time periods since 1998 to 2018 (the pressure profile shifted to the left). By analyzing Figure 5.15 the production of PPL06 has been decreased at the same WHP pressure of ~130 psig around 3 ton/hour after the reinjection, such a decrease could be due to the presence of water inside the reservoir and blockage of the steam flow (the steam relative permeability has been decreased, refer to section 5.3.4 liquid−saturation analysis). Additionally, there is a possibility that the injected−fluid traveled away from PPL06 towards the other producers (i.e. PPL02A, PPL04, refer to section 5.3.3). Therefor in the next section we analyzed the production behavior of neighboring wellbores.

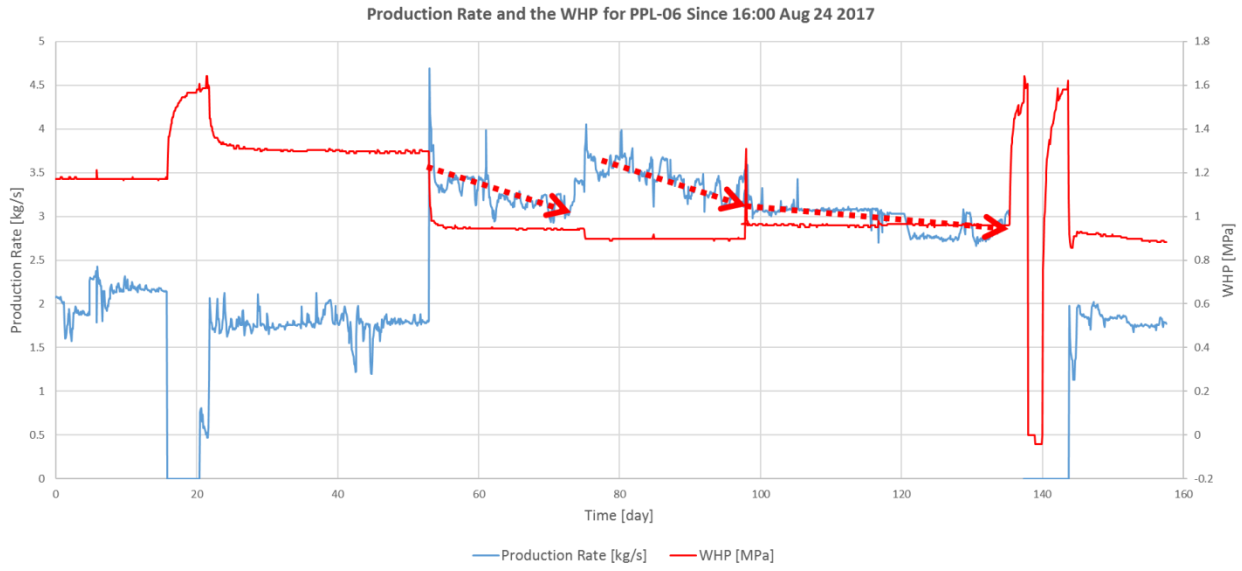

Figure 5.15 The production history of PPL06 Starting from 25 July 2017 to 22 December 2017. Red dotted arrows show the production rate reduction (reservoir pressure reduction).

5.4.3 Reinjection Analysis for PPL06 effects on the neighboring wellbores

Considering the location of PPL−06 the nearest wellbores which are most likely

being connected through the estimated fault network are PPL−02, PPL−02A, PPL−04A and PPL−04 (see Figure 2.6). These wells could be affected by the injection of water at PPL−06 (Figure 5.8). Based on the available data, the distances of bottom−hole location of PPL−02A and PPL−02 from PPL−06 are, 351.65 m and 983.17 m, respectively. Although PPL−06 is far from PPL−04 and PPL−04A, considering figure 2.6 there is an estimated−fault which might be intersected by PPL−06, PPL−02A, PPL−02, PPL−04, and PPL04A. This estimated−fault could have a high permeability along the fault zone, which connected some of these wellbores[17]. Since PPL06 shows a production decline after the reinjection experiment (Figure 5.8), the injected mass should either be stored in porous media as liquid, or travel away from PPL−06. In Figure 5.16, it is suspected that the enhanced steam production at well PPL−02A (an increase of production by 15.2% from 46 to 53 tons/hr, 7 ton/hour increase) might be due to the injection at PPL−06 specially during the period from 12 Jan to 18 Jan 2018, since the shut−in period for this wellbore was 9−10 Jan 2018. In addition, the presence of the estimated−fault with possible high permeable zone might affect the production of PPL−04 (Figure 5.17) in particular during and after the reinjection operation of PPL−06 (12 Jan to 25 Jan 2018). The steam production of PPL−04 increased by 28.3% (from 12 to 15.4 tons/hr) due to the possible connection via the fault after the reinjection at PPL06.

Total electricity generation is increased after the injection at the Patuha geothermal field by 12.6% (from 50 to 56.3 MW) Figure 5.18.

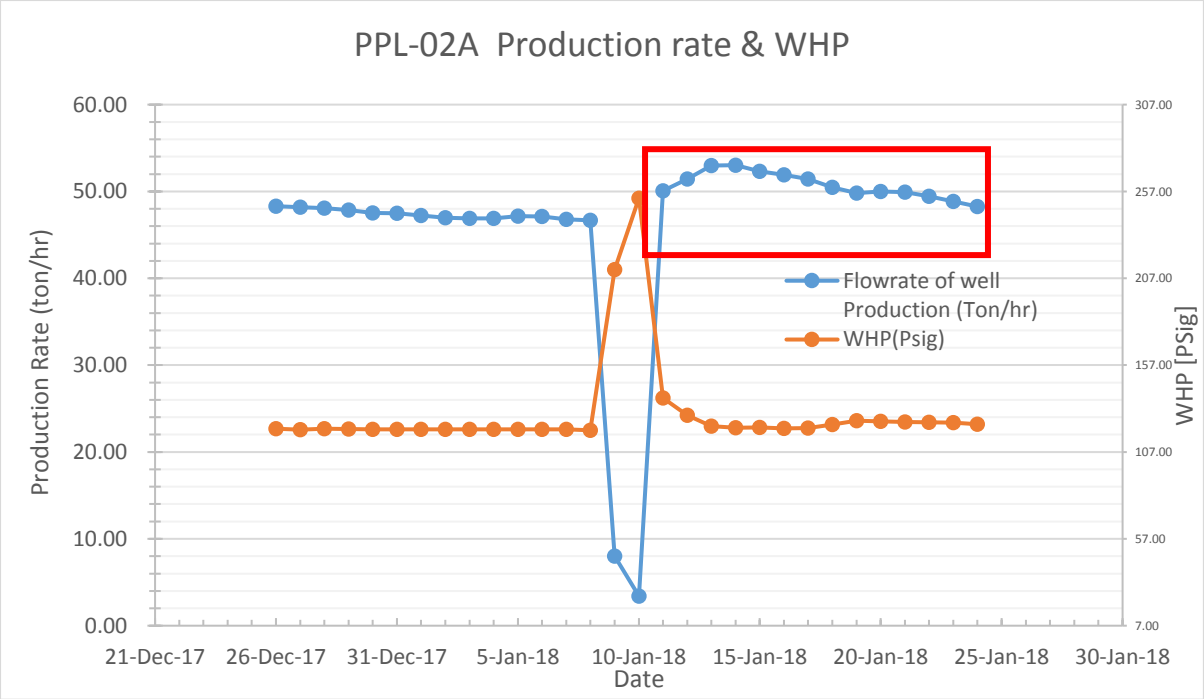

[17] However, since the underground pathways are very complex additional studies (e.g. tracer tests) are required to evaluate and enhance the quality and reliability of the presented analysis.

Figure 5.16 Production history and WHP of PPL02A during January 2018.

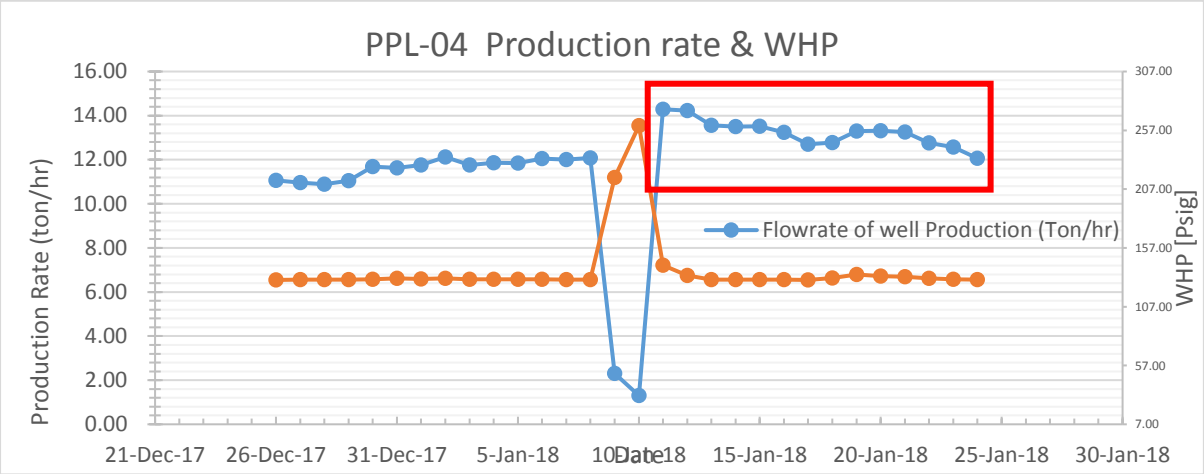

Figure 5.17 Production history and WHP of PPL04 during January 2018.

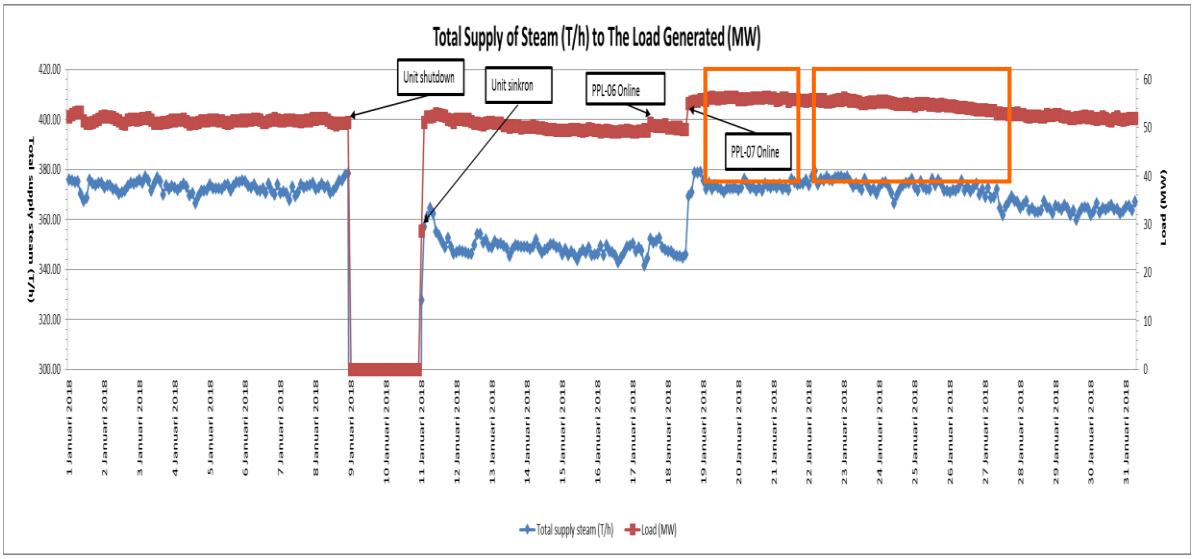

Figure 5.18 Total electricity generation and Steam production

5.5 Numerical Analysis of injection at PPL-06

5.5.1 Reinjection model

Cold water injection is a coupled process of heat and multi−phase mass transfer. This process is severely non−linear which makes the computation strongly expensive. Therefore, a computer simulator is required to solve the non−linear equations. A simplified numerical model has been developed by taking advantage of TOUGH2 simulator (see chapter. 3) which provides insights into the injection at PPL−06 and its effects on the near producers by analyzing and studying the pressure, temperature, and liquid saturation distribution along the reservoir. As it was explained these three wellbores (i.e. PPL−06, PPL−02A, and PPL−04) might be connected by a fault which is permeable along the fracture, while it is assumed to be impermeable in normal direction (perpendicular to the fault), Figure 2.6.

5.5.2 Model geometry, properties, boundary and initial conditions

A $2{,}164\ \text{m} \times 2{,}640\ \text{m} \times 2{,}540\ \text{m}\ (X \times Y \times Z)$ was generated (see Figure 5.19) for the reinjection experiment at PPL−06. The vapor zone is selected to be from 480 to −390 (Figure 5.19), this depth has been selected based on the measured values presented in Figure 5.9 and 5.10, which is corresponding to the measured−depth of the vapor zone at the depth of 800 m to 1670 m. The fault is assumed as a vertical fault (section 2.2). The thickness of the fault as it is explained in section 5.2.1 has been selected 2.5 m (the fractured medium considered as a continuum porous medium). The open hole section of PPL−06 which has intersected with the fault is assumed to be 180 m (Figure 5.11). The intersection length for PPL−02A and PPL04 with the fault are assumed to be 40 m, although enough data was not available to select the exact numbers; the numbers were chosen based on the depth of the mentioned wells in table 2.1. The properties that has been used for the simulation is listed in Table. 5.2. The reservoir boundaries are impermeable and the initial pressure and the temperature of all domains are 1.7 MPa and 240 ℃, respectively. It was assumed that the permeability, porosity, pressure, and temperature are homogeneously distributed along the fault and vapor−zone (−390 m to 480 m Z−

coordinate at the model scale). The formation permeability above (0 m to 800 m at the field corresponding to Z−coordinate of 480 m to 1270 m at the model) and below (1670 m to 2540 m at the field corresponding to −390m to −1270) the vapor zone is 1×10^{-21} m^2, the flow cannot pass the fault in the direction of negative X (see Figure 3.18), however there could be a communication with the reservoir zone at the positive X direction with the fault since the vapor zone (from 800m to 1670 at the field scale depth and 480m to −390 at the model scale size Z direction) permeability is 0.547×10^{-17} m^2.

Table 5.2 the properties used for the reinjection simulation at PPL-06

Property	Value
Formation density*	$2600\ kg/m^3$
Rock specific heat*	$1000\ J/kg\,℃$
Formation heat conductivity*	$1.8\ W/m\,℃$
Fault Permeability***	$1.227\times10^{-12}m^2$
Rock mass Permeability*	$0.574\times10^{-17}m^2$
Fault Porosity*	0.1
Formation Porosity*	0.048
Relative Permeability Function **	$Corvey's\ curves$ (1954) $S_{lr}=0.3, S_{gl}=0.05$
Reservoir Pressure ***	$1.7\ MPa$
Reservoir Temperature ***	240 ℃
Injection Enthalpy	$0.1258\times10^6\ kJ/kg$ (~29.5 ℃)

*Data from previous numerical studies for Patuha (Schotanus, 2013).

**Typical Values for numerical modeling of cold water injection into super−heated vapor−dominated formations (Pruess, 1980; Calore, 1986; Pruess, 1987), see equation 3.9.

***Data from section 5.3.1

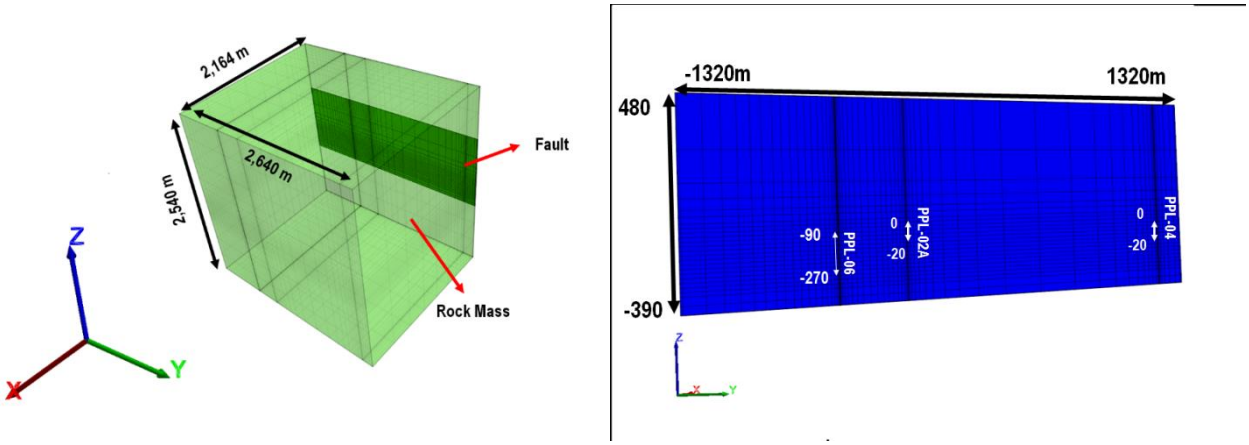

Figure 5.19 Geometry of the reinjection at PPL-06 the connecting fault (fracture) and PPL-02A and PPL-04 (see also Figure 2.6), left geometry is showing the whole doming including the rock mass, right geometry is representing the fault and the wellbores (numbers are in m), the thickness of the fault zone is 2.5 m.

Due to the fact that the uncertainties of the underground fluid flow are high, and the data from the injection test is limited, instead of adding more uncertainties to the simulation model and making the results more complex by including, for instance, the production of PPL−2A and PPL−04 of which not much data was available (e.g. the number, permeability, depth, and thickness of the feed zones are not known), it was decided to study the pressure, temperature, and liquid saturation in the reservoir zone during and after the injection at PPL−06. The location of the two other wellbores (connected by the fault) are shown in Figure 5.19. The elements near all the wellbores are discretized fine enough to strengthen the reliability of the results. In this model, the wellbores are simulated as a high permeable elements at which the porosity is 1. The allocated−parameters to the wellbore elements gives insights into the fluid flow behavior inside the wellbore during the injection.

By this simplified model a series of sensitivity analysis have been carried. The purposes of these sensitivity analyses are as follow:

- To study and analyze the pressure, temperature, and liquid saturation distribution along the fault, and in particular at the location of PPL−02A and PPL−04 when the injection schedule is following the actual injection plan carried out on January 12, 2018 (Figure 5.8) with homogeneous permeability input of $1.227 \times 10^{-12} m^2$ as it was calculated in section 5.3.1. Moreover, the pressure at the wellbore element was monitored and compared with the measure pressure at the depth during the injection test (Figure 5.14).
- To analyze the long−term injection test at PPL−06 and the effects on the reservoir zone at the Patuha geothermal field.

The results of the sensitivity analyses are presented and discussed in the next paragraphs.

5.5.3 Sensitivity analysis of the injection operation on PPL-06

As it was explained by analyzing the pressure, temperature, and liquid saturation distribution, with the assumption that the permeability, porosity, and intimal pressure and temperature are homogeneously distributed along the fault, the efforts have been taken to evaluate whether the injection plume could reach to the vicinity of the other two wells (i.e. PPL−02A, and PPL−04), with the given permeability (calculated in section 5.3.1). Therefore, the important parameter here is the permeability[18].

[18] Needless to say that this simplified assumption might not be the case in reality, instead the permeability might be varying inside the reservoir widely.

5.5.4 Discussion on the cold water injection behavior into the wellbore

By analyzing the wellbore elements, as the injection starts the simulation shows that the wellbore is under two-phase condition. Similarly, as it has been explained in section 2.4.3, when the injection is in two phase zone, the saturation pressure and the saturation temperature are dependent on each other (following the Figure 3.5). However, the pressure (and equivalently the corresponding saturation temperature) and the liquid saturation along the well are not uniform; instead most of the liquid (similar to the real case) will rain down (due to its buoyancy) causing a decline in the saturation temperature of the bottom-hole. Consequently, the corresponding saturation pressure will decline, while the saturation pressure at the shallower well elements are higher and since the permeability in the wellbore elements (in Z direction) is much higher than the fault system the fluid will flow downward. The saturation temperature of the bottom-hole declining, and consequently its corresponding saturation pressure will decline to the point that the saturation pressure will drop under the dominant element-pressure; also thanks to continuous liquid injection into the element-pressure will build up and finally mass state inside the element will be single-phase water, and since then the pressure in this element will continuously build up. Meanwhile, the shallower elements are in two-phase condition and they have lower pressure than the bottom-hole element, thus the downward-flow (inside the wellbore) would decrease significantly and the cold fluid starts entering the near wellbore elements. As the cold fluid goes inside the vapor-zone element (which has the initial pressure and temperature of the reservoir), it cools down and follows figures 3.7 & 3.8 (see also Section 3.3.2, 3.3.3, Figure 2.13) to two phase-zone state, and then the cooler fluid will enter the next downstream element. Similar process will happen for bottom-hole element with a delay since firstly the saturation pressure is decreasing significantly (due to temperature reduction, and the wellbore element pressure is lower than the next element of vapor-zone), and later after transition to single-phase liquid the pressure starts building up and entering the reservoir elements.

As it has been fully discussed in section 2.4.3 the reduction in pressure at PPL-06 is most likely due to the reduction in temperature and transiting to the two-phase condition at the wellbore and the near well region. The pressure records for the similar injection schedule at PPL-06 at the depth of 1390 m were compared with the measured field data in Figure 5.20. Although, the relative permeability (section 3.3.3, e.g. equation 3.9) is an unknown sensitive value (e.g. the S_lr: residual liquid saturation and S_gr: residual gas saturation are assumed), the pressure trends and values are in sufficient agreement with the field data. This observation supports the concept that was explained in section 2.4.3.

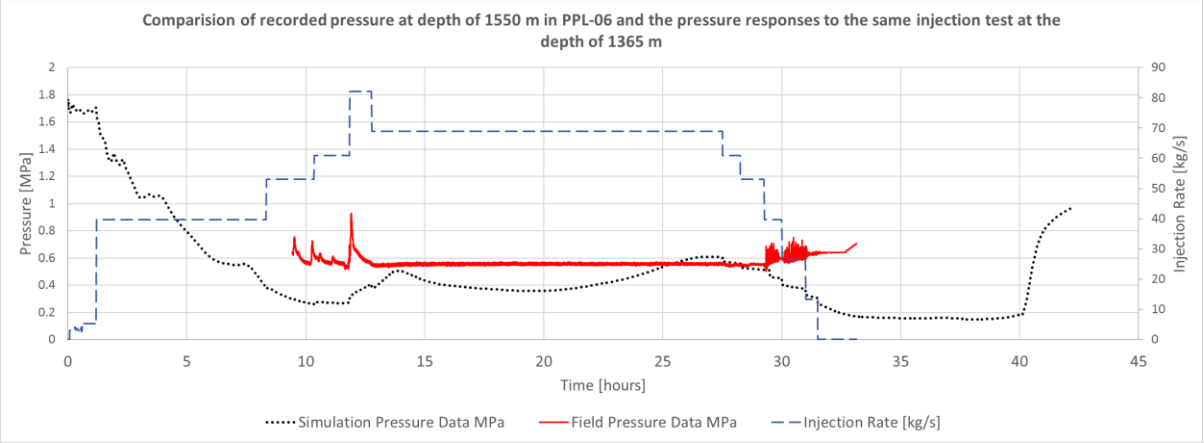

Figure 5.20 Comparison of the measured field data with the simulated injection data at PPL-06 (k=1 D).

5.5.5 Discussion on the pressure, temperature, and liquid saturation distribution along the fault vapor zone of the Patuha field during injection at PPL-06

In Figure 5.21 the pressure distribution for a series of different absolute permeabilities k_1=1.22 D, k_2=2.55D, k_3=5.55D, k_4=10.55D, and k_5=15.55D after 33 hours of injection (same as Figure 5.8, 1 hour after the shut−in) are compared. The results of the pressure distribution under the assumption of homogenous permeability along the fault as well as no production of PPL−02A and PPL−04 show that for the calculated permeability, i.e. k_1(section 5.3.1), the pressure distribution did not reach at PPL−02A and PPL−04. Therefore, under this assumptions the production increase reported in section 5.3.1, Figures 5.16 and 5.17 is not caused by the injection at PPL−06. In order to find the least required permeability to see the pressure support to the mentioned wellbores different permeabilities were simulated and the results presented in Figure 5.21, considering the given condition in order to affect the production of PPL−02A and PPL−04 the permeability should be higher than 15.55. This permeability value does not look to be a practical value in a real field therefore the production improvement at PPL−02A and PPL−04 (Figures 5.16 and 5.17), under this assumptions cannot be caused by the injection at PPL−06.

Figure 5.22 shows the temperature distribution modeled with the mentioned premeabilities; the shape of the temperature distribution is expected, since as it was explained in this section earlier, the bottom of the hole has a lower temperature (colder fluid) in compare with that of shallower elements, and therefore the effects of thermal front propagation (see section 3.3.1) near the bottom hole is stronger than that of the shallower parts.

Figure 5.23 shows the liquid saturation for all the modeled permeabilities. By looking at the liquid−phase saturation distribution near the wellbore, the poor production of PPL−06 after the injection test could be explained. Since the saturation of the liquid has been increased near the wellbore, the relative permeability of the steam has been decreased consequently (see Figure 5.24).

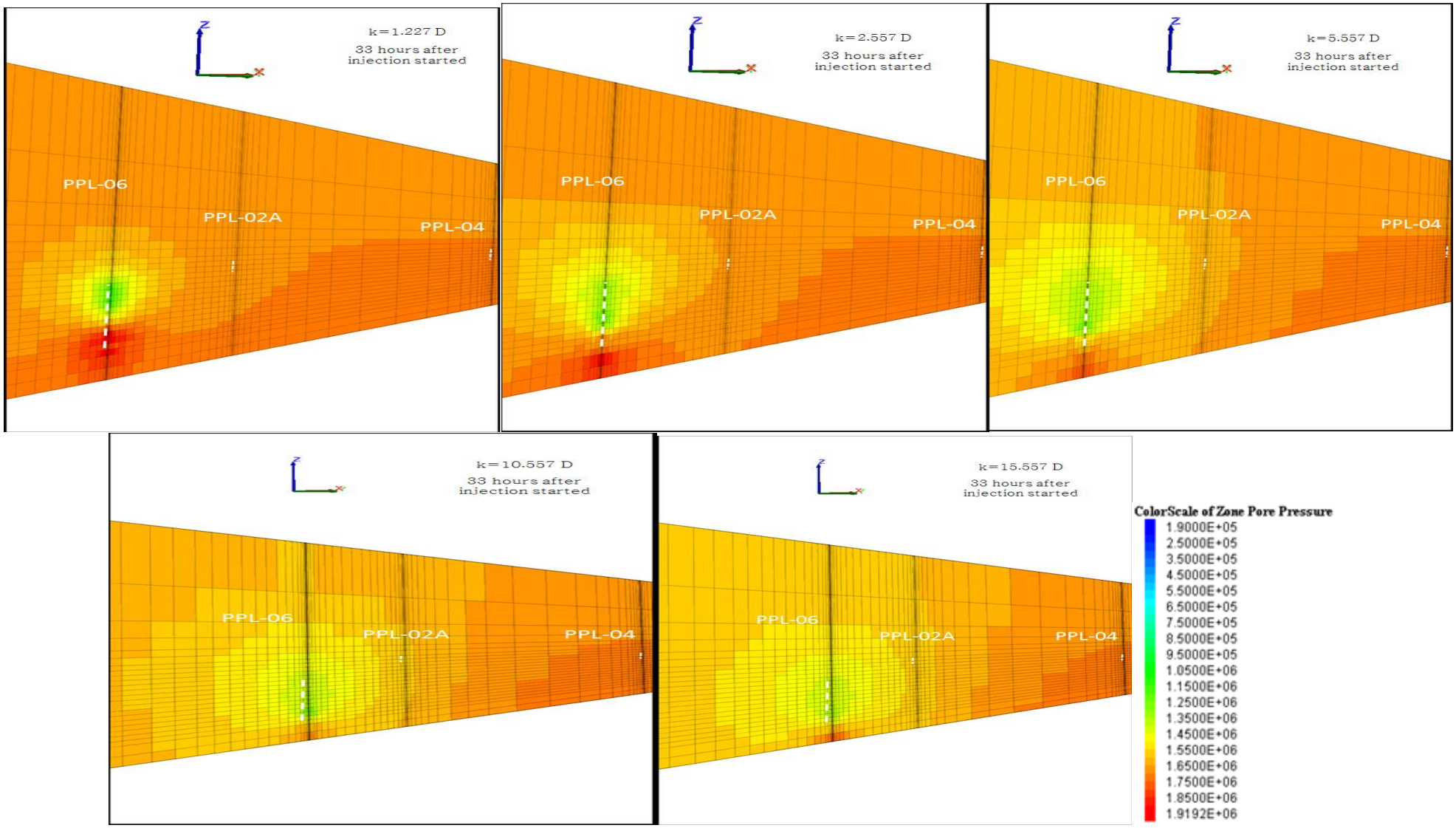

Figure 5.21 The pressure distribution 1 hour after injection stopped according to Figure 5.8, for k_1=1.22 D, k_2=2.55D, k_3=5.55D, k_4=10.55D, and k_5=15.55D, the pressure legend is in [Pa].

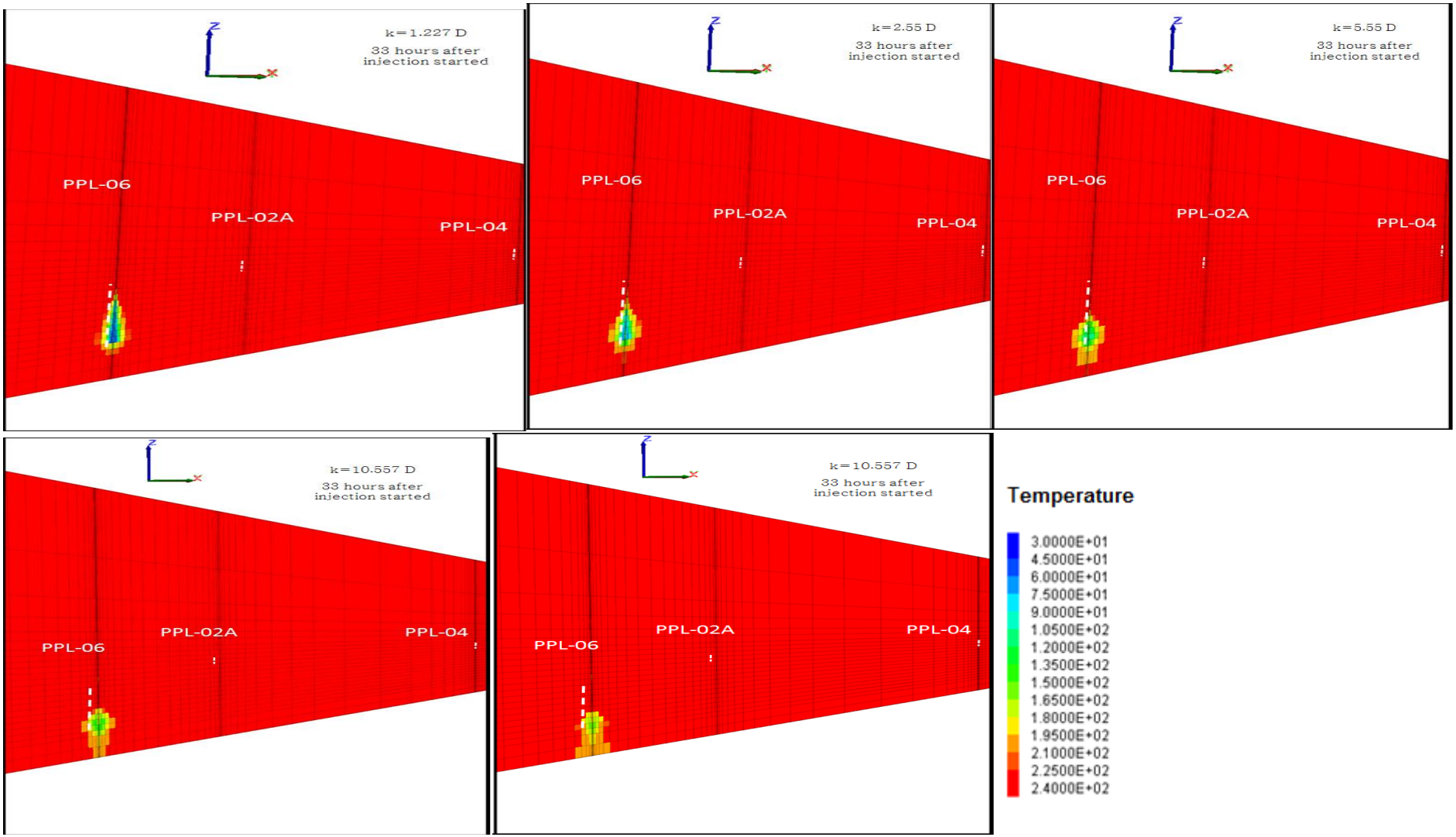

Figure 5.22 the temperature distribution 1 hour after injection stopped according to Figure 5.8, for k1=1.22 D, k2=2.55D, k3=5.55D, k4=10.55D, and k5=15.55D, the temperature legend is in °C.

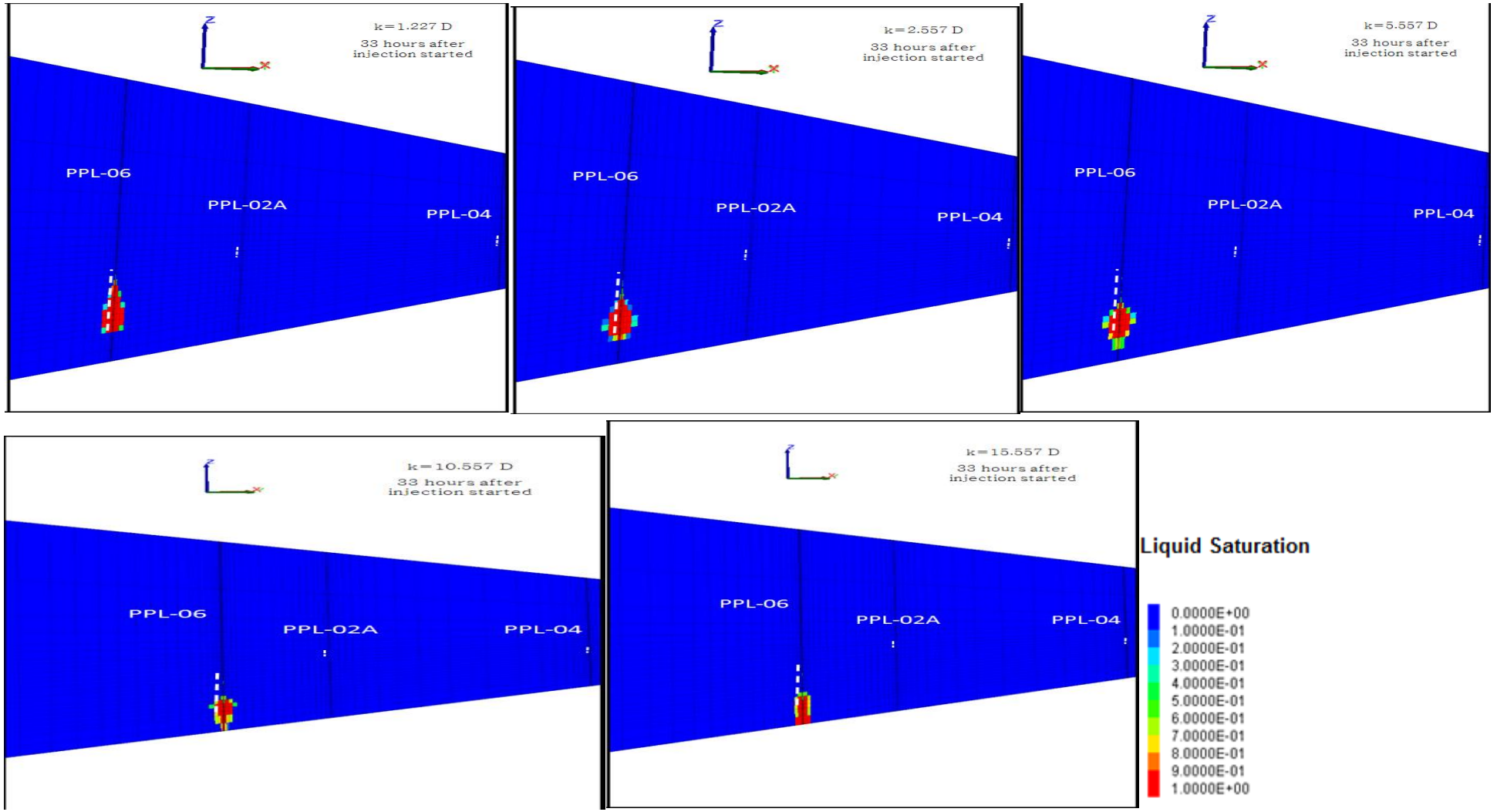

Figure 5.23 The liquid saturation distribution 1 hour after injection stopped according to Figure 5.8, for k1=1.22 D, k2=2.55D, k3=5.55D, k4=10.55D, and k5=15.55D. The formed high saturation liquid zone is believed to be the main reason of production reduction of PPL-06 after injection test see Figure 5.15.

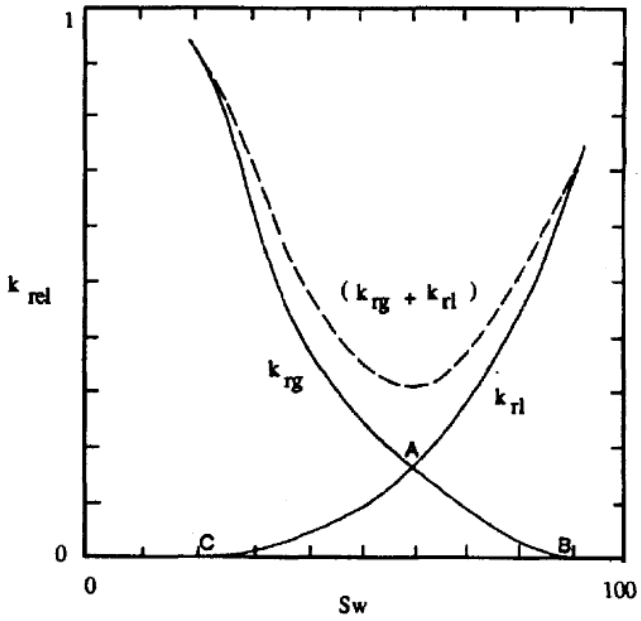

Figure 5.24 Typical example of relative permeability curve, point "C" is the saturation of irreducible water, point "B" is the critical gas saturation at the saturation less than "B" the gas-phase is not mobile. Point A is the saturation at which the relative permeabilities of the gas- and liquid-phase become equal (Honarpour, 2018).

More simulation studies have been conducted to analyze the injection at PPL−06. In this section, the permeability was kept constant at k_1=1.227 D, and the injection schedule has been altered. Firstly, the results of the injection according to Figure 5.7 is reviewed. As it was explained, this injection test has been was designed pursuing multitude purposes. One of the conservative aspect of the designing process of this very first injection test at PPL−06 was to minimize the risk of seismic event as well as the risk of the cold water break−through, therefore the injection test has been designed with relatively low injection rate to monitor and evaluate the reservoir responses for reservoir characterizations and the future injection test designs at the Patuha field. Figure 5.25 shows the simulated pressure at the depth of 1365 m at PPL−06 corresponding to proposed injection test (Figure 5.7). One could conclude that the test has failed to reach any stable pressure value during the injection test, therefore, no injectivity index could be calculated based on the developed concept at chapter 4. The main reason to this unstabilized pressure is that the liquid zone near the wellbore was not formed, as it is shown in figure 5.26. However, under the given conditions (i.e. homogeneous permeability and zero−production of PPL−02A and PPL−04) the pressure distribution has reached PPL−02A as it is shown in Figure 5.27, while the temperature at PPL−02A is still at the reservoir temperature, as Figure 5.28 represents. Thus, although this test failed to measure the injectivity index at PPL−06, it could increase the production of PPL−02A by pressure support without any change in the produced temperature. Note that after production from PPL−02A the draw−down pressure near the wellbore will propagate and the pressure support of PPL−06 will increase the production of PPL−02A. The production decline at PPL−06 after this injection test is also expected due to liquid saturation increase, and consequently lower relative permeability of steam.

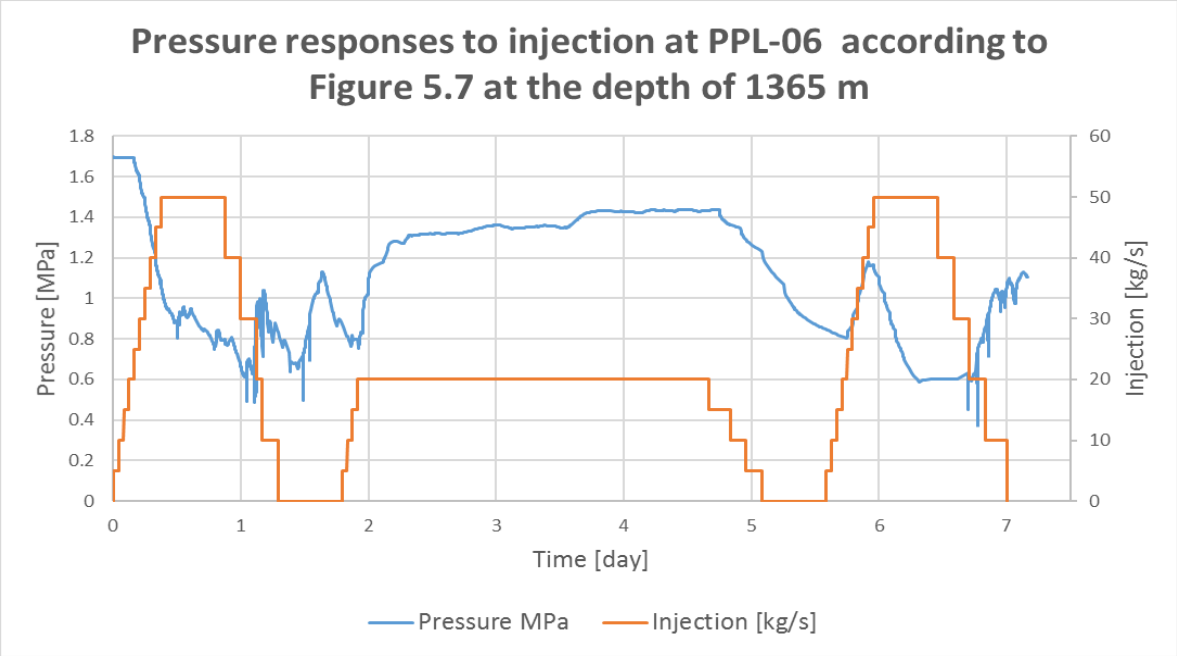

Figure 5.25 the pressure responses to the injection test designed for one week, Figure 5.7

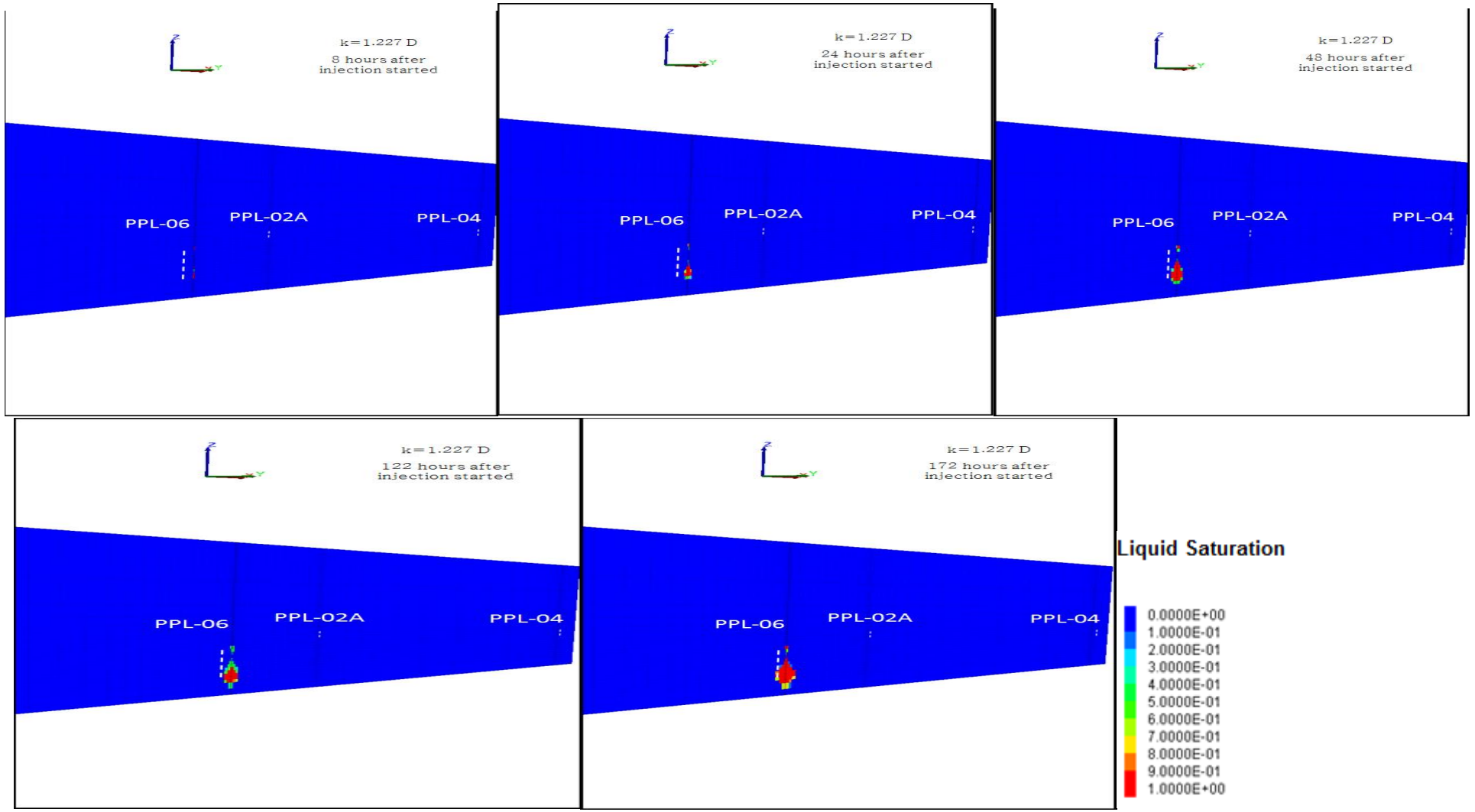

Figure 5.26 the liquid saturation distribution around PPL-06 corresponding to the injection proposed test in Figure 5.7 (Figure 5.25) in different time period after injection started (the simulation finished at 172 hours). The injection test failed to create a fully single-liquid-phase zone near the wellbore.

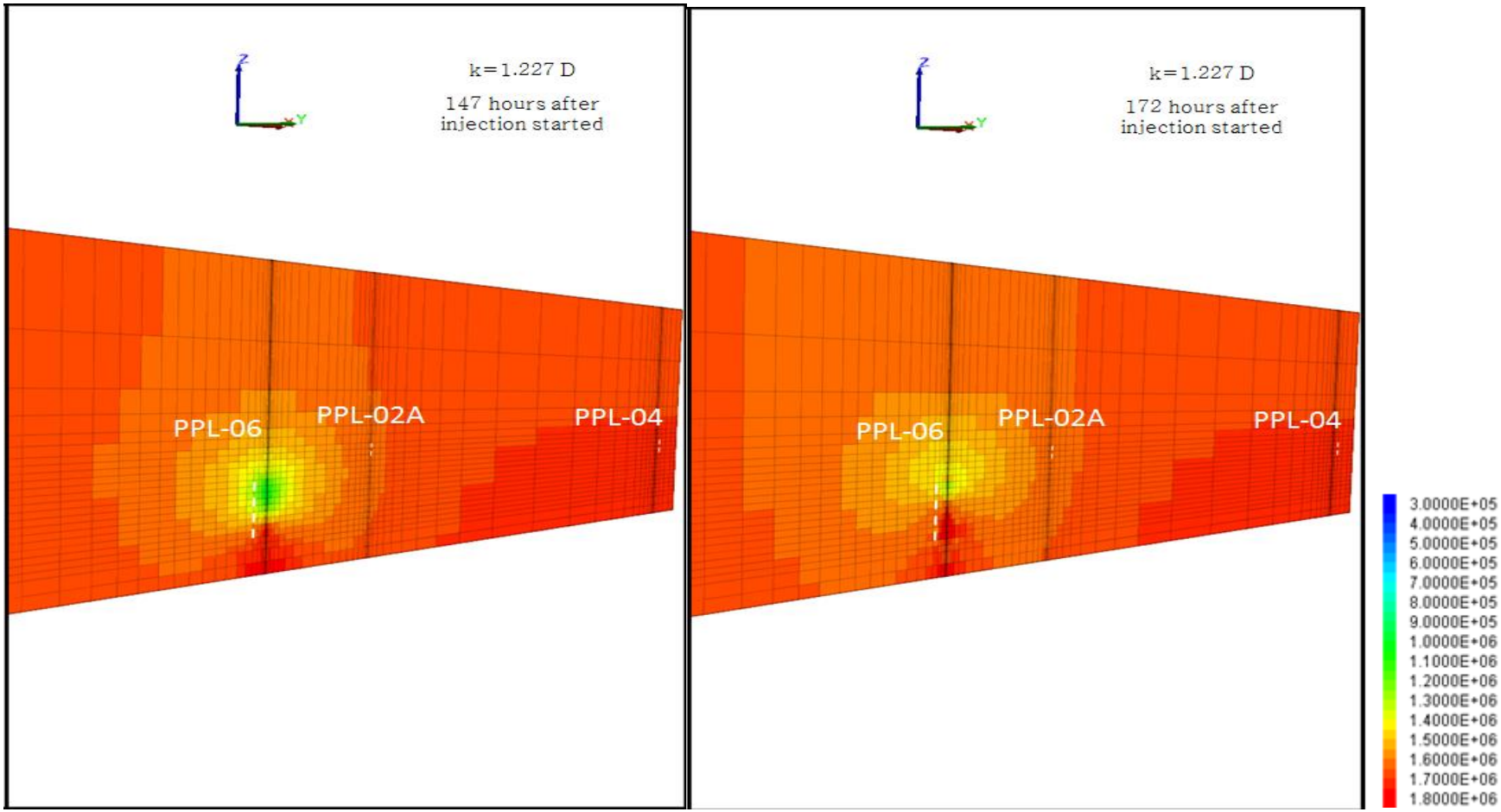

Figure 5.27 the pressure distribution around PPL-06 corresponding to the injection proposed test in Figure 5.7 (Figure 5.25) 147 hours (~6 days), and 172 hours (~7days) after injection started. The pressure dies off as the injection sopped after 168 hours (7 days). The pressure distribution has been reached to PPL-02A with the homogeneous permeability of 1.227 D, the pressure legend is in [Pa].

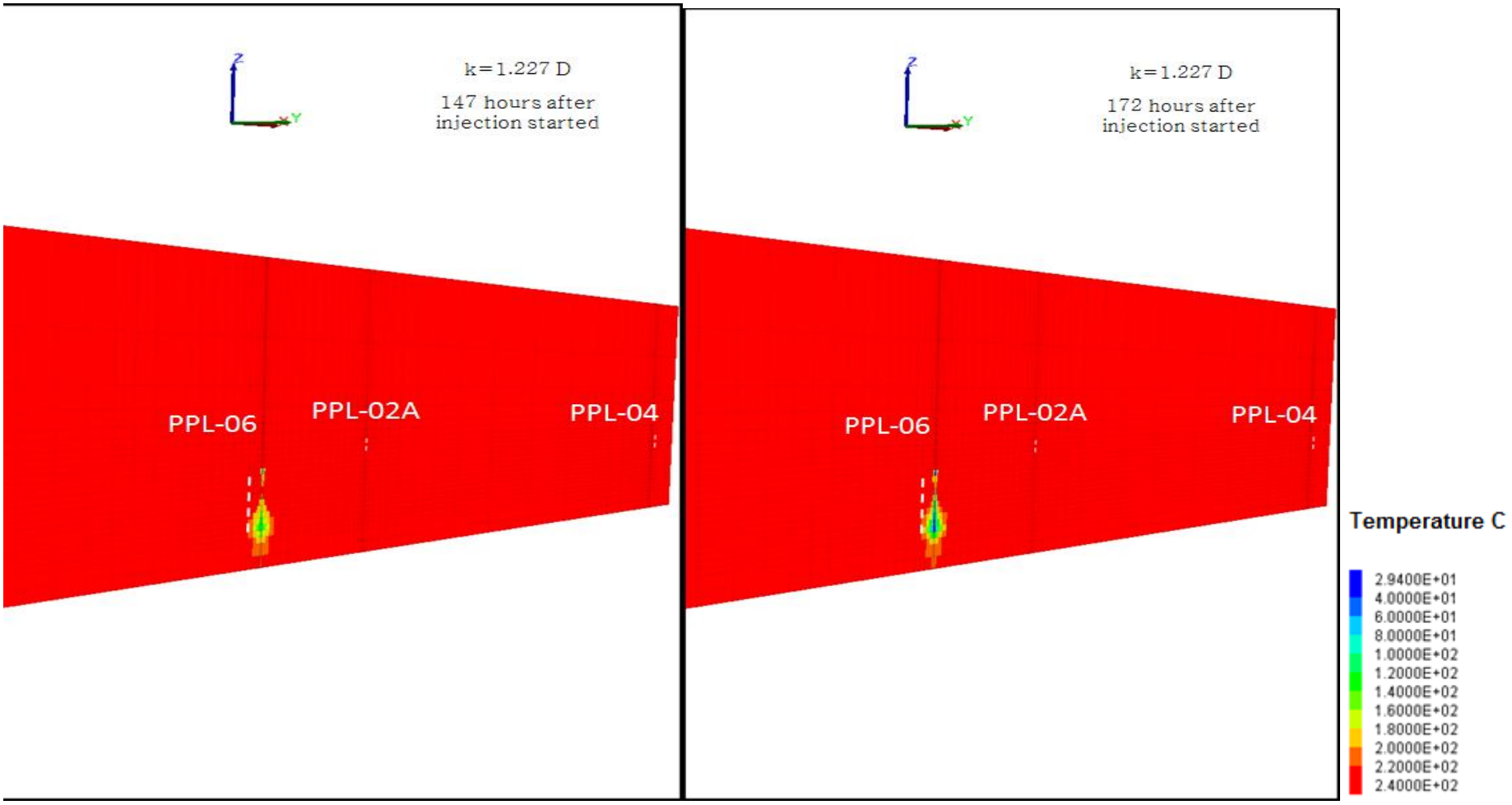

Figure 5.28 the temperature distribution around PPL-06 corresponding to the injection proposed test in Figure 5.7 (Figure 5.25) 147 hours (~6 days), and 172 hours (~7days) after injection started. The injection sopped after 168 hours (7 days). The temperature has not reached to PPL-02A with the homogeneous permeability of 1.227 D, the temperature legend is in °C.

As the next step, an injection test has been designed to evaluate the reservoir responses for long term injection at PPL−06. Therefore, an injection test as it is shown in Figure 5.29 was simulated. This injection test was designed considering the available sources at the Patuha field, in particular the available condensate to be injected at PPL−06. This test is similar to the actual injection test carried out on January 12, 2018 at PPL−06 with a maximum injection rate of 68.9 kg/s, however this maximum injection rate is extended for two months, also the step−down injection rates were extended to 10 hours to record the possible stabilized pressures. The simulated pressure results are presented in Figure 5.29. At around 103 hours after the initiation of the injection test a fully single−phase−liquid zone has been created around PPL−06 (see Figure 5.30A, D), from this point the pressure starts slightly and smoothly building up, as it is expected in single−phase−liquid reservoirs. However, the pressure is still building up as the constant injection rate of 68.9 kg/s is applied, which endorses that the typical injectivity test for vapor−dominated reservoir are not suitable and a specific strategy is required to measure the injectivity index as it was fully discussed in chapter 4. Figure 5.31A represents the step−down−rate stabilized pressures and the calculated injectivity index based on equation 4.1. Finally, as the injection started the pressure distribution reached PPL−02A after approximately 8 days. This pressure support became stronger specially after ~20 days of injection, and after ~50 days the pressure at PPL−02A has increased around 1 MPa (see Figure 5.32). According to equation 5.2, such an increase in the reservoir pressure could increase the steam production of PPL−02A ~2.5times higher, which is equal to 16.8 MWe, or 120.456 t/h based on table 2.1. The temperature at PPL−02A also was not affected by the injection after 64 days, as it is shown in Figure 5.33. The liquid saturation distribution, Figure 5.30E, suggests that at the Patuha field with the estimated−vertical−fault, the injection wells should be located at deeper zone to reduce the risks of cold−water thermal breakout. Based on this numerical simulation it is suggested that the injection starts at lower rate with a relatively long−term injection test (in the order of 30 days e.g. Figure B.2), this is considered to be beneficial for the production improvement at the Patuha field. However, further evaluation of the system is required to understand the underground fluid paths.

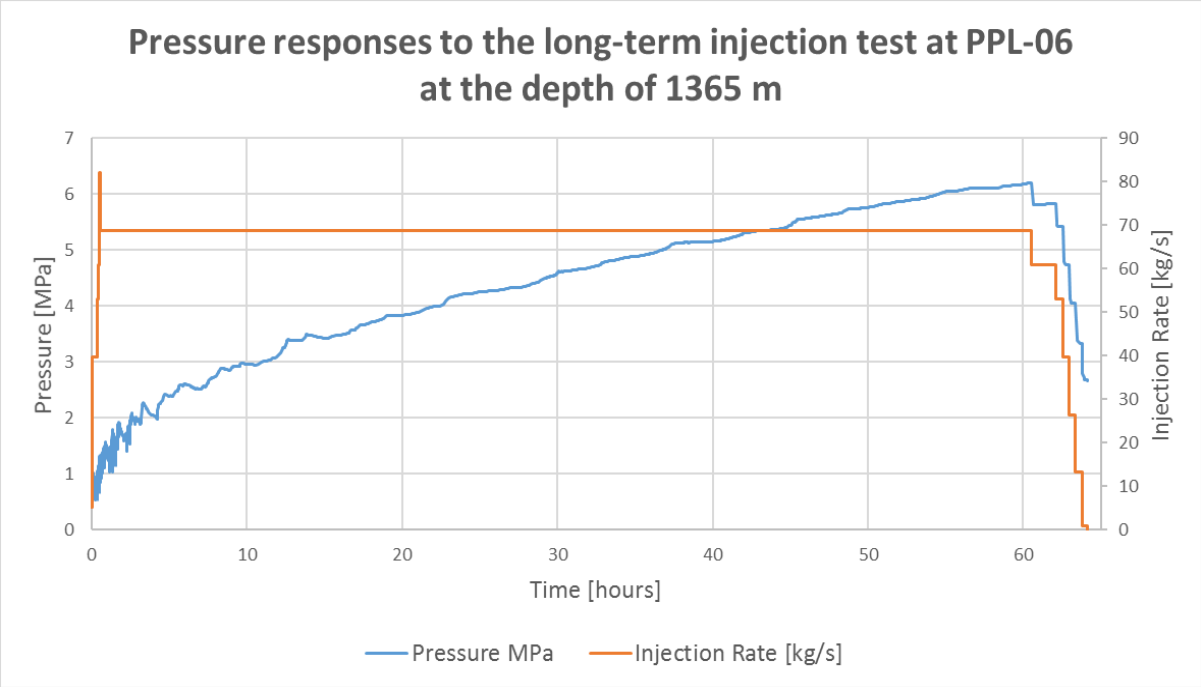

Figure 5.29 the long-term injection test and the recorded pressure of the simulation at the depth of 1365 m of PPL-06. The pressure has not stabilized during the constant step-up injection rate, it, however, stabilized at the step-down injection rate.

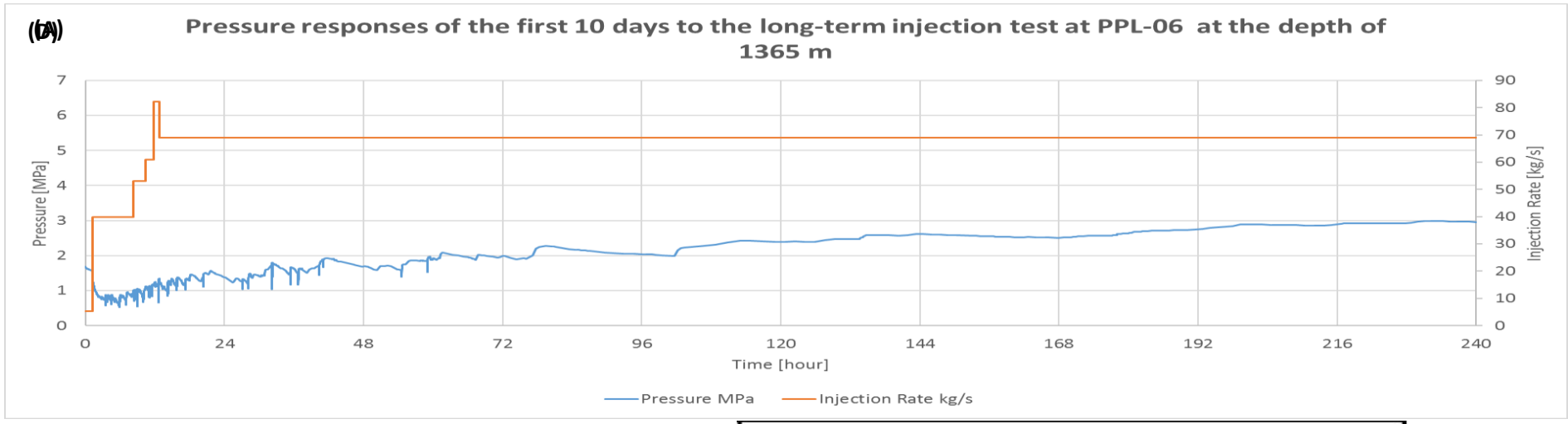
(A)
Pressure responses of the first 10 days to the long-term injection test at PPL-06 at the depth of 1365 m
Pressure [MPa]
Injection Rate [kg/s]
Time [hour]
0
24
48
72
96
120
144
168
192
216
240
Pressure MPa
Injection Rate kg/s

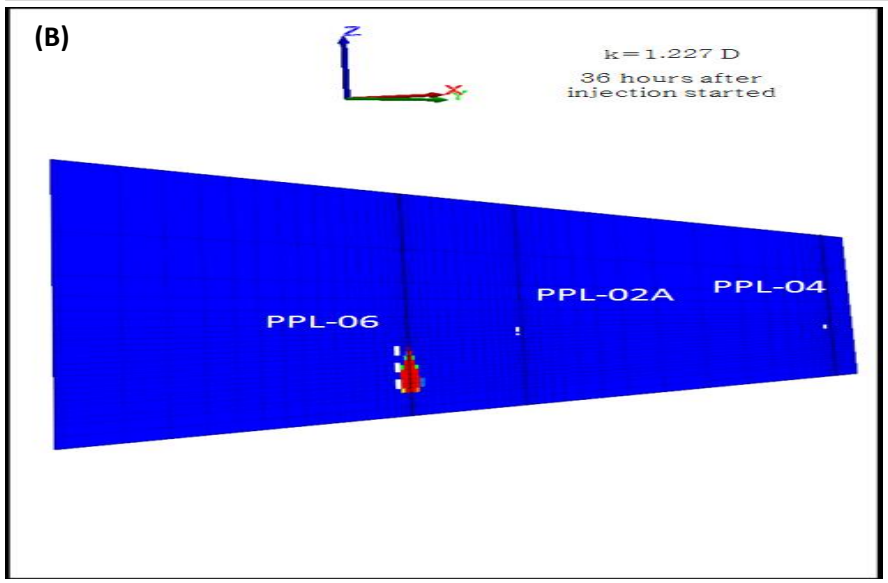
(B)
k=1.227 D
36 hours after injection started
PPL-06
PPL-02A
PPL-04

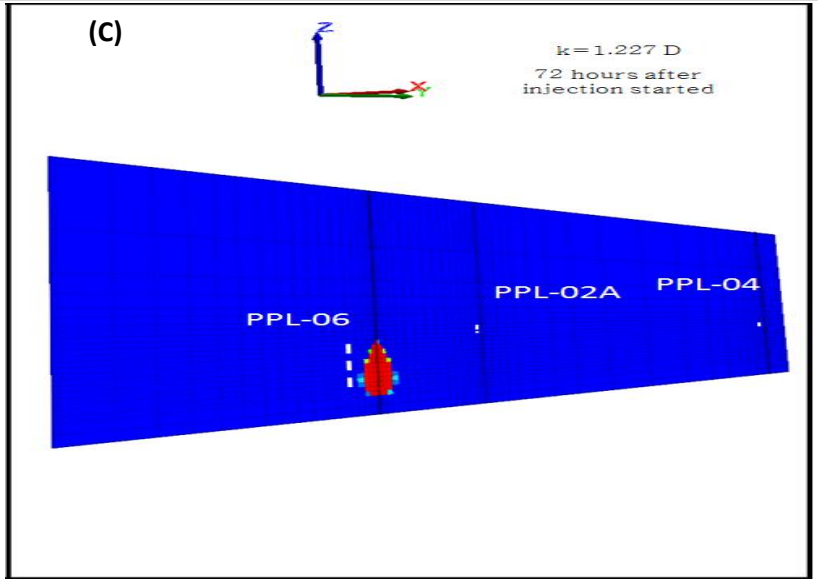
(C)
k=1.227 D
72 hours after injection started
PPL-06
PPL-02A
PPL-04

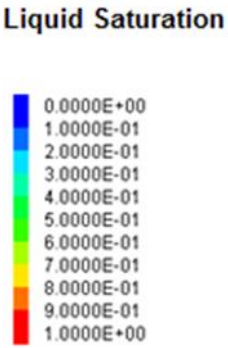
Liquid Saturation
0.0000E+00
1.0000E-01
2.0000E-01
3.0000E-01
4.0000E-01
5.0000E-01
6.0000E-01
7.0000E-01
8.0000E-01
9.0000E-01
1.0000E+00

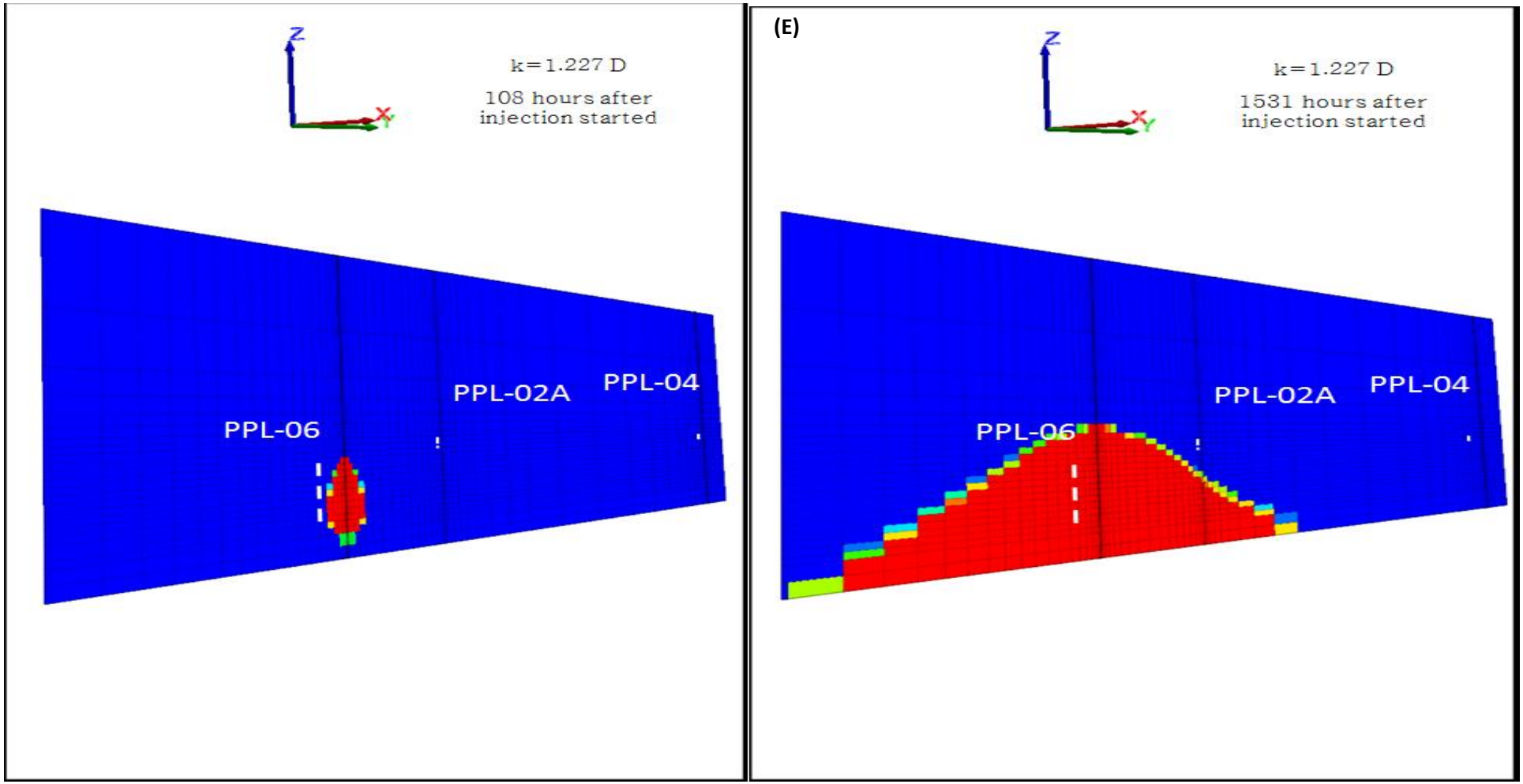

Figure 5.30 A) Pressure responses of the first 10 days to the long-term injection test at PPL-06 at the depth of 1365 m. Liquid-saturation distribution after B) 36 hours, C) 72 hours, D) 108 hours, and E)1531 hours (~64 days, when the injection has stopped). The single-phase liquid zone was fully formed around 103 (D) after the injection test started. The pressure also increased smoothly and slightly after 103 hours after injection (A).

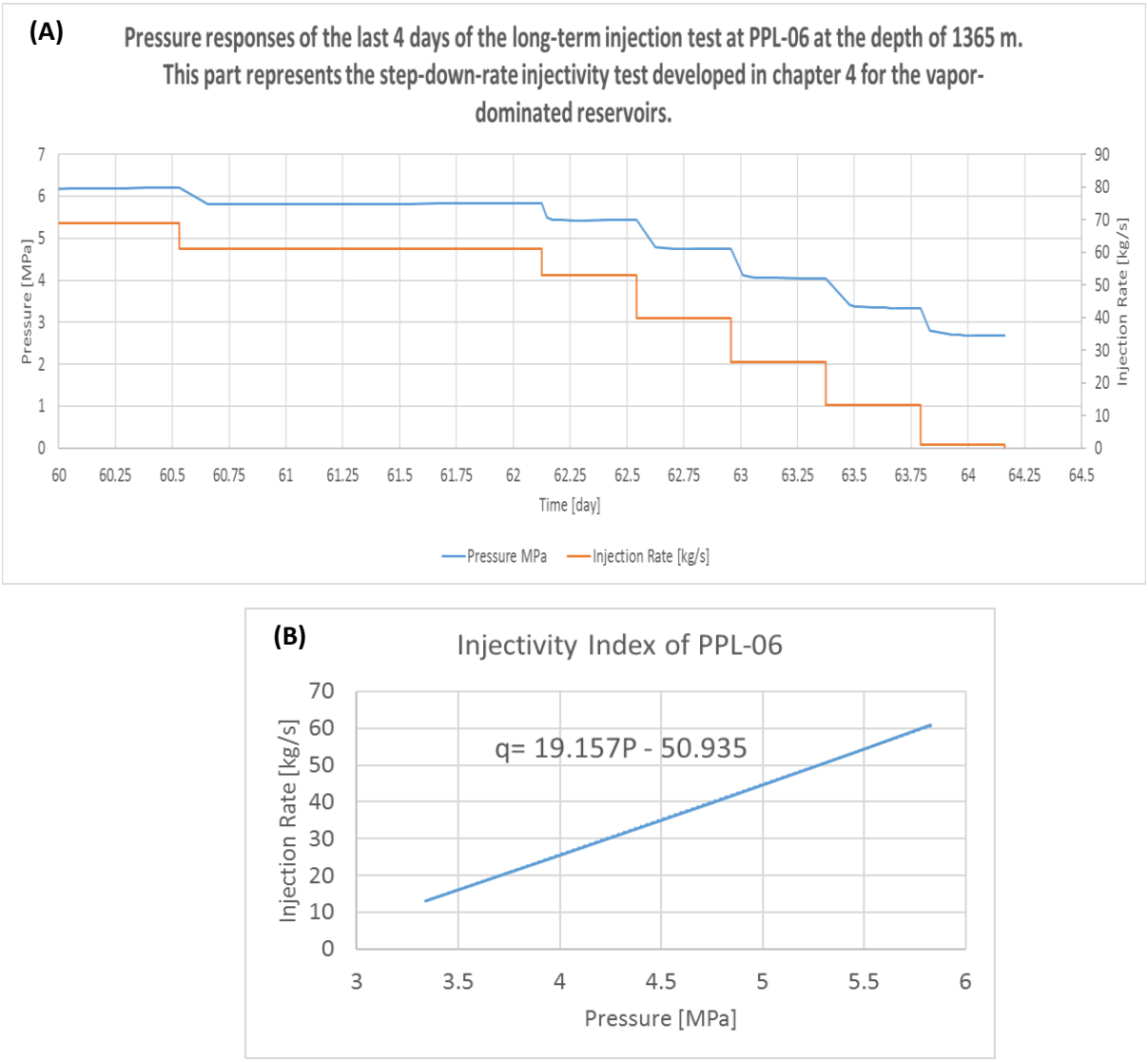

Figure 5.31 A) shows the pressure responses at the last 4 days of long-term injection test at PPL-06 at the depth of 1365 m. B) represents the injectivity index value calculated from the stabilized pressure at A.

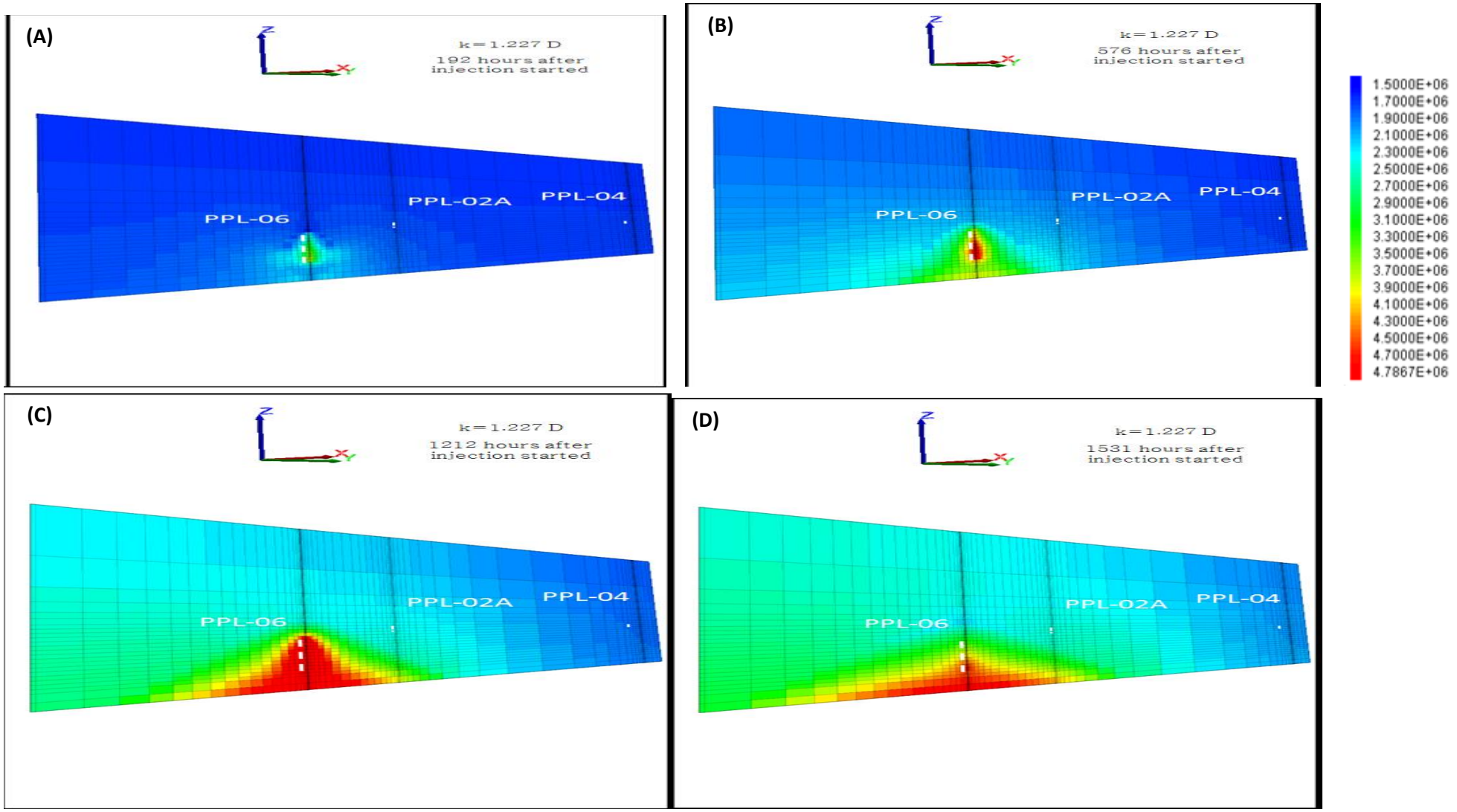

Figure 5.32 the pressure distribution during the long-term injection test along the fault connecting PPL-06, PPL-02A, and PPL-04 after A) 192 hours (8 days), B) 576 hours (24 days), C) 1212 hours (50.5 days), and D) 1531 hours (~64 days, the end of the injection) after injection. The pressure has been increased round 1 MPa after 50 days of injection (C & D). , the pressure legend is in [Pa].

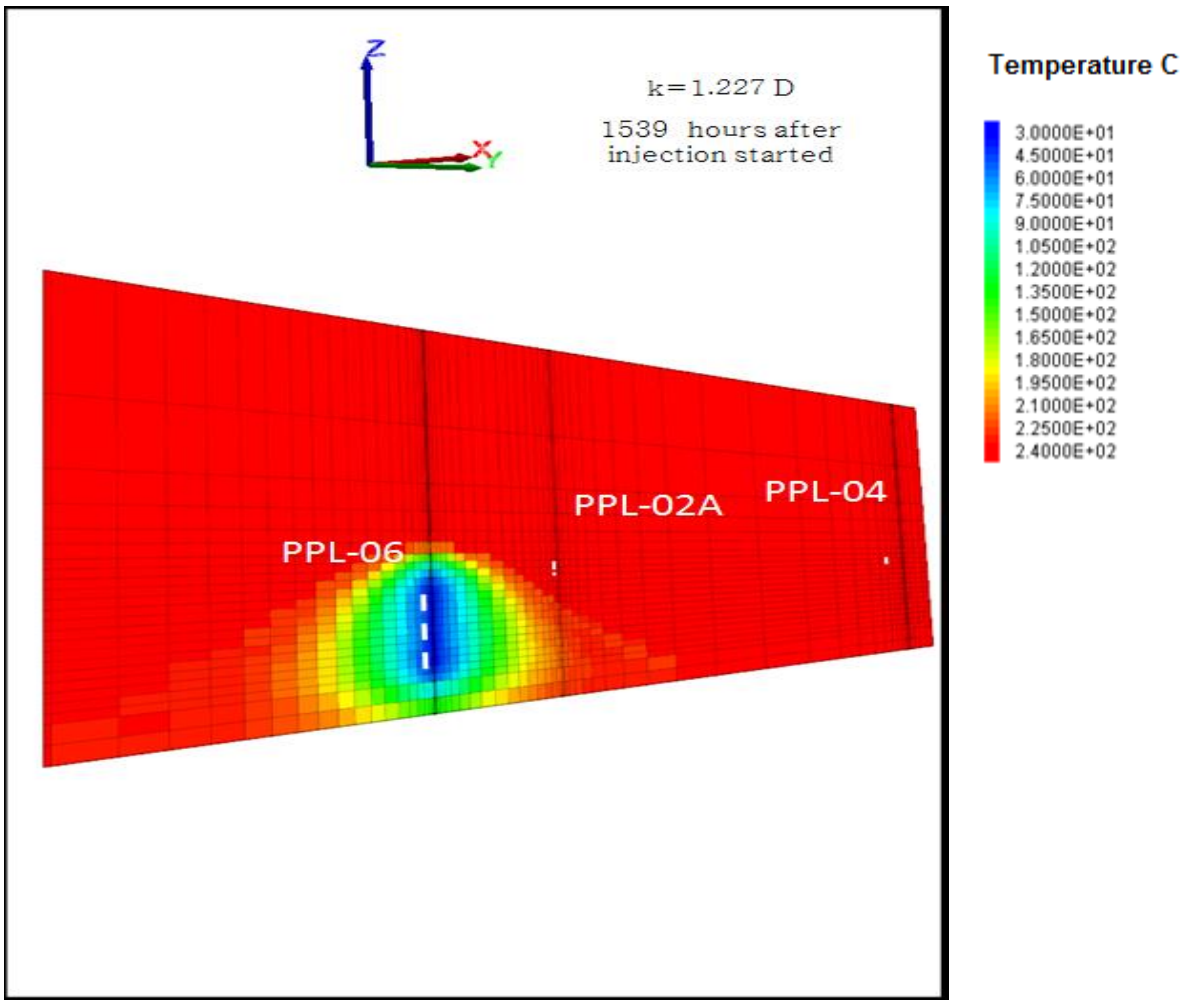

Figure 5.33 the temperature distribution after the long term injection finished (1539 hours, or ~64 days). The cold fluid did not reach the vicinity of PPL-02A.

Chapter 6. Conclusion

Efforts have been taken to collect the data, and to review the characteristics of vapor-dominated systems. The field-data-analysis showed that the observed-production-decline at the Patuha field might not be caused by poor permeability (or poor connection between well and the surrounding reservoir). The preliminary analysis on the injection test conducted on PPL-01A and -01B indicated that the wellhead pressure (WHP) is abnormally decreasing as the injection starts, and the WHP could even drop to negative values. Numerical simulation (an equivalent continuum approach) has been employed to study the observed negative pressure at the Patuha field. The results of this investigation on the factors which may cause the negative WHP could be summarized as the effect of the phase changes and the high permeable infinite zone; as the cold water penetrates the hot reservoir the pressure in part of the reservoir connected with the wellbore drops to two-phase saturated-condition (see section 2.4.3, 3.3.2, and 3.3.3), due to temperature decline. The temperature decline stops as the thermal equilibrium at prevailed saturated-condition is met. If we consider the high-permeable zone (fracture) as a gigantic element (or a huge container for simplicity, see Figure 2.14) the pressure will not build up to transit to the single-liquid-phase zone as long as the boundaries are not met by the injected fluid. Instead, it remains at the two-phase saturated condition (the flat minimum pressure at Figure 3.7).

Due to the unusual observed-pressure behavior of the wellbore during injection, it is impossible to use the typical injectivity test performed at the geothermal fields (e.g. the results of this test is used to monitor and study the permeability evolution of the reservoir and wellbore due to fluid extraction, or injection over the life span of the field). According to the results of the aforementioned numerical analyses on the abnormal pressure responses during well-injection, a proper injectivity test to quantify the injectivity index of a vapor-dominated reservoir was developed in this study. To be able to obtain reasonable pressure data from vapor-dominated systems, one way is to create a single-phase-liquid region close to the wellbore during injectivity test. The aim of this single-phase liquid region is to eliminate the effects of condensation of steam during cold water injection, therefore we are able to measure the injectivity (absolute permeability) of the reservoir near the wellbore, or physical characterization of the formation regardless of the suturing fluid. To do so, injectivity test should be done by two flowrate trends, including increasing, high injection rate, and decreasing. The increasing rate trend is necessary to avoid any thermal shock to the wellbore (e.g. casing) as well as monitoring the associated seismic events. During the increasing flowrate, steam condensation is expected and the single phase will be created near the wellbore. The data from decreasing flowrate trend might be used to obtain the injectivity index (section 4.2.1).

Further field-data analyses together with the extensive review of other vapor-dominated systems revealed that the production decline of vapor-dominated reservoirs is arising from the characteristics of the system. These systems own a very low permeable matrix surrounded the vapor-zone (due to the evolution process explained in section 1.4.4); consequently, the natural recharge to replenish the discharged-fluid of the reservoir is very low (if not impossible). Therefore, similar to all other vapor-dominated fields, the Patuha field is running out of in-situ fluid due to excessive steam production. This fact has been also endorsed by observation of production of super-heated-steam from PPL-06. This observation was implied as that the liquid existing at the porous rock to boils supplying the produced-steam is traveling far away from the wellbore (see sections 1.4.6 and 2.4.4). Therefore, the new formed-steam is additionally heated up, resulting in the production of super-heated steam.

While the in-situ fluid is running out, the remaining heat is enormous (less than 10% of the initial heat could be recovered by producing the initial dwelling fluid). Thus, this study suggests that to artificially recover the remaining heat by reinjection. The designing of the reinjection operation is a difficult challenge. The difficulties is arising from the unknown complex underground fluid-flow-path. Tracer test is the best tool to assist the designing of the reinjection test. However, this test was not performed at the Patuha field. Therefore, a detailed study was conducted by means of reviewing lessons from other reinjection experiments at vapor-dominated reservoirs, analyzing field-data, and running numerical simulation. Accordingly, an injection strategy for PPL-01B and PPL-01A has been proposed and currently is being applied at the site. Based on the proposed strategy, the condensate-injection was switched from PPL-0B to PPL-01A (since 24/11/2017), because not only was there no evidence of observed production improvement or pressure support during nearly two decades of injection, but also based on the field-data this well was drilled at the peripheral of the reservoir, and most likely did not lead the reinjected fluid to the reservoir zone. The reinjection at PPL-01A drilled inside the reservoir could potentially increase the chance of pressure support or production improvement, however, the data has not been received yet by the author to make a full analysis.

A multi-purpose injection test was designed for PPL-06. The main goals were not only to improve the production of near wellbores, but also to measure the reservoir properties including injectivtiy index, the depth, thickness, permeability, pressure, and temperature of the high-permeable zone(s). The actual injection test (conducted on January 12, 2018) was modified from the proposed-injection plan to meet the available sources at the field. The injectivity test concept developed for the vapor-dominated reservoir employed as part of the injection plan, however, it was not successfully done since the test was not performed long enough to create the single-phase-liquid zone near the wellbore. Based on the analysis of the results of the injection test at PPL-06, the depth, thickness, in-situ permeability (for the first time), pressure and temperature of the high-permeable zone were measured. The observation of the production improvements of PPL-02A and PPL-04 during the injection at PPL-06 were suspected if it was caused by the injection. Therefore,

based on the data a numerical model (using equivalent continuum approach) was employed to simulate the fracture zone as an equivalent porous medium. The numerical model was developed to analyze the injection experiment at PPl-06. The simulation was conducted applying two key assumptions, the fault zone was modeled with a homogenous permeability as the in-put and no production at PPL-04 and PPL-02A was modeled since not sufficient production data was available. The sensitivity analysis carried out with the actual injection test at PPL-06 revealed that in order to expect any production improvement at the aforementioned producers the fault permeability should be higher than 15.5 D. This high permeability value does not seem to be practical. Therefore, considering the key assumptions the injection at PPL-06 could not have affected the production of PPL-04 and PPL-02A. The further analysis of the actual injection plan revealed that the observed production decline (Figure 5.15) of PPL-06 after the actual injection test is due to the partial formation of single-phase-liquid zone near the production zone, which consequently decreased the gas relative permeability (Figure 5.24). The numerical simulation also suggested that the wellbore was under two-phase condition during the injection, therefore the test failed to obey the concept of injectivity test developed for vapor-dominated reservoirs. Additionally, the simulation was able to grasp the observed-pressure-decline during the injection (Figure 5.20) at PPL-06, however, further studies and analysis in particular on the relative permeability is required for a better match.

Based on the developed model, two more injection tests have been modeled. The first injection test was same as the initial proposed injection test for one week in the reservoir with the same calculated homogenous permeability of 1.227 D (Figure 5.7). Although, this injection test (presuming the two key assumptions) failed to form the single-liquid-phase zone (to measure the injectivity index), it could support the pressure at PPL-02A. Similarly due to formation of partial single-liquid-phase zone near the well, the steam production of PPL-06 will decrease.

A relatively long injection test has been conducted with the given key assumptions. The injection rate are similar with the actual injection test at PPL-06, however, the injection rate of 68.9 kg/s was extended for (~65 days) and the decreasing trend injection steps were extended to 10 hours each (Figure 5.29). The simulation results revealed that under the given assumption, not only the production at other producers (in particular at PPL-02A) would be improved (it actually could be increased by 2.5 times) by pressure support, the temperature will not change at the producers (no thermal breakthrough was observed). The production of the Patuha field would be increased if PPL-06 is injected with a proper injection schedule. This wellbore is currently producing less than 1.5 MWe, however, simulations show that injection at this wellbore could increase the production of PPL-02A up to 12.45 MWe. The injectivity index was measure by the developed concept at this simulation. Moreover, the results support the idea of choosing the depth of the injection well as deep as possible to reduce the risk of cold water thermal breakthrough. The analysis also showed that the minimum required time to reach the

single-liquid-phase zone under the injection rate of 68.9 kg/s (with the aforementioned assumptions) is ~105 hours which is around 5 days.

In order to take the proper reinjection strategic management, it is vital to find out the best optimum location and depth, however, the reinjection strategy should be updated by a proper the monitoring of the production rate and enthalpy of all the system over the time. Tracer tests are important tool for a design of a successful reinjection plan. The location and the strategy of reinjection is most often empirical and site-specific depending on the setting of the given geothermal system. However, we can learn from other vapor-dominated systems. In terms of the location and depth of the injector wells, infield reinjection, which required the drilling of the injection well in the vicinity of the producers (less than 1~2 km) in vapor-dominated system is the key in maintaining steam productivity of the fields as it is reported in the literature in Kamojang, Larderello, and The Geysers (the largest vapor-dominated reservoir in the world). The optimum depth for infield reinjection in this system varies, depending on reservoir structure. For example, the reinjection target is preferred to be deeper than production zones at Kamojang, above the reservoir at Larderello and at same depth as the reservoir at The Geysers. These strategies are selected to provide enough recharge and allow good residence time for injected fluid to heat up. However, among all these vapor-dominated systems Kamojang is the closest geothermal setting, since they are both in central Java and in volcanic region and islandic-arc system. Also, it is believed that faults and fractures in both fields have similar dipping angle between approximately 75° and 90°. Therefore, it was more meaningful to take the similar strategy as the first experiment to inject at the deeper zone in Patuha.

By the results of this study, the current strategy of the field owner of the Patuha field which is drilling new producers (makeup wells) was strongly argued. It may increase the production rate for a short period, but it would have significant effect on the production decline rate. It has been suggested as the proper strategy to inject at least 60 % of the produced fluid close enough to the producers (less than 1~2 km) to improve or maintain the reservoir pressure and the production rate. However, this strategy needs to be investigated more deeply, with field scale injection tests. The injection test at PPL-06 and the reinjection strategy for PPL-01A and PPL-01B were suggested based on the available sources. The main reasons for injection at PPL-06 were the fact that it is one of the deepest wells of the field, it is producing small amount of super-heated steam, and the observed reservoir pressure decline over the production time. Additionally, the results of the numerical simulation supports that injection at deeper zones at the Patuha field would be beneficial. In many cases, for example the Geysers the poor producer has been converted to a successful injector in a way that the reinjection practice increased the production rate at the near connected producers.

Reference

A.R. Aqui, S. Z. (2011). Permeability Enhancement of Conventional Geothermal Wells. *New Zealand Geothermal Workshop 2011 Proceedings*.

Agency, I. E. (2017). *Electricity Information 2017*.

Allis, R. (2000). *Insights on the formation of vapor-dominated geothermal systems.* Paper presented at the Proceedings World Geothermal Congress.

Aqui, A., & Zarrouk, S. (2011). *Permeability enhancement of conventional geothermal wells.* Paper presented at the New Zealand Geothermal Workshop.

Arias, A., Dini, I., Casini, M., Fiordelisi, A., Perticone, I., & Dell'Aiuto, P. (2010). *Geoscientific feature update of the Larderello–Travale geothermal system (Italy) for a regional numerical modeling.* Paper presented at the Proceedings world geothermal congress.

Armstead, H., & Tester, J. (1987). Heat mining: a new source of energy, 29. *West 35th Street, New York NY, 10001*.

Armstead, H. C. H., & Tester, J. W. (1986). Heat mining.

Axelsson, G. (2012). Role and management of geothermal reinjection. *001226914*.

Axelsson, G. (2013a). Geothermal well testing. *Short Course V on Conceptual Modelling of Geothermal Systems", organized by UNU-GTP and LaGeo, in Santa Tecla, El Salvador*.

Axelsson, G. (2013b). *Tracer tests in geothermal resource management.* Paper presented at the EPJ Web of Conferences.

Axelsson, G., Thórhallsson, S., & Björnsson, G. (2006). *Stimulation of geothermal wells in basaltic rock in Iceland.* Paper presented at the Enhanced geothermal innovative network for Europe Workshop.

Axelsson G., a. B. G. (1987). *Analysis of Production Data from Fractured Liquid Dominated Geothermal Reservoirs in Iceland*. Paper presented at the Geothermal Resources Council Transactions.

Ayling, B. F., Hogarth, R. A., & Rose, P. E. (2016). Tracer testing at the Habanero EGS site, central Australia. *Geothermics, 63*, 15-26. doi:https://doi.org/10.1016/j.geothermics.2015.03.008

Barbier, E. (2002). Geothermal energy technology and current status: an overview. *Renewable and Sustainable Energy Reviews, 6*(1), 3-65. doi:https://doi.org/10.1016/S1364-0321(02)00002-3

Barker, B., Gulati, M., Bryan, M., & Riedel, K. (1992). Geysers reservoir performance. *Monograph on The Geysers Geothermal Field, 17*, 167-177.

Beall, J. J., Enedy, S., & W. T. Box, J. (1989). Recovery of injected condensate as steam in the south Geysers field. *Geothermal Resources Council Transactions, 13*, 351-358.

Bjornsson, G., & ISOR, I. G. (2004). *Reservoir conditions at 3-6 km depth in the Hellisheidi geothermal field, SW-Iceland, estimated by deep drilling, cold water injection and seismic monitoring.* Paper presented at the Proceedings.

Bodvarsson, G. (1972). Thermal problems in the siting of reinjection wells. *Geothermics, 1*(2), 63-66.

Bodvarsson, G. S., Benson, S. M., Sigurdsson, O., Stefansson, V., & Eliasson, E. T. (1984). The Krafla geothermal field, Iceland: 1. Analysis of well test data. *Water Resources Research, 20*(11), 1515-1530.

Breede, K., Dzebisashvili, K., Liu, X., & Falcone, G. (2013). A systematic review of enhanced (or engineered) geothermal systems: past, present and future. *Geothermal Energy, 1*(1), 4. doi:10.1186/2195-9706-1-4

Bruel, D. (2002). Impact of induced thermal stresses during circulation tests in an engineered fractured geothermal reservoir: example of the Soultz-sous-Forets European hot fractured rock geothermal project, Rhine Graben, France. *Oil & Gas Science and Technology, 57*(5), 459-470.

Calore, C., Pruess, K., & Celati, R. (1986). *Modeling studies of cold water injection into fluid-depleted, vapor-dominated geothermal reservoirs*. Retrieved from

Cappetti, G., & Ceppatelli, L. (2005). *Geothermal Power Generation in Italy: 2000-2004 Update Report.* Paper presented at the Proceedings.
Cappetti, G., Parisi, L., Ridolfi, A., & Stefani, G. (1995). *Fifteen years of reinjection in the Larderello-Valle Secolo area: analysis of the production data.* Paper presented at the Proceedings.
Cappetti, G., & Stefani, G. (1994). Strategies for sustaining production at Larderello. *Bulletin of the Geothermal Resources Council, 23*(9), 303-306.
Cataldi, R. (1993). Review of historiographic aspects of geothermal energy in the Mediterranean and Mesoamerican areas prior to the Modern Age. *Geo-Heat Center Quarterly Bulletin;(United States), 15*(1).
Cathles, L. M. (1977). An analysis of the cooling of intrusives by ground-water convection which includes boiling. *Economic Geology, 72*(5), 804-826. doi:10.2113/gsecongeo.72.5.804
Chun, K. (2013). *Fracture propagation under poro-thermally induced stress using the displacement discontinuity method.* Paper presented at the Proceedings of the Thirty-Eighth Workshop on Geothermal Reservoir Engineering, Stanford University, Stanford, California.
Clifton, R., Brown, U., & Wang, J. (1991). *Modeling of In-Situ Stress Change Due to Cold Fluid Injection.* Paper presented at the International Arctic Technology Conference.
Clotworthy, A., & Hingoyon, C. (1995). *Injectivity Testing for Vapour Dominated Feed Zones*. Retrieved from
Commission, E. (2006). European Commission, 2009. White paper, Adapting to climate change: Towards a European framework for action, Belgium: European Commission,.
Commission, E. (2009). White paper, Adapting to climate change: Towards a European framework for action, Belgium: European Commission.
Committee, I. F. (1967). A formulation of the thermodynamic properties of ordinary water substance. *Wiley Online Library*.
Diaz, A. R., Kaya, E., & Zarrouk, S. J. (2016). Reinjection in geothermal fields− A worldwide review update. *Renewable and Sustainable Energy Reviews, 53*, 105-162.
Dobson, P., Asanuma, H., Huenges, E., Poletto, F., Reinsch, T., & Sanjuan, B. (2017). *Supercritical geothermal systems-a review of past studies and ongoing research activities.* Paper presented at the 42nd Workshop on Geothermal Reservoir Engineering.
Donaldson, I. G. (1962). Temperature gradients in the upper layers of the earth's crust due to convective water flows. . *J. Geophys. Res. 67, 3449-3459.*
Dunn, J. C., & Hardee, H. C. (1981). Superconvecting geothermal zones. *Journal of Volcanology and Geothermal Research, 11*(2), 189-201. doi:https://doi.org/10.1016/0377-0273(81)90022-6
Dusseault, M. (1993). *Stress changes in thermal operations.* Paper presented at the SPE International Thermal Operations Symposium.
Dwikorianto, T., Abidin, Z., & Kamah, Y. (2005). *Tracer injection evaluation in Kamojang geothermal field, West Java, Indonesia.* Paper presented at the Proc. World Geothermal Congress 2005, Antalya, Turkey, 24–29 April.
Dwikorianto, T., Zuhro, A. A., & Yani, A. (2010). Sustainable development of the Kamojang geothermal field. *Geothermics, 39*(4), 391-399.
Economic, W. (2015). Global Risks Reports - World Economic Forum. Retrieved from http://reports.weforum.org/global-risks-2015/
Edenhofer, O., Pichs-Madruga, R., Sokona, Y., Seyboth, K., Matschoss, P., Kadner, S., . . . Schlömer, S. (2011). IPCC special report on renewable energy sources and climate change mitigation. *Prepared By Working Group III of the Intergovernmental Panel on Climate Change, Cambridge University Press, Cambridge, UK*.
Elsworth, D. (1989). Thermal permeability enhancement of blocky rocks: One-dimensional flows. *International Journal of Rock Mechanics and Mining Sciences & Geomechanics Abstracts, 26*(3), 329-339. doi:https://doi.org/10.1016/0148-9062(89)91981-5
Enedy, S., Enedy, K., & Maney, J. (1991). *Reservoir response to injection in the Southeast Geysers*. Retrieved from

Enedy, S. L. (2014). Benefit of a Typical Injection Well at The Geysers Field. *Geothermal Resources Council Transactions, 38*, 985-989.
Faust, C. R. (1976). Numerical simulation of fluid flow and energy transport in liquid-and vapor-dominated hydrothermal systems.
Finnie, I., Cooper, G., & Berlie, J. (1979). *Fracture propagation in rock by transient cooling.* Paper presented at the International Journal of Rock Mechanics and Mining Sciences & Geomechanics Abstracts.
Fitzgerald, S. D., & Woods, A. W. (1995). On vapour flow in a hot porous layer. *Journal of Fluid Mechanics, 293*, 1-23.
Flores-Armenta, M., and R. Tovar-Aguado. (2008). Thermal Fracturing of Well H-40, Los Humeros Geothermal Field. *Geothermal Resources Council Transactions, 32*, 445-448.
Flores, M., Davies, D., Couples, G., & Palsson, B. (2005). *Stimulation of geothermal wells, can we afford it.* Paper presented at the Proceedings World Geothermal Congress, Antalya, Turkey.
Fradkin L. J., S. M. L., and McNabb A. (1981). On identification and validation of some geothermal models. *Water Resources Research, 17*(4), 929-936. doi:doi:10.1029/WR017i004p00929
Fridleifsson, I. B. (2001). Geothermal energy for the benefit of the people. *Renewable and Sustainable Energy Reviews, 5*(3), 299-312. doi:https://doi.org/10.1016/S1364-0321(01)00002-8
FUKUDA, D., KUWANO, T., & ITOI, R. (2013). Two-Phase Tracer Tests Using Alcohols at the Matsukawa Vapor-Dominated Geothermal Reservoir: Evaluation of Responses to Water Injection and Prediction of Production Interference. *Journal of the Geothermal Research Society of Japan, 35*(2), 69-81.
Fukuda, D., Kuwano, T., & Itoi, R. (2018). Estimation of the steam fraction of injected water at the Matsukawa vapor-dominated geothermal field using two-component, two-phase tracers. *Geothermics, 71*, 167-177.
Garg, S. K., & Combs, J. (1997). Use of slim holes with liquid feedzones for geothermal reservoir assessment. *Geothermics, 26*(2), 153-178. doi:https://doi.org/10.1016/S0375-6505(96)00038-7
Geyer, J. F., & Nemat-Nasser, S. (1982). Experimental investigation of thermally induced interacting cracks in brittle solids. *International Journal of Solids and Structures, 18*(4), 349-356.
Ghassemi, A., Nygren, A., & Cheng, A. (2008). Effects of heat extraction on fracture aperture: A poro–thermoelastic analysis. *Geothermics, 37*(5), 525-539. doi:https://doi.org/10.1016/j.geothermics.2008.06.001
Ghassemi, A., Tarasovs, S., & Cheng, A. H. D. (2003). An integral equation solution for three-dimensional heat extraction from planar fracture in hot dry rock. *International Journal for Numerical and Analytical Methods in Geomechanics, 27*(12), 989-1004. doi:doi:10.1002/nag.308
Ghassemi, A., Tarasovs, S., & Cheng, A. H. D. (2005). Integral equation solution of heat extraction-induced thermal stress in enhanced geothermal reservoirs. *International Journal for Numerical and Analytical Methods in Geomechanics, 29*(8), 829-844. doi:doi:10.1002/nag.440
Ghassemi, A., Tarasovs, S., & Cheng, A. H. D. (2007). A 3-D study of the effects of thermomechanical loads on fracture slip in enhanced geothermal reservoirs. *International Journal of Rock Mechanics and Mining Sciences, 44*(8), 1132-1148. doi:https://doi.org/10.1016/j.ijrmms.2007.07.016
Goyal, K., & Box Jr, W. (1992). *Injection recovery based on production data in Unit 13 and Unit 16 areas of The Geysers field*. Retrieved from
Goyal K. P., a. B. W. T. J. (1990). Reservoir Response To Production: Castle Rock Springs Area, East Geysers, California, U.S.A: Society of Petroleum Engineers.
Goyal, K. P. (1995). Injection recovery factors in various areas of the southeast Geysers, California. *Geothermics, 24*(2), 167-186. doi:https://doi.org/10.1016/0375-6505(95)91146-B

Goyal, K. P. (1999). Injection related cooling in the Unit 13 area of theSoutheast Geysers, California, usa. *Geothermics, 28*(1), 3-19. doi:https://doi.org/10.1016/S0375-6505(98)00042-X
Grant, M. A., & Bixley, P. F. (2011) *Geothermal Reservoir Engineering (Second Edition)*. Boston: Academic Press.
Grant, M. A., Clearwater, J., Quinão, J., Bixley, P. F., & Le Brun, M. (2013). *Thermal stimulation of geothermal wells: a review of field data.* Paper presented at the Proceedings.
Grant, M. A., Donaldson, I.G., and Bixley, P.F. (1982). *Geothermal Reservoir Engineering*. New York: Academic Press.
Gringarten, A., Witherspoon, P., & Ohnishi, Y. (1975). Theory of heat extraction from fractured hot dry rock. *Journal of Geophysical Research, 80*(8), 1120-1124.
Gunnarsson, G., & Energy, O. R. (2011). *Mastering reinjection in the Hellisheidi field, SW-Iceland: a story of successes and failures.* Paper presented at the Proc., 36th Workshop on geothermal reservoir engineering, Stanford University.
Gunnarsson, G., Kristjánsson, B. R., Gunnarsson, I., & Júlíusson, B. M. (2015). *Reinjection into a fractured reservoir—induced seismicity and other challenges in operating reinjection wells in the Hellisheiði Field, SW-Iceland.* Paper presented at the Proceedings world geothermal congress.
Hall, R. (2002). Cenozoic geological and plate tectonic evolution of SE Asia and the SW Pacific: computer-based reconstructions, model and animations. *Journal of Asian Earth Sciences, 20*(4), 353-431.
Hanano, M. (2003). Sustainable steam production in the Matsukawa geothermal field, Japan. *Geothermics, 32*(3), 311-324. doi:https://doi.org/10.1016/S0375-6505(03)00023-3
Hanano, M., Ohmiya, T., & Sato, K. (1991). Reinjection experiment at the matsukawa vapor-dominated geothermal field: Increase in steam production and secondary heat recovery from the reservoir. *Geothermics, 20*(5), 279-289. doi:https://doi.org/10.1016/0375-6505(91)90021-M
Héðinsdóttir, H. (2014). *Mechanisms of injectivity enhancement in the thermal stimulation of geothermal wells.* (Master), ETH Zürich.
Holm, A. (2010). Geothermal Energy: International Market Update.
Honarpour, M. M. (2018). *Relative permeability of petroleum reservoirs*: CRC press.
Hornbrook, J. W. (1994). *The Effects of Adsorption on Injection into and Production from Vapor Dominated Geothermal Reservoirs.* Ph. D. thesis, Stanford University, California.
Horne, R. (1985). Reservoir engineering aspects of reinjection. *Geothermics, 14*(2-3), 449-457.
Horne, R. N. (1985). Reservoir engineering aspects of reinjection. *Geothermics, 14*(2), 449-457. doi:https://doi.org/10.1016/0375-6505(85)90082-3
Hurst, A. W., & Dibble, R. R. (1981). Bathymetry, heat output and convection in Ruapehu Crater Lake, New Zealand. *Journal of Volcanology and Geothermal Research, 9*(2), 215-236. doi:https://doi.org/10.1016/0377-0273(81)90005-6
James, R. (1968). Wairakei and Larderello geothermal power systems compared. *N. Z. J. Sci. Technol., 11 (1968)*, 706-719.
Jansen, G., & Miller, S. A. (2017). On the role of thermal stresses during hydraulic stimulation of geothermal reservoirs. *Geofluids, 2017*.
Kajugus, S. I. (2015). *Geothermal Reservoir Evaluation Using Well Testing and Analytical Modelling-Case Example: Reykjanes Geothermal System, SW Iceland.* (Doctoral dissertation), University of Iceland.
Karner, S. L., & Renner, J. (2005). *Stimulation techniques used in enhanced geothermal systems: perspectives from geomechanics and rock physics*. Retrieved from
Kaya, E. (2016a). Modelling reinjection into vapour-dominated two-phase systems: Part 1—Experiments on model design. *Geothermics, 60*, 175-195.
Kaya, E. (2016b). Modelling reinjection into vapour-dominated two-phase systems: Part 2-reinjection experiments on the 3D Model. *Geothermics, 60*, 196-217.

Kaya, E., Zarrouk, S. J., & O'Sullivan, M. J. (2011). Reinjection in geothermal fields: A review of worldwide experience. *Renewable and Sustainable Energy Reviews, 15*(1), 47-68. doi:https://doi.org/10.1016/j.rser.2010.07.032

Khan, M. A., & Truschel, J. (2010). The Geysers geothermal field, an injection success story. *GRC Trans, 34*, 1239-1242.

Kitao, K., Ariki, K., Watanabe, H., & Wakita, K. (1995). Cold-water well stimulation experiments in the Sumikawa geothermal field, Japan. *Bulletin of the Geothermal Resources Council, 24*(2), 53-61.

Kohl, T., Evansi, K. F., Hopkirk, R. J., & Rybach, L. (1995). Coupled hydraulic, thermal and mechanical considerations for the simulation of hot dry rock reservoirs. *Geothermics, 24*(3), 345-359. doi:https://doi.org/10.1016/0375-6505(95)00013-G

KPMG. (2012). Expect the Unexpected: Building business value in a changing world, London.

KPMG. (2014). Future State 2030: The Global Megatrends and Shaping Gov- ernments, London.

Kurashige, M., Furuzumi, M., & Kamijo, S. (1997). Rough size estimation of a thermally fractured zone in an infinite hot rock mass. *Journal of thermal stresses, 20*(7), 729-747.

Layman, E. B., & Soemarinda, S. (2003). *The Patuha vapor-dominated resource West Java, Indonesia.* Paper presented at the Proceedings of the 28th Workshop on Geothermal Reservoir Engineering, Stanford University.

Mahagyo, R. P., Molling, P. A., & Hidayaturrobi, A. D. (2010). *Review of baseline geochemical model and the impact of production at the darajat geothermal field, Indonesia.* Paper presented at the Proc., the World Geothermal Congress, Bali, Indonesia.

Marconcini, R., McEdwards, D., Neri, G., Ruffilli, C., Schroeder, R., Weres, O., & Witherspoon, P. (1977). *Modeling vapor dominated geothermal reservoirs*. Retrieved from

Maria, R. B. S. (1996). *OPTIMIZATION OF INJECTION INTO VAPOR-DOMINATED GEOTHERMAL RESERVOIRS CONSIDERING ADSORPTION.* Stanford University.

Matek, B. (2016). Annual U.S. & Global Geothermal: Power Production Report.

Mock, J. E., Tester, J. W., & Wright, P. M. (1997). Geothermal energy from the earth: its potential impact as an environmentally sustainable resource. *Annual review of Energy and the Environment, 22*(1), 305-356.

Mohammadzadeh Bina, S., Jalilinasrabady, S., Fujii, H., & Pambudi, N. A. (2018). Classification of geothermal resources in Indonesia by applying exergy concept. *Renewable and Sustainable Energy Reviews, 93*, 499-506. doi:https://doi.org/10.1016/j.rser.2018.05.018

Nathenson, M. (1975). *Some reservoir engineering calculations for the vapor-dominated system at Larderello, Italy* (2331-1258). Retrieved from

Newman, R. S. (2018). *Numerical Modeling of Cold Water Injection into Supercritical Geothermal Reservoirs* (Master's), Reykjavík University.

Nicholson, K. (2012). *Geothermal fluids: chemistry and exploration techniques*: Springer Science & Business Media.

Nishijima, J., & Naritomi, K. (2017). Interpretation of gravity data to delineate underground structure in the Beppu geothermal field, central Kyushu, Japan. *Journal of Hydrology: Regional Studies, 11*, 84-95. doi:https://doi.org/10.1016/j.ejrh.2015.11.022

O'Sullivan, M., & Pruess, K. (1980). Analysis of injection testing of geothermal reservoirs.

Olasolo, P., Juárez, M., Morales, M., & Liarte, I. (2016). Enhanced geothermal systems (EGS): A review. *Renewable and Sustainable Energy Reviews, 56*, 133-144.

Pambudi, N. A., Itoi, R., Jalilinasrabady, S., & Jaelani, K. (2014). Exergy analysis and optimization of Dieng single-flash geothermal power plant. *Energy Conversion and Management, 78*, 405-411.

Park S, Kim KI, Xie L, Kwon S, Yoo H, Min KB, . . . P, M. (2018). Observations and analyses of the first hydraulic stimulations in a fractured geothermal reservoir in Pohang, South Korea. *International Journal of Rock Mechanics and Mining Sciences (In prepration)*.

Parmentier, E. M., & Schedl, A. (1981). Thermal Aureoles of Igneous Intrusions: Some Possible Indications of Hydrothermal Convective Cooling. *The Journal of Geology, 89*(1), 1-22. doi:10.1086/628561
Perkins, T., & Gonzalez, J. (1985). The effect of thermoelastic stresses on injection well fracturing. *Society of Petroleum Engineers Journal, 25*(01), 78-88.
Portier, S., André, L., & Vuataz, F.-D. (2007). Review on chemical stimulation techniques in oil industry and applications to geothermal systems. *Engine, work package, 4*, 32.
Pruess, K. (1990). Modeling of geothermal reservoirs: fundamental processes, computer simulation and field applications. *Geothermics, 19*(1), 3-15.
Pruess, K. (1995). Numerical simulation of water injection into vapor-dominated reservoirs.
Pruess, K. (1996). *Injection plume behavior in fractured, vapor-dominated reservoirs*. Retrieved from
Pruess, K., Calore, C., Celati, R., & Wu, Y. (1987). An analytical solution for heat transfer at a boiling front moving through a porous medium. *International journal of heat and mass transfer, 30*(12), 2595-2602.
Pruess, K., Calore, C., Celati, R., & Wu, Y. S. (1987). An analytical solution for heat transfer at a boiling front moving through a porous medium. *International journal of heat and mass transfer, 30*(12), 2595-2602. doi:https://doi.org/10.1016/0017-9310(87)90140-2
Pruess, K., & Enedy, S. (1993). Numerical modeling of injection experiments at The Geysers.
Pruess, K., & Narasimhan, T. (1982). On fluid reserves and the production of superheated steam from fractured, vapor-dominated geothermal reservoirs. *Journal of Geophysical Research: Solid Earth, 87*(B11), 9329-9339.
Pruess, K., & Narasimhan, T. (1982). *Practical method for modeling fluid and heat flow in fractured porous media*. Retrieved from
Pruess, K., Oldenburg, C., & Moridis, G. (2011). *TOUGH2 user's guide version 2.1*. Retrieved from
Pruess, K., & Truesdell, A. H. (1980). A numerical simulation of the natural evolution of vapor-dominated hydrothermal systems.
Report, I. (2014). Fifth Assessment Report - Mitigation of Climate Change. *IPCC. Available at: https://www.ipcc.ch/report/ar5/wg3/*.
Romitti, Y. (2015). The International Geothermal Market At a Glance.
Rutagarama, U. (2012). *The role of well testing in geothermal resource assessment.* (Masters Thesis), University of Iceland.
Sanyal, S. K., & Enedy, S. L. (2011). *Fifty years of power generation at the Geysers geothermal field, California–the lessons learned.* Paper presented at the 36th workshop on geothermal reservoir engineering, Stanford, California.
Saptadji, N. M., Artika, Y., & No, J. G. (2012). *Surface water potential analysis and groundwater conservation concept at Kamojang geothermal field.* Paper presented at the Proc., 37th Workshop on Geothermal Reservoir Engineering.
Sass, J. H. (1993). *Potential of hot-dry-rock geothermal energy in the eastern United States [microform] : a report to the United States Congress under Section 2502 of Public Law 102-486 (The Energy Policy Act of 1992) / U.S. Geological Survey in collaboration with the U.S. Department of Energy*. [Menlo Park, Calif.?] : [Denver, Co: The Survey ; Books and Open-File Reports Section, distributor.
Sawin, J. L., Sverrisson, F., Seyboth, K., Adib, R., Murdock, H. E., Lins, C., . . . Williamson, L. E. (2016). Renewables 2016 Global Status Report. Key findings. A Record Breaking Year for Renewable Energy: New Installations, Policy Targets, Investment and Jobs. Mainstreaming renewables: guidance for policy makers.
Schotanus, M. (2013). *The Patuha geothermal system: a numerical model of a vapor-dominated system.*
Schroeder, R. C., O'sullivan, M., Pruess, K., Celati, R., & Ruffilli, C. (1982). Reinjection studies of vapor-dominated systems. *Geothermics, 11*(2), 93-119.

Siega, C. H., M. Grant, and T. Powell. (2009). Enhancing Injection Well Performance by Cold Water Stimulation in Rotokawa and Kawerau Geothermal Fields*., Proceedings, PNOC-EDC Conference, Manilla, Philippines 2009. 7p*.

Siratovich, P. A., Sass, I., Homuth, S., & Bjornsson, A. (2011). *Thermal stimulation of geothermal reservoirs and laboratory investigation of thermally-induced fractures.* Paper presented at the Proc., Geothermal Resources Council Annual Meeting.

Siratovich, P. A., Villeneuve, M. C., Cole, J. W., Kennedy, B. M., & Bégué, F. (2015). Saturated heating and quenching of three crustal rocks and implications for thermal stimulation of permeability in geothermal reservoirs. *International Journal of Rock Mechanics and Mining Sciences, 80*, 265-280. doi:https://doi.org/10.1016/j.ijrmms.2015.09.023

Skea, J., Anderson, D., Green, T., Gross, R., Heptonstall, P., & Leach, M. (2008). Intermittent renewable generation and the cost of maintaining power system reliability. *IET generation, transmission & distribution, 2*(1), 82-89.

Slevinsky, B. (2002). *A model for analysis of injection-well thermal fractures.* Paper presented at the SPE Annual Technical Conference and Exhibition.

Smith, R., & Shaw, H. (1978). Igneous-related geothermal systems. *Assessment of geothermal resources of the United States*, 12-17.

Stefansson, V.-đ. (1997). Geothermal reinjection experience. *Geothermics, 26*(1), 99-139. doi:https://doi.org/10.1016/S0375-6505(96)00035-1

Stephens, G., & Voight, B. (1982). Hydraulic fracturing theory for conditions of thermal stress. *International Journal of Rock Mechanics and Mining Sciences & Geomechanics Abstracts, 19*(6), 279-284. doi:https://doi.org/10.1016/0148-9062(82)91364-X

Stimac, J., Goff, F., & Goff, C. J. (2015). Chapter 46 - Intrusion-Related Geothermal Systems A2 - Sigurdsson, Haraldur *The Encyclopedia of Volcanoes (Second Edition)* (pp. 799-822). Amsterdam: Academic Press.

Tarasovs, S., & Ghassemi, A. (2011). *Propagation of a system of cracks under thermal stress.* Paper presented at the 45th US Rock Mechanics/Geomechanics Symposium.

Tester, J., Herzog, H., Chen, Z., Potter, R., & Frank, M. (1994). Prospects for universal geothermal energy from heat mining. *Science & Global Security, 5*(1), 99-121.

Tester, J. W., Anderson, B. J., Batchelor, A. S., Blackwell, D. D., DiPippo, R., Drake, E. M., . . . Nichols, K. (2006). Impact of enhanced geothermal systems on US energy supply in the twenty-first century. *Philosophical Transactions of the Royal Society of London A: Mathematical, Physical and Engineering Sciences, 365*(1853), 1057-1094.

Thomas, R. P., Chapman, R. H., Dykstra, H., & Stockton, A. (1981). *A reservoir assessment of The Geysers geothermal field*. Retrieved from

Truesdell, A. H., & White, D. E. (1973). Production of superheated steam from vapor-dominated geothermal reservoirs. *Geothermics, 2*(3), 154-173. doi:https://doi.org/10.1016/0375-6505(73)90022-9

Tsypkin, G. G. e., Calore, C., & Marcolini, M. (2006). Mathematical modeling of cold water injection into a depleted high-temperature geothermal reservoir. *High temperature, 44*(3), 450-457.

Weres, O., Tsao, K., & Wood, B. (1977). *Resource, technology, and environment at the geysers*. Retrieved from

West Japan Engineering Consultants (West JEC), I. I. r. (2007). *Feasibility study for Patuha geothermal power development: Final feasibility report.* Retrieved from

White, D., Muffler, L., & Truesdell, A. (1971). Vapor-dominated hydrothermal systems compared with hot-water systems. *Economic Geology, 66*(1), 75-97.

Witherspoon, P. A., Wang, J. S., Iwai, K., & Gale, J. E. (1980). Validity of cubic law for fluid flow in a deformable rock fracture. *Water Resources Research, 16*(6), 1016-1024.

Wohletz, K., & Heiken, G. (1992). *Volcanology and geothermal energy* (Vol. 432): University of California Press Berkeley.

Woods, A. W. (2014). *Flow in Porous Rocks: Energy and Environmental Applications*. Cambridge: Cambridge University Press.

Yoo, H. (2018). *Numerical modeling of hydraulic stimulation at a fractured geothermal reservoir* (Master's), Seoul National University

Yoshioka, K., Izgec, B., & Pasikki, R. (2008). *Optimization of geothermal well stimulation design using a geomechanical reservoir simulator.* Paper presented at the Proceedings, Thirty-Third Workshop on Geothrmal Reservoir Engineering.

Yoshioka, K., Pasikki, R. G., Suryata, I., & Riedel, K. L. (2009). *Hydraulic Stimulation Techniques Applied to Injection Wells at the Salak Geothermal Field, Indonesia.* Paper presented at the SPE Western Regional Meeting.

Appendix A. Full detailed injection design PPL-06

This executive summary is intended to provide the reader a quick review of the most important points of the current report. Apparently, for additional information and detailed-support the reader is referred to the main document.

1. Purpose

The poor production of PPL06 is believed to be caused by one or a combination of the following factors:

- Lack of in-situ immobile water to be replenished the produced-steam: increase in produced enthalpy and decline in steam production are believed to be caused by this issue.
- Small fracture network or lack of a pre-existing fracture network
- Poor connection between wellbore and the pre-existing fractures

2. Pre Stimulation/Injection Test

Pre stimulation/injection test has been designed to not only ensure the cause of poor production, but to pursue the following purposes:

- Pre-stimulation/injection characterization
  - Observation of the reservoir response
- To check the difference with somewhat higher injection rate
- Test reservoir seismic responses during injection and shut-in period
- Possible measurement of Injectivity index
- Identification of the most impermeable zone
- Implement and test traffic light system of seismic risk management
- Establish amplitude-ML relationship to be used for traffic light system

Since the injection starts, based on the contribution of the most permeable interval(s) one of the following scenarios is expected. However, based on the previous injection experiences in other vapor-dominated fields including Kamojang, as well as the injection experiences in other well bores in the Patuha, it is expected the first scenario happens:

I. Injection into the vapor zone

a. Due to low pressure, the injected-water will go mainly to this zone and if this scenario is the case, then the wellhead pressure is continuously decreasing; due to phase change of hot steam to water there would be void space and there would be a suction into the reservoir. The fracture network is large enough, and/or the matrix is accepting the water. In this case, the fluid will either flow towards the producers while it is heating up and improve the overall production of

the field, or replenish the produced-fluid, and after a temporary period of shut in and heat up in addition to the preexisting steam the amount of production will improve. We may confirm the interval of flow contribution by spinner log/pressure/temperature logging.

II. Injection into vapor zone filling the small fracture network or filling the porous medium and reaching the impermeable boundaries
    a. If this is the case, the wellhead pressure may increase after a while of continuous decreasing; in this case, once WHP starts increasing, by doing a step rate test we may measure the minimum principle stress, and tune the injection rate of the second injection stage in order to design a thermo-hydro-shearing stimulation. It also has to be confirmed, which interval is contributing to the fluid flow dominantly by spinner log/pressure/temperature logging.

III. Injection into vapor zone due to poor connection with the well is not possible
    a. In this case, the injection may just happen into the liquid zone and the wellhead pressure will increase from the first moment; if this is the case, then the use of packer to isolate the liquid zone from the vapor zone is proposed. Similarly, due to limitation of budget and the expenses of the proppant agent in high environment, by doing a step rate test we may measure the minimum principle stress, and tune the injection rate of the second injection stage in order to design a thermo-hydro-shearing stimulation. The importance of application of spinner log/pressure/temperature logging is apparent.

The flowchart has covered all the aforementioned scenarios (Figure 3.4). For the first almost 5 days (4.5 days), the test has been designed with relatively higher injection rate. In this period also three injection trends including increasing, decreasing, and constant injection rate has been implemented. The main goal of increasing and decreasing and injection at high rate for relatively long time is that to create a single-phase liquid region close to the wellbore during injection test, same as what is being done in Dieng filed. The aim of this single-phase liquid region is to eliminate the effects of condensation of steam during cold-water injection and measuring an injectivity. To do so, injectivity test should be done by two flowrate trends, including increasing and decreasing. During the increasing flowrate, steam condensation is expected and the single phase will be created near the wellbore. The data from decreasing flowrate trend may be used to obtain injectivity index. Since the decreasing injection rate is relatively long enough we may reach stable wellhead pressure. This method has been used successfully in Philippine (Clotworthy & Hingoyon, 1995). Hence, by taking advantage of this method we may repeat this test at the end of the second stage (long injection) period in order to analyze the injectivity index.

It is also noteworthy to emphasize again that by a proper spinner and temperature/pressure log, we may recognize the interval with higher permeability

zone, which could be either in vapor zone or in liquid zone. This Idea is coming from the drilling report of PPL06 since the circulation data shows there is not much lost in the vapor zone, which could be a good evidence of poor connectivity of this zone with the wellbore or a poor fracture network. On the other hand, the injection at high rate, if the fracture zone is small, will fill out the fracture network in the vapor zone, which is already filled with steam and since then the wellhead pressure will increase. However, it is essential to confirm such an injection is going through the vapor zone by pressure/temperature logging or spinner log. If this is the case, by doing a step rate test we may measure the minimum principle stress, and tune the injection rate of the second injection stage in order to design a thermo-hydro-shearing stimulation.

If it was not the case and the wellhead pressure of PPL06 is decreasing as injection is going on as it is expected like other injection experiences in Patuha, we may do the same as other vapor dominated system as they did the same reinjection experiment to enhance the heat production.

In fact, this short pre stimulation/injection test includes two injectivity tests and a short soft hydraulic stimulation of PPL06. These two injectivity tests are before and after the short soft hydraulic stimulation test in order to analyze the injectivity improvement (Figure A.1).

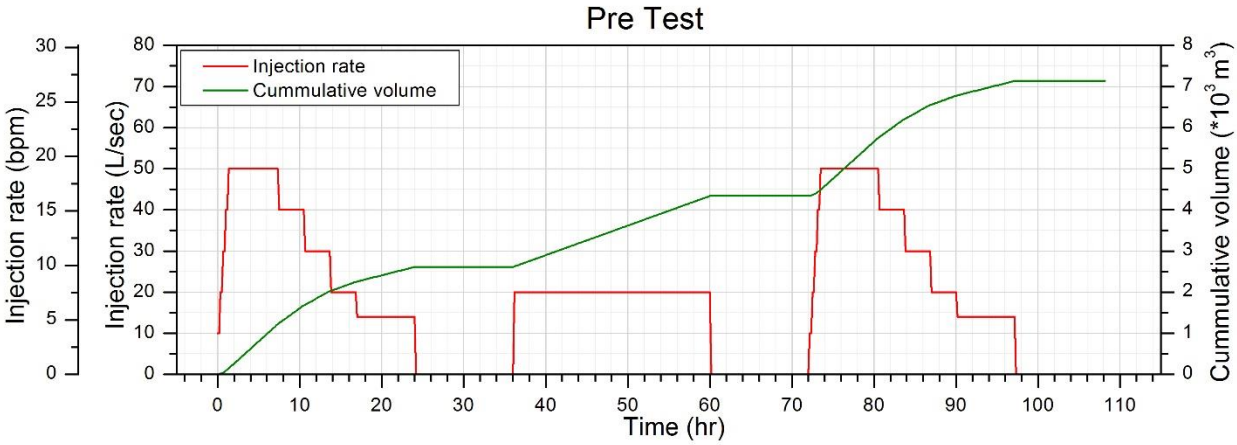

Figure. A.1 The injection scheme and the cumulative injection volume of the first 4.5 days

3. Monitoring System

It is vital to observe the responses of the reservoir carefully by an exact monitoring plan to formulate the most appropriate field strategy management.

Key considerations in the pre injection test will be;

- Wellhead pressure monitoring of PPL06
- Pressure and Temperature logging/ Spinner logging in PPL06 are extremely important to make the right decision (before-during-after injection)
    - In order to find the most contributing intervals (high permeable zones) if it is the vapor zone or the liquid zone

        - It is recommended to do it with every different rate, however, if not possible just at the maximum rate and shut in period to recognize the contributing intervals

- Pressure and steam/hot water flow rate as well as temperature and enthalpy rate of other producers
- Induced Microseismicity rate (number of event/time)
- Magnitude of Induced Microseismicity
- (Possibly) regional extent of induced microseismicity
- It is highly recommended to supplement enough water prior to injection
    - Using retention tanks or storage ponds prior to reinjection will be helpful to reduce the risk of presentation of silica scaling and also injection of high rate or hot water will also reduce the risk of silica scaling

4. Long-term Injection Design in Vapor-Dominated System

1. Tracer Test

Underground flow paths are complex and a distance above ground is not necessarily representing the distance below ground. Tracer testing is, therefore, one of the most important tools for the geothermal reservoir engineer. As it was mentioned, due to the complex underground flow paths, it is not possible to totally design a reinjection scheme until the wells have already been tested and the underground flow paths mapped by tracer tests (T Dwikorianto et al., 2005). Furthermore, it is not yet clear whether the full effects of reinjection water breakthrough are detectable unless full-scale, field-wide test is in progress. Some progress in this case is being made, but reinjection schemes are likely to be designed conservatively in the meantime. The problem of injectivity loss has been overcome in some fields, based on the reports, and increases of injectivity have even been observed.

2. Silica Scaling Problem

In some cases, though, chemical precipitation continues to be a difficulty and is a major cost penalty to the geothermal power-station in particular silica scaling. However, in the case of Patuha, PPL01B is under injection for relatively long time and there is no report of reduction in permeability or injectivity. Nevertheless, in case, to reduce the risk of silica scaling since there would be an external water supply for injection test, it is highly recommended to control the water component. Also as it was mentioned, based on the experiences the high injection rate, higher temperature, as well as using retention tanks or storage ponds prior to reinjection will be helpful

to reduce the risk of presentation of silica scaling (Diaz et al., 2016; R. Horne, 1985; Pambudi, Itoi, Jalilinasrabady, & Jaelani, 2014).

Finally, the design of reinjection is most often empirical and site−specific, however, there are some generic similarities depending on the characteristic of the system. This test is also designed based on these similarities and the reported field experiences. Therefore, the results of this test will be used in order to find the best optimum reinjection strategy. Nonetheless, based on the analysis the current reinjection strategy proposed here as stop injection in PPL01−B and instead start injection in PPL01−A which is drilled into the center as well as carrying out an injection test in PPL06 is believed to have promising effects on the production of the field. The response of the reservoir must be observed carefully by an exact monitoring plan to formulate the most appropriate field strategy management. Although, there is a temporary halt in production of PPL06 due to one month injection, an overall improvement in production is expected. It is worthy to mention that in other vapor dominated systems, also the poor producer has converted to a successful injector in a way that the reinjection practice is designed for a longer period in the order of years and the overall improvement in production is positive as for example The Geysers, and Larderello.

All in all, the reinjection plan is suggested as below, this injection is started with a relatively smaller injection rate in compare with the pre stimulation/injection test since the distance of the bottom holes of PPL06 and the nearest production well PPL02 AST is 351.65 m. This injection experiment requires continuous monitoring of production rate and temperature of all the producers since the underground flow path are complex. Due to this complexities, there is no guarantee that the closer wellbore will response to injection faster than the other producers as in case in Matsukawa geothermal field. Figure A. 2. Shows the overall view of injection plan. In fact, this injection plan has been designed to satisfy all the expected scenarios, however, the injection rate and accordingly the total injection volume might be tuned due to mitigation plan, or the operation of soft hydraulic stimulation.

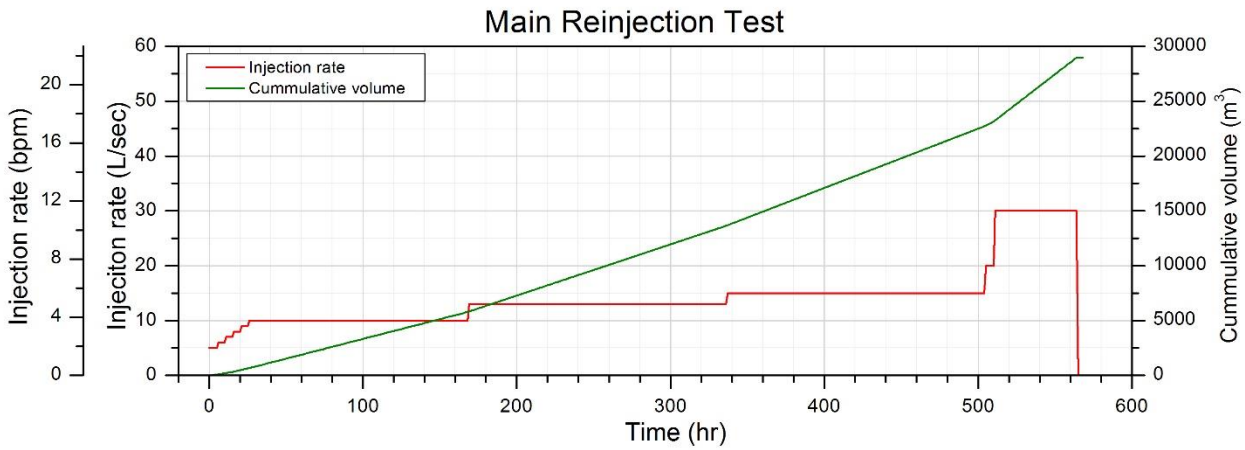

Figure. A .2. The main injection scheme and the cumulative injection volume of the first 25.5 days

Appendix B. Thermal Stimulation

Thermal stimulation relies on the thermal contraction induced by a significant temperature difference between the cold injection fluid against the hot rock formation (to create new fractures) and the enhancement of near wellbore permeability. Thermal cracking is attained by alternately injecting cold fluid and allowing the well to heat up the formation as thermal recovery ensues. Cold fluids may include cooling tower condensate, fresh water, seawater, or cold waste brine (A.R. Aqui, 2011; Flores, Davies, Couples, & Palsson, 2005). Three mechanisms are considered responsible for the success of thermal stimulations:

1. The cleaning of debris or mineral deposits from open fractures intercepted by the wellbore during drilling
2. The re-opening of pre-existing fractures by thermal contraction
3. The creation of new fractures from the thermal stress exerted on the reservoir rocks (Gudni Axelsson et al., 2006).

In practice, although, it has been estimated that all three mechanisms are contributing on the wellbore stimulation, the first is the most likely when post-drilling stimulation is carried out right after the well has been drilled. The second and third mechanisms are thought to be responsible for significant gains in wells that have previously been used as injectors or producers (Flores-Armenta, 2008). Such a hydraulic stimulation (mainly below the formation breakdown pressure) has been used in many geothermal fields; accordingly, based on limited reports, in all the cases the permeability improvement has been observed (A.R. Aqui, 2011; Paul A Siratovich et al., 2011). Table B.1 shows some of the reported thermal stimulation results all over the world. Generally speaking, based on the recorded thermal stimulation applications the injection pressure and temperature range between 10 to 60 bars and 20℃ (sourced from nearby fresh water sources) up to 165℃ (sourced from separated geothermal brine from power plant infrastructure), respectively. In terms of the thermal stimulation duration, it can vary from hours after well has been drilled to several months of long term, often cyclic injection. There are several methods of injection which have been used in EGSs all over the world:

1. Long term cold water injection, i.e. the Southern Negros Geothermal Production Field, Philippines (Aqui & Zarrouk, 2011).
2. Cyclic hot water and cold water injection, i.e. the Salak field, Indonesia (Yoshioka et al., 2009).
3. Cyclic cold water injection and shut in, i.e. Los Humeros geothermal field in Pue, Mexico (Flores-Armenta, 2008).

For long term injection in situ stress will vary due to thermal elasticity. Thermal effects on in situ stress are expressed as:

$$\sigma_3 = \frac{\nu}{1-\nu}(OB - \alpha P_{Res}) + P_{Res} + \frac{E}{1-\nu^2}[\varepsilon_3 + \nu\varepsilon_1 + (1+\nu)\beta\,\Delta T] \quad \text{(B.1)}$$

Where, σ_3, is the minimum horizontal stress, $\varepsilon_3$and ε_1, are the minimum and maximum horizontal strains, respectively, α, is Biot's parameter, β, is coefficient of thermal expansion, ν, is the Poisson's ratio, E, is Young's Modulus, OB, is the overburden pressure, and, P_{Res}, is the formation pore pressure (reservoir pressure). However, the change in stress due to temperature changes directly relates to the temperature change, ΔT, and to the modulus (Young's modulus) of the rock. Since the location of many EGS projects is usually in basement, crystalline rock, modulus can often be very high in the order of 10×10^6 pounds per square inch (psi) or 6.9×10^4 Mega Pascal (MPa), and cooling (negative ΔT) can potentially create very large positive (tensile or reduction in the in situ stress) stress changes. To discuss in more details, Ghassemi et al., (2007) have suggested that the fracture propagation can be explained by the fact that the cooling effect of the injected fluid results in pore pressure reduction that increases effective stress near the wellbore but reduces the total stress in the reservoir itself (A. Ghassemi et al., 2007; Héðinsdóttir, 2014). The reduction in total reservoir stress results in fewer shear failures and a higher instability due to tensile failure. Therefore, the resultant fractures have significant permeability. The subsequent cooling increases stress at the fracture tip, and the fracture itself grows due to the stress differential. In geothermal real field practice, Siega et al., (2009) reported that the long term injection of cold water has shown significant improvement in fluid handling capacities in injection wells at the Rotokawa and Kawerau fields, New Zealand (Siega, 2009). Additionally, based on literature review, it seems that the more temperature difference (in the order of > ~150℃), and the larger coefficient of thermal expansion (9.57E−06 1/℉), the larger effect of thermal stimulation can be expected. Furthermore, Yokiosha et al., (2008) by taking advantage of geomechanical reservoir simulator showed that the use of higher injection pressure and a cooler injection fluid temperature leads to improved injectivity. In addition, they found through their modeling that the cycling of injection does have long lasting benefits, but these are overcome through utilization of a longer−scale higher pressure and cooler injection scheme(Yoshioka, Izgec, & Pasikki, 2008). It has been also confirmed with other researchers (by field observation reports) that the thermal cycling in production wells showed to be an effective technique by rapidly cooling and heating the wellbore; the stresses are enhanced at the reservoir−well interface and there is permeability improvement (Bjornsson & ISOR, 2004; Kitao, Ariki, Watanabe, & Wakita, 1995).

In terms of the prediction of the stimulation duration, Grant et al., (2013), based on the available data in Rotokawa and Kawerau fields in New Zealand, suggested that the expected pattern is an increase like t^n, where n is 0.4−0.7 – in fact when the injectivity index is plotted versus time, there should be a linear trend on log−log scale (Figure B.1). Moreover, they claimed that the sustained deviation below this trend suggests deposition during the injection. Finally, they concluded that the permeability of hot fractured rock increases strongly with decrease in temperature. They even stated that the increase is due to thermal contraction of the rock, and causes permeability changes much greater than those due to pressure changes. As a matter of fact, such a statement has been confirmed by the report by

Aqui and Zarrouk (2011) when the well in the Southern Negros Geothermal Production field in Philippine was firstly tried to be hydraulically fractured, but it was not successful, while the low pressure injection of cold water has improved the permeability of the formation considerably (see appendix A for more details). This process cannot continue indefinitely, as it depends on the existence of a temperature contrast; but it has been observed to continue for a few years, as it was observed with other researchers (Aqui & Zarrouk, 2011; Malcolm A Grant et al., 2013; Yoshioka et al., 2009). There is a new suggested technique, by which it is recommended to drill the well with low temperature drilling fluid (i.e. water), in order to have considerably stimulated formation at the end of drilling, and lately with continued injection, injectivity continues to increase, such a method has been applied in Rotokawa and Kawerau fields in New Zealand (Malcolm A Grant et al., 2013).

Table B.1. Thermal stimulation comparison from various geothermal fields

Field/ Test Wells	Injection Rate (kg/s)	Initial Injectivity Index (kg/s)/bar	Post Stimulation Injectivity Index (kg/s)/bar
Hellisheidi (HE-08)	50-60	2	6-7
Sumikawa (SA-1; SA-2; SA-4)	3-110	11.1;13.3;9.2	18.2; 15.5;11.2
Los Humeros (H-40)	1.3-33	Initial Injection Capacity Less than 1.4 kg/s	Final Injection Capacity In Excess of 30.5 kg/s
Boulliante (BO-4)	26	0.9	1.4
Salak (Awi-11-6OH. Awi 11-5)	60-250	2.01; 1.09	4.03, 2.56
Kawerau (KA43; KA44)	25-60	6.4;5.5	12.5;26.9
Rotokawa (RK21; RK23)	11-39	0.75;4.2	0.83;10

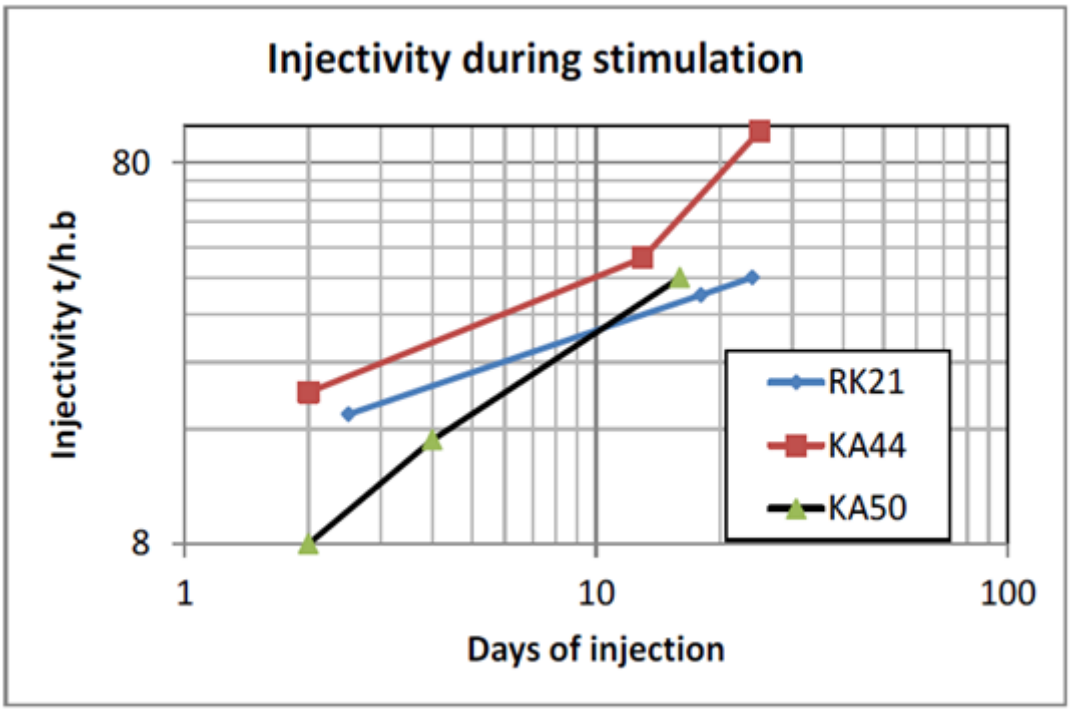

Figure B. 1. injectivity (ton/hour.bar) of RK21, KA44, KA50 during stimulation days (Malcolm A Grant et al., 2013).

To specifically address the question whether the permeability improvement of the thermal stimulation is irreversible or not. An example of thermal stimulation will be briefly discussed in the following.

The Krafla geothermal field has been found to be complex, consisting of two zones. A shallow liquid-dominated zone with temperature of approximately 210 ℃ whereas the deeper zone is a two phase system with temperatures >300℃. The Krafla high-temperature field of Northern Iceland is a field in which thermal stimulation of geothermal well bores has been performed as a standard procedure over the many decades the field has been in operation. This example is the well KJ-14 in Krafla geothermal field, Iceland was thermally stimulated right after drilling completed (figure B.2). Cold water (20℃) was being injected immediately after the completion of the well in 1980s. The permeability improvement, represented here as the circulation loss, was considerably observed, and this well was one of the most productive well in the Krafla region, yielding 15 kg/s of steam during initial production testing. Therefore, based on this information, it can be inferred that the permeability improvement is irreversible, till mineral deposition happens and reduce the permeability. After the stimulation procedure, the well became one of the best producers in the field. The increase in permeability is attributed to the cleaning of drill cuttings from permeable fractures, opening of sealed fractures and possibly the creation of new fractures (G. S. Bodvarsson, Benson, Sigurdsson, Stefansson, & Eliasson, 1984; Paul A Siratovich et al., 2011).

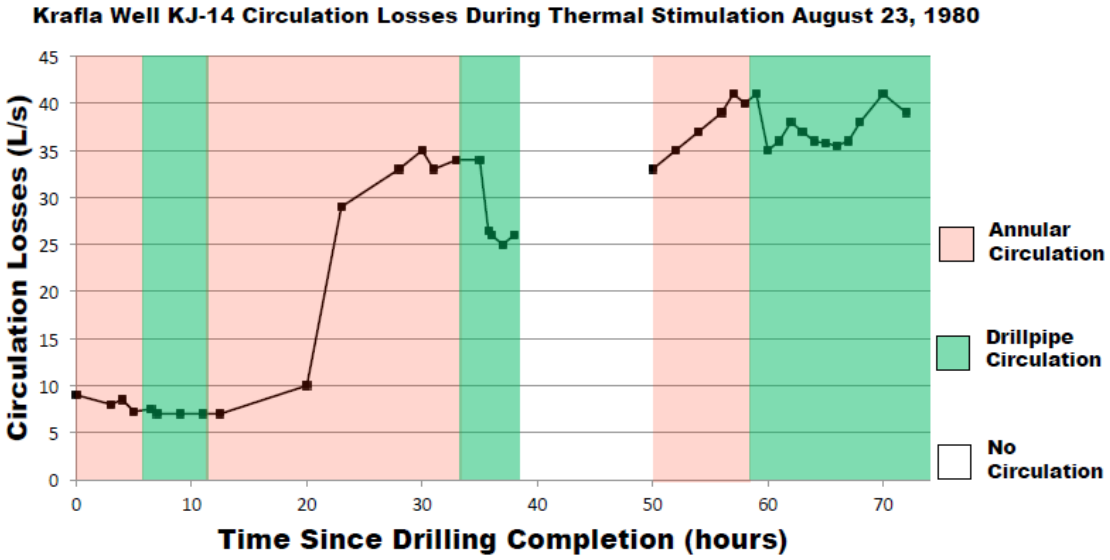

Figure B. 2. Observed circulation losses following drilling of well KJ-14 at Krafla geothermal field, Iceland. Thermal Stimulation of the well began almost immediately after drilling, and the circulation losses were recorded once fluid was injected into the well. The break in the middle is a warming period when no injection occurred (Paul A Siratovich et al., 2011).

Although, the theory and mechanics that control how reservoirs react to thermal stresses has not been well understood yet and it is still the subject of ongoing investigations. All in all, thermal stimulation has been a mechanism that has huge potential to improve geothermal reservoir–well interaction and has seen many successful applications. Moreover, the running time of the pumps would be the main cost of such a stimulation method(Yoshioka et al., 2009).